Government of Western Australia

Department of
Mines and Petroleum

REPORT
118

GEOCHEMICAL EVOLUTION OF RHYOLITES OF THE TALBOT SUB-BASIN AND ASSOCIATED FELSIC UNITS OF THE WARAKURNA SUPERSUITE

by RH Smithies, HM Howard, CL Kirkland, M Werner, CC Medlin, MTD Wingate, and JB Cliff

Geological Survey of Western Australia

Government of Western Australia
Department of Mines and Petroleum

REPORT 118

GEOCHEMICAL EVOLUTION OF RHYOLITES OF THE TALBOT SUB-BASIN AND ASSOCIATED FELSIC UNITS OF THE WARAKURNA SUPERSUITE

by
RH Smithies, HM Howard, CL Kirkland, M Werner[1], CC Medlin[2], MTD Wingate, and JB Cliff[3]

[1] Geological Survey of South Australia, GPO Box 1264, Adelaide SA 5001

[2] School of Geosciences, Monash University, Wellington Road, Clayton Victoria 3800

[3] The Centre for Microscopy, Characterisation and Analysis, The University of Western Australia, Crawley WA 6009

Perth 2013

Geological Survey of Western Australia

REFERENCE
The recommended reference for this publication is:
Smithies, RH, Howard, HM, Kirkland, CL, Werner, M, Medlin, CC, Wingate, MTD, and Cliff, JB 2013, Geochemical evolution of rhyolites of the Talbot Sub-basin and associated felsic units of the Warakurna Supersuite: Geological Survey of Western Australia, Report 118, 74p.

National Library of Australia Cataloguing-in-Publication entry

Author:	Smithies, R. H., author.
Title:	Geochemical evolution of rhyolites of the Talbot Sub-basin and associated felsic units of the Warakurna Supersuite / RH Smithies, HM Howard, CL Kirkland, M Werner, CC Medlin, MTD Wingate and JB Cliff.
ISBN:	9781741684926 (Electronic document)
Subjects:	Rhyolite--Western Australia--Musgrave Block. Volcanism--Western Australia--Musgrave Block. Geology--Western Australia--Musgrave Block.
Other Authors/Contributors:	Howard, H. M., author. Kirkland, C. L., author. Werner, M., author. Medlin, C. C., author. Wingate, M. T. D. (Michael Thomas David), author. Cliff, John B., author. Geological Survey of Western Australia.
Dewey Number:	552.3099415

ISSN 0508–4741

Grid references in this publication refer to the Geocentric Datum of Australia 1994 (GDA94). Locations mentioned in the text are referenced using Map Grid Australia (MGA) coordinates, Zone 52. All locations are quoted to at least the nearest 100 m.

Volcanological and some geochemical aspects relating specifically to the Pussy Cat Group (i.e. the Kathleen Ignimbrite and porphyritic rhyolite intrusions) form part of the PhD thesis of CC Medlin (in prep.) at Monash University, Victoria.

NGAANYATJARRA COUNCIL (Aboriginal Corporation)

John de Laeter Centre
Isotope Research for the Earth and Environment

U–Pb measurements were conducted using the SHRIMP II ion microprobes at the John de Laeter Centre of Isotope Research at Curtin University in Perth, Australia. Isotope analyses were funded in part by the Western Australian Government Exploration Incentive Scheme (EIS).

Copy editor: A Forbes
Cartography: M Prause
Desktop publishing: RL Hitchings
Printed by Images on Paper, Perth, Western Australia

Published 2013 by Geological Survey of Western Australia
This Report is published in digital format (PDF), as part of a digital dataset, and is available online at <www.dmp.wa.gov.au/GSWApublications>.

Further details of geological publications and maps produced by the Geological Survey of Western Australia are available from:
Information Centre
Department of Mines and Petroleum
100 Plain Street
EAST PERTH WESTERN AUSTRALIA 6004
Telephone: +61 8 9222 3459 Facsimile: +61 8 9222 3444
www.dmp.wa.gov.au/GSWApublications

Cover photograph: Spherulites in rhyolite of the Mount Palgrave Group – Talbot Sub-basin. 'Teddy Bear's Arsehole' (Malvaceae: *Sida platycalyx*) seed pod 2 cm in diameter for scale

Contents

Appendix

Figures

Tables

Geochemical evolution of rhyolites of the Talbot Sub-basin and associated felsic units of the Warakurna Supersuite

by

RH Smithies, HM Howard, CL Kirkland, M Werner[1], CC Medlin[2], MTD Wingate, and JB Cliff[3]

Abstract

Large-volume felsic volcanic sequences yield valuable information about crustal architecture, crust–mantle interactions, and regional tectonic evolution. Eruptions of super-volcano size (i.e. >450 km^3 of material erupted) are very rare in the geological record. We present new geological, geochemical, isotopic, and geochronological data from the felsic volcanic sequences of the Bentley Supergroup in the Mesoproterozoic Ngaanyatjarra Rift, which includes several volcanic deposits of super-volcano size.

The Ngaanyatjarra Rift in central Australia is the main crustal expression of the Mesoproterozoic Giles Event. This event included emplacement of the regional Alcurra Dolerite dyke swarm during the evolution of the early (c. 1075 Ma) Warakurna Large Igneous Province (LIP), but magmatism continued for >50 m.y. thereafter and included the development of a silicic LIP over a period of >30 m.y., formed by a series of large rhyolite eruptions, including some of super-volcano size, interleaved with regional tholeiitic basalt flows. These formed the Talbot Sub-basin and, on a more regional basis, represent the dominant stratigraphic component of the Bentley Basin — the fill of the Ngaanyatjarra Rift.

In the Talbot Sub-basin, at least 20 separate felsic volcanic units can be recognized, forming layers of very high-temperature (some >900ºC) rhyolitic and rheomorphic ignimbrites and rhyolitic flows. All of these are isotopically juvenile, reflecting direct mantle extraction with only minimal crustal input. Combining preserved volumes of extruded basalt with volumes of parental basalt required to produce the felsic volcanic rocks gives a minimum of 227 000 km^3 of mantle-derived magma to produce the total preserved felsic and mafic volcanic pile of the Talbot Sub-basin. Notably, of the total required mantle-derived magma, <5% erupted as basalt. The Talbot Sub-basin is only one of several sub-basins of the Bentley Basin. At least five additional felsic units are recognized within the other, less well-studied, sub-basins. Extrapolating magma volume calculations for the Talbot Sub-basin across these other sub-basins provides speculative estimates of initial volumes of mantle-derived magma of approximately 2.19×10^6 km^3. These calculations ignore the giant layered Giles (G1) intrusions and associated massive gabbros (G2) of the Warakurna Supersuite, the basalts of the lower Kunmarnara Group into which those intrusions were emplaced, and the rocks of the Warakurna LIP.

Mantle-derived magmatism of more than 30 m.y. duration in a single isolated region is difficult to relate to a mantle plume. Even a conservative drift rate of 2 cm/year removes the crustal plate by more than 600 km from an stationary asthenospheric plume source, and much farther if we consider the entire duration of the Giles Event. Nor does the duration of magmatism favour a fortuitous sequence, or cluster, of plumes. Rather, the region reflects a zone of persistently very high crustal temperatures linked to a crustal architecture established as amalgamation of Proterozoic cratonic Australia locked the region between three thick and rigid cratonic masses. From c. 1220 to 1020 Ma, it was the site of one of the world's largest and longest-lived (c. 1220 to 1150 Ma) belts of mid-crustal ultrahigh-temperature conditions, the site of one of the world's largest layered mafic intrusions (the 1078 to 1075 Ma Giles intrusion), the focal point of the c. 1075 Ma Warakurna LIP, and the site of possibly the worlds longest-lived sequence of high-temperature super-volcano eruptions, forming possibly the world's most voluminous juvenile input of felsic material into the crust outside a subduction zone. Throughout the Giles Event, the magmatic and tectonic evolution of this thermally weakened zone was possibly a far-field response to tectonic processes operating along the margins of the combined Proterozoic Australian craton. Crustal structure and thermal history were the primary controls on magmatic and tectonic evolution, rather than deep-seated mantle upwelling or mantle plume activity.

KEYWORDS: Mesoproterozoic Giles Event, Musgrave Province, felsic volcanics, geochemistry, geochronology, petrogenesis, igneous petrology, tectonics, stratigraphy

[1] Geological Survey of South Australia, GPO Box 1264, Adelaide SA 5001

[2] School of Geosciences, Monash University, Wellington Road, Clayton Victoria 3800

[3] The Centre for Microscopy, Characterisation and Analysis, The University of Western Australia, Crawley WA 6009

Introduction

The Ngaanyatjarra Rift is the main structural expression of the Mesoproterozoic Giles Event (Evins et al., 2010), in central Australia, which saw the earlier Mesoproterozoic rocks of the Musgrave Province extensively intruded and covered by bimodal magmatic rocks of the Warakurna Supersuite (Fig. 1). The Giles Event was also responsible for the craton-scale mafic rocks of the Warakurna Large Igneous Province, including the Alcurra Dolerite dyke swarm (e.g. Wingate et al., 2004). Volcanic rocks of the Warakurna Supersuite (Bentley Supergroup) are the dominant stratigraphic component of the Bentley Basin — the fill of the Ngaanyatjarra Rift. One of the best-preserved bimodal volcanic sequences is in the far southwest of the Musgrave region within the Talbot Sub-basin, where it comprises a series of basalt flows and interleaved, thick, and regionally continuous layers of very high-temperature rhyolitic ignimbrites, rheomorphic ignimbrites and flows, some with volumes reflecting super-volcano eruptions. Volcanic activity in the Talbot Sub-basin lasted for more than 30 Ma and all magmas there are of mantle-derived tholeiitic descent, with very minimal crustal contamination. The size, volume, duration, composition, source, and tectonic setting of these rocks make the Talbot Sub-basin unique in the global geological record. This Report provides a detailed description of the stratigraphy and lithological diversity within the Talbot Sub-basin. It describes the geochemical and chronological evolution of the felsic magmas and the implications of their development for the tectonic evolution of the region.

Regional geological setting

Volcanic rocks of the Bentley Basin overlie earlier Mesoproterozoic rocks of the Musgrave Province and are locally overlain by Neoproterozoic sedimentary rocks of the Amadeus and Officer Basins (Fig. 1). The Musgrave Province itself is an east-trending Mesoproterozoic belt up to 800 km long and 350 km wide, bounded to the north and south by Neoproterozoic to Palaeozoic basins. It lies at the convergence of Australia's main Proterozoic structural trends that reflect the amalgamation of the North, West, and South Australian Cratons (Fig. 1). The broad lithological framework of the province has been established (Daniels, 1974; Glikson et al., 1996; Edgoose et al., 2004; Howard et al., 2006, 2007, 2011a; Evins et al., 2009, 2010; Smithies et al., 2009, 2010; King, 2008; Kelsey et al., 2009), although some aspects of its tectonic evolution are still debated (e.g. Li, 2000; Giles et al., 2004; Betts and Giles, 2006; Wade et al., 2006, 2008; Cawood and Korsch, 2008).

A recent study of Hf isotopes in zircons from magmatic and sedimentary rocks throughout the Musgrave Province (Kirkland et al., 2013a) indicates that the unexposed basement in the region is dominated by two major juvenile crustal formation events — one at 1600–1550 Ma and a possibly more significant event at 1950–1900 Ma. Although no juvenile rocks or crystals are known from c. 1900 Ma, radiogenic addition to the crust at this time is required to account for consistent Nd and Hf evolution patterns that show no indication of mixing processes (Kirkland et al., 2013a).

Outcrop in the west Musgrave Province is dominated by granites formed during several Mesoproterozoic events (Fig. 2). The oldest of these is a recently identified, and hitherto un-named, event that involved intrusion and possible extrusion of felsic calc-alkaline magmas of the Papulankutja Supersuite and contemporaneous redistribution of this material into local sedimentary basins at c. 1400 Ma (Howard et al., 2011b; Kirkland et al., 2013a). Subsequent major events include the 1345–1293 Ma Mount West Orogeny, the 1220–1150 Ma Musgrave Orogeny, and the 1085–1040 Ma Giles Event (Fig. 2; Wade et al., 2008; Smithies et al., 2009, 2010, 2011; Howard et al., 2011b).

The Mount West Orogeny is the oldest clearly recognizable event in the region. During this period, calc-alkaline granites of the Wankanki Supersuite were emplaced mainly within the central and southeastern part of the west Musgrave Province (Fig. 2; Smithies et al., 2009; Evins et al., 2009). Crystallization ages range from c. 1345 to 1293 Ma (Gray, 1971; Sun et al., 1996; White et al., 1999; Bodorkos and Wingate, 2008; Bodorkos et al., 2008a–e; Kirkland et al., 2008a–f; Smithies et al., 2009), but are concentrated between c. 1326 and 1312 Ma. Rocks of the Wankanki Supersuite are typically metaluminous, calcic to calc-alkaline granodiorites and monzogranites with strong compositional similarities to the Phanerozoic granites of the Andean continental arc (Smithies et al., 2010). The Mount West Orogeny may reflect a final subduction and accretion event in the amalgamation of the North, West, and South Australian Cratons (Giles et al., 2004; Betts and Giles, 2006; Smithies et al., 2009, 2010; Kirkland et al., 2013a).

The 1220–1150 Ma Musgrave Orogeny involved mylonitic deformation, granulite-facies metamorphism, and widespread crustal reworking. The dominant northwest structural trend of the west Musgrave Province reflects a crustal architecture established during or before the Musgrave Orogeny and was locally modified and reactivated during later events. There is no clear evidence for significant compressional deformation associated with the prolonged orogeny, although northeast-trending folds are an early structural development (e.g. Aitken et. al., 2012). The orogeny appears to have been essentially intracratonic (Wade et al., 2008; Smithies et al., 2009, 2010).

Orthopyroxene-bearing (charnockitic) and locally rapakivi-textured granites of the Pitjantjatjara Supersuite intruded the mid-crust more or less continuously throughout the Musgrave Orogeny. They are ferroan and typically alkali-calcic granites with significant rare earth element (REE) and high field strength element (HFSE) enrichments. In all areas, the earliest Pitjantjatjara intrusions are strongly Yb-depleted granites formed through deep-crustal melting under garnet-present conditions. A transition from these to Yb-undepleted granites formed at lower melting pressures is diachronous, migrating from the northeast to the southwest of the province from c. 1220 to 1200 Ma. This transition has

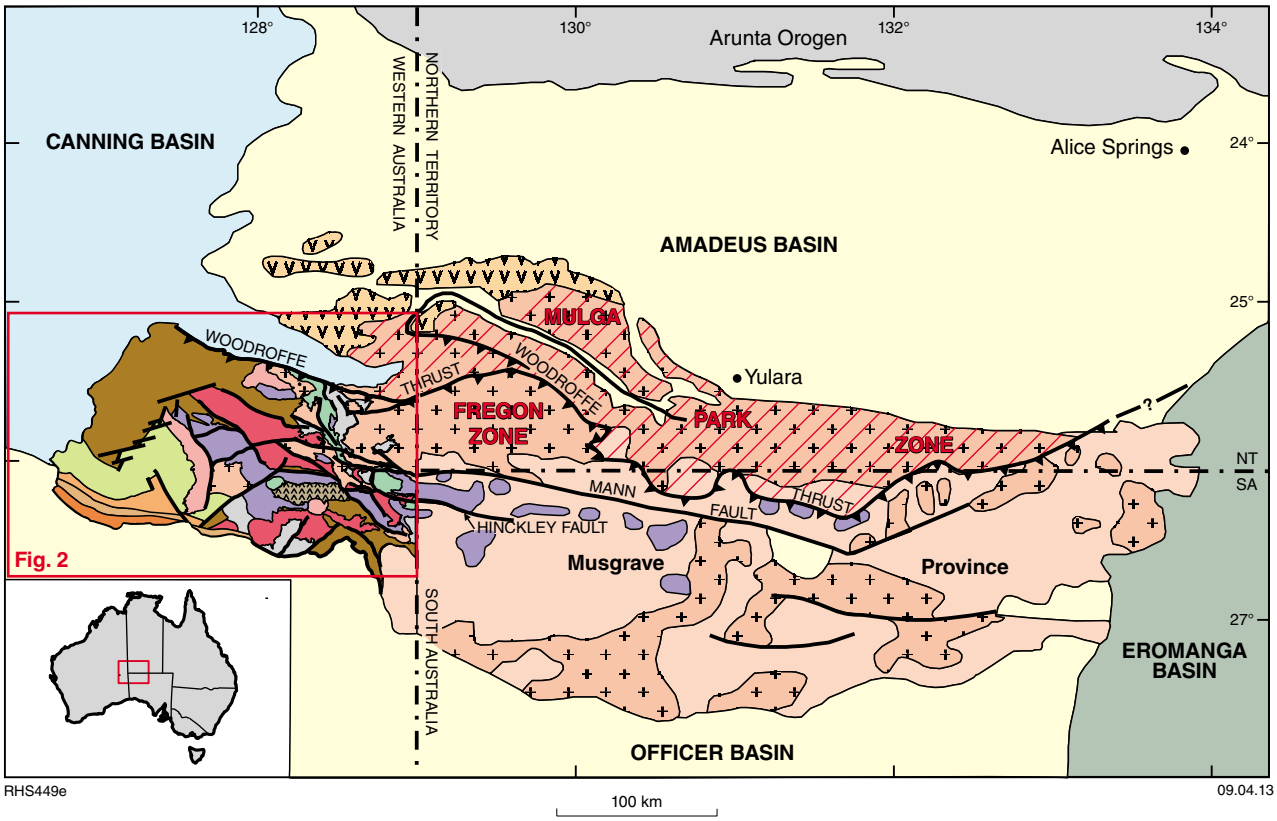

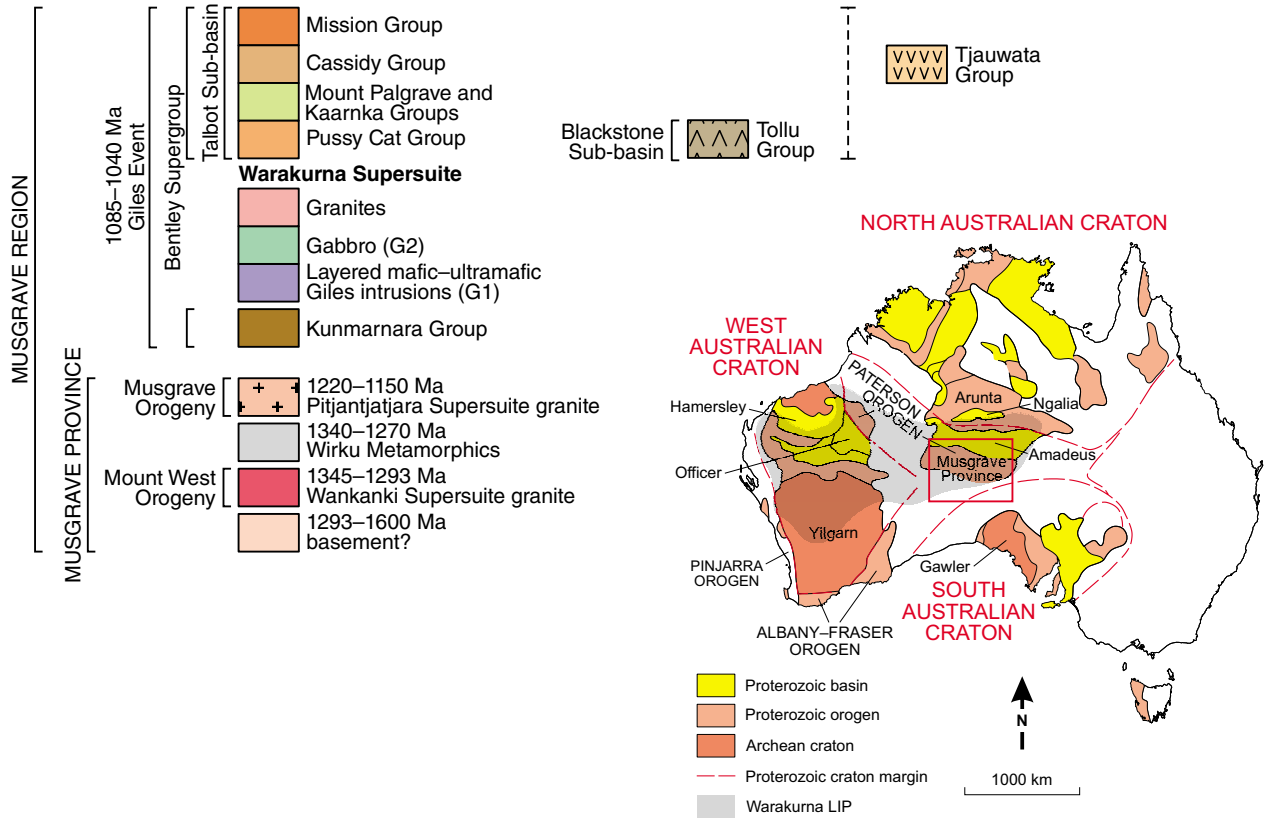

Figure 1. Tectonic map of Australia (modified from Myers et al., 1996) showing the location of the Musgrave Province and a generalized regional geological map of the Musgrave region (modified from Glikson et al., 1996; Edgoose et al., 2004)

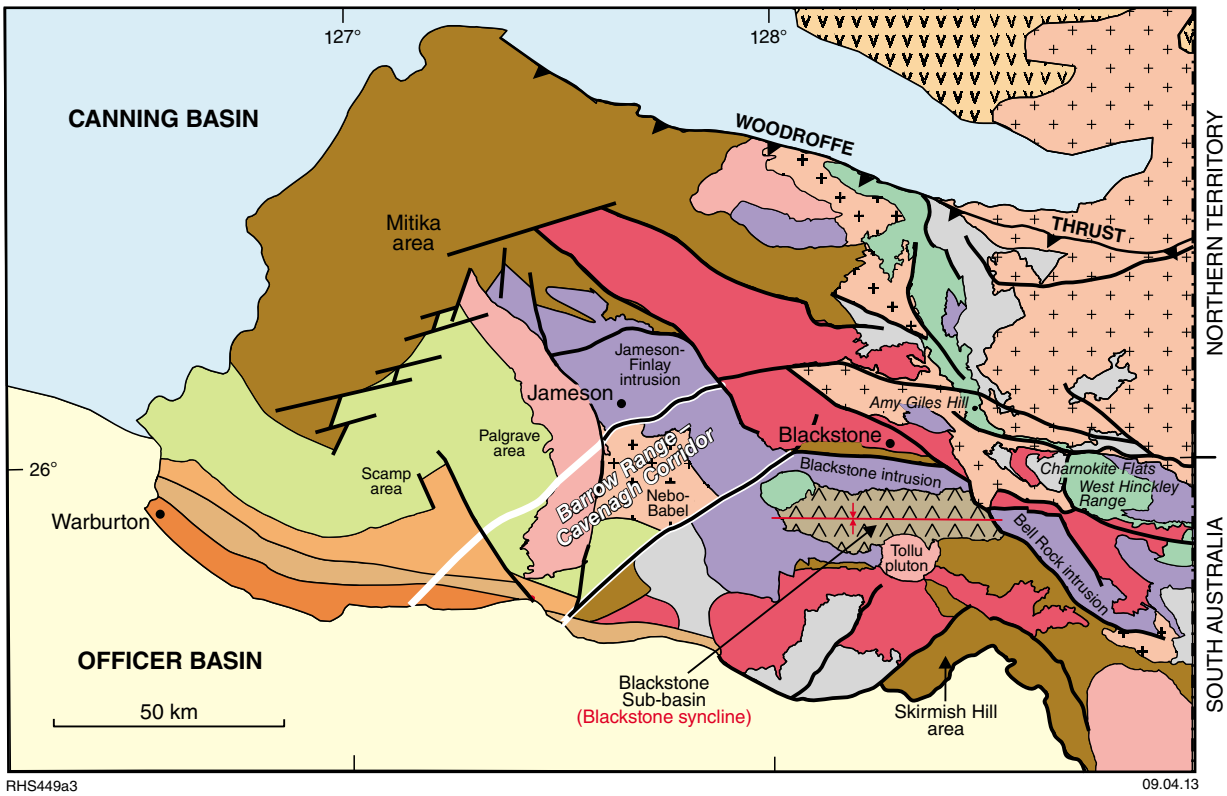

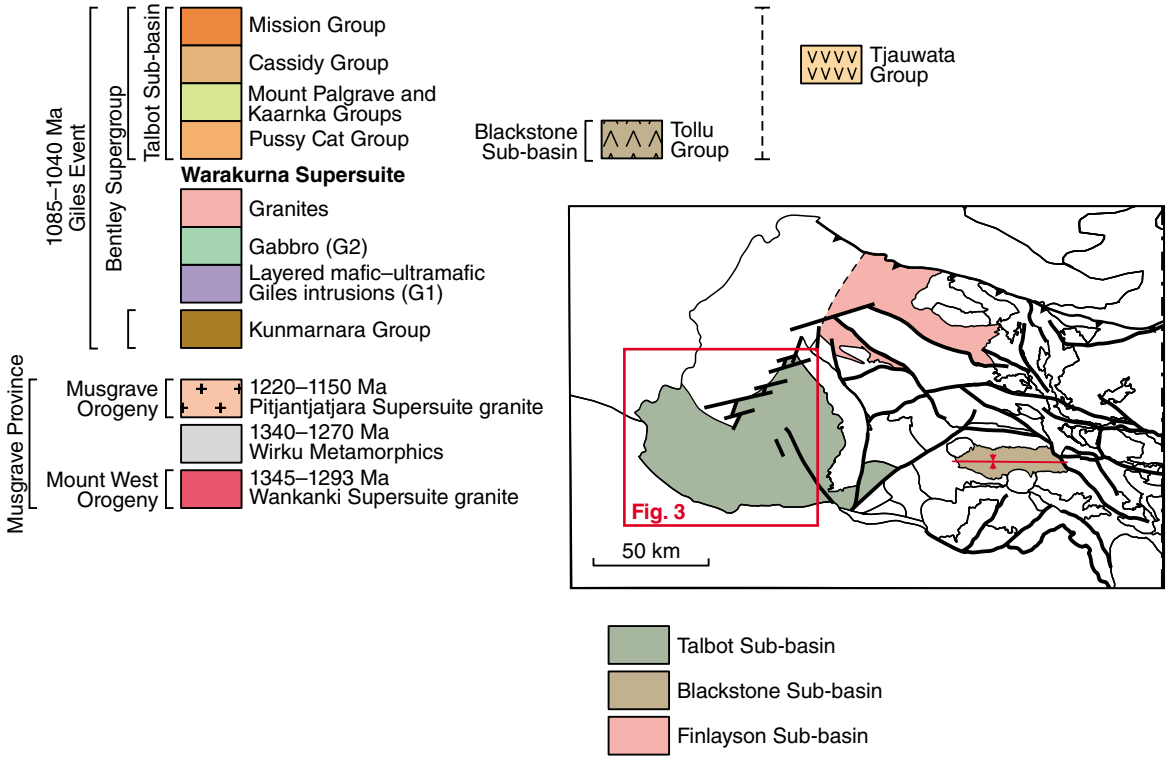

Figure 2. Simplified interpreted bedrock geology of the west Musgrave Province, also showing the preserved extent of the various sub-basins of the Bentley Basin

been attributed to progressive removal (delamination) of the lower crust and lithosphere, previously thickened during the Mount West Orogeny (Smithies et al., 2010, 2011).

The Pitjantjatjara granites were emplaced at temperatures of up to 1000ºC (Smithies et al., 2010, 2011) and intrusion coincided with a newly recognized 70–100 m.y. period of regional ultrahigh-temperature (UHT) metamorphism (e.g. King, 2008; Kelsey et al., 2009; Smithies et al., 2010, 2011), characterized by temperatures in the lower to mid crust of >1000°C along a geothermal gradient ≥35–40°C km^{-1} (e.g. King, 2008; Kelsey et al., 2009). These thermal conditions are consistent with complete removal of the lithospheric mantle during the early Musgrave Orogeny delamination event and the thermal limits on the amount of crust sustainable below the level of intrusion, as well as isotopic constraints, which together imply a significant (>50%) mantle-derived source component to the Pitjantjatjara Supersuite. The duration of this long-lived UHT magmatic event suggest that it was related to intrinsic features of the lithosphere, rather than to a specific thermal anomaly within the asthenosphere. Smithies et al. (2010, 2011) suggested that the lithospheric architecture of the region — locked at the junction of three thick cratonic masses — played a major role in Mesoproterozoic evolution.

Age constraints on the interval between the end of the Musgrave Orogeny and the beginning of the Giles Event (about 35–65 m.y.) provide a minimum range, and data presented later in this Report suggest continuous zircon-forming events throughout this period. There is no suggestion that the prevailing intracontinental tectonic setting during the Giles Event fundamentally differed from that of the Musgrave Orogeny, so it is possible that the two events could justifiably be viewed as a continuum (Smithies et al., 2010). The UHT conditions that characterized the Musgrave Orogeny indicate very thin, dry and refractory crust, perhaps with little or no lithosphere, and this likely approximated the thermal state of the crust at the beginning of the Giles Event.

The 1085–1040 Ma Giles Event, Warakurna Supersuite, and Ngaanyatjarra Rift

Regional tectonic overview

The volcanic rocks of the Bentley Supergroup (Figs 2 and 3) formed during the Mesoproterozoic Giles Event. Mafic magmatic elements of this event are recognized in outcrop as dolerite dykes and sills across approximately 1.5 million square kilometres of central and Western Australia (Fig. 1). This craton-scale mafic magmatism appears to be very restricted in age to c. 1075 Ma, providing a basis for grouping the igneous rocks into a large igneous province — the Warakurna Large Igneous Province (Wingate et al., 2004; Morris and Pirajno, 2005). In the Musgrave region, and in the area around Bloods Range (Tjauwata Group) in the Northern Territory (Fig. 1), extensive intrusion and extrusion of voluminous mafic magmas also occurred at c. 1075 Ma. However, in these regions it was contemporaneous with felsic magmatism, and voluminous mafic and felsic magmatism occurred more or less continuously for at least 10 m.y. before and 35 m.y. after the craton-scale c. 1075 Ma event. Thus, the Warakurna Large Igneous Province should be regarded simply as a component of the Giles Event rather that the expression of it, and the Warakurna Supersuite is the magmatic expression of the entire c. 1085–1040 Ma magmatic history of the Giles Event. In the west Musgrave Province, the Warakurna Supersuite incorporates more than 10 geochemically and chronologically distinct phases of mafic magmatism and 25 phases of felsic magmatism.

The Giles Event has been interpreted as the result of a single mantle plume (Wingate et al., 2004; Morris and Pirajno, 2005; Godel et al., 2011), but the c. 45 m.y. (minimum) duration of mantle-derived igneous activity suggests the event reflects a more complex geodynamic setting.

The magmatic and structural history of the Giles Event in the Musgrave region chronicles the formation and evolution of a long-lived, failed intracontinental rift called the Ngaanyatjarra Rift (Evins et al., 2010). According to Aitken et al. (2012), the Ngaanyatjarra Rift is an excellent example of magmatism-dominated rifting, where magmatic addition to the crust was able to keep pace with, or out pace, crustal thinning. In this respect it shares similarities with other Proterozoic rifts such as the Transvaal Rift in South Africa and the Midcontinent Rift of North America. Although the overall regional structural regime appears to have been primarily extensional, the amount of extension was quite limited and the crust was actually thickened as a result of co-located magmatic additions (Aitken et al., 2012). Active faults were steep and movement primarily normal and, at least in some cases, facilitated accommodation of large upper-crustal magma chambers.

The Bentley Basin represents the extent of the volcanosedimentary fill of the Ngaanyatjarra Rift. These volcanosedimentary rocks (including siliciclastic and minor calcareous sediments) form the Bentley Supergroup, which includes the Tjauwata Group in the Bloods Range area of the Northern Territory (e.g. Edgoose et al., 2004). In the west Musgrave Province, the Bentley Basin can be subdivided into at least two rhyolite-dominated sub-basins (Fig. 2): the Talbot Sub-basin in the area west of the Jameson Community, and the smaller Blackstone Sub-basin in the area south of the Blackstone Community. A third, poorly defined sub-basin, the Finlayson Sub-basin, lies to the north of Blackstone and Jameson Communities. In addition, recent mapping has identified the basal components of the Bentley Supergroup — the Kunmarnara Group — overlying the northern parts of the west Musgrave Province (Mitika area, Fig. 2), possibly linking the Talbot Sub-basin and the Bloods Range area of southern Northern Territory, and the immediately adjacent parts of Western Australia, as a single continuous depositional basin. To the east, components of the Kunmarnara Group are exposed at Skirmish Hill (Fig. 2),

and are interpreted to extend into the westernmost parts of South Australia. Based on these occurrences, the minimum original extent of the Bentley Basin was approximately 50 000 km^2.

Geological history of the Ngaanyatjarra Rift

In the Musgrave region, the earliest preserved lithological manifestation of the Giles Event is a succession of quartz sandstones, pebbly sandstones and conglomerates (MacDougall Formation), basalts (Mummawarrawarra Basalt), and minor amounts of felsic volcanic rocks, forming the Kunmarnara Group (Fig. 2). The equivalent units of the Tjauwata Group include the Karukali Quartzite and the Mount Harris Basalt (Edgoose et al., 2004). These are the basal units of the Bentley Supergroup (Howard, et al., 2011b; Evins et al., 2010) and have been interpreted to represent the basal succession to the Ngaanyatjarra Rift (Evins et al., 2010). There are no direct maximum age constraints on deposition, other than the minimum age constraint on high-grade metamorphism related to the Musgrave Orogeny, at c. 1120 Ma. Minimum depositional age constraints are based on crystallization ages of the oldest igneous rocks to intrude the Kunmarnara Group — c. 1090 Ma in the Bloods Range (Edgoose et al., 2004) and c. 1078 Ma in the west Musgrave Province (Sun et al., 1996; Howard et al., 2011b).

The next recognizable event was emplacement of the layered mafic–ultramafic Giles intrusions (G1). These dominate outcrop in the Musgrave region, forming the elevated west-northwest-trending spine, and have intruded mainly along, or near, the bounding faults separating the various major lithotectonic zones of the Musgrave Province basement (Fig. 2). Troctolite, gabbronorite, and gabbro dominate. Ultramafic units are also present, but are cumulate rocks related to mafic, rather than ultramafic, magmas. The layered bodies reach a maximum cumulative thickness of ~10 km in the Jameson area and the present outcrop extent clearly understates the original size of some of the intrusions. It is very likely that the major troctolitic Bell Rock, Blackstone, and Jameson–Finlay intrusions of the Giles Event are tectonically dislocated parts of a single intrusion. If this is the case, this intrusion might have originally been greater than 170 km long, 25 km wide, and up to 10 km thick, making it one of the largest mafic magma chambers on Earth. Preserved country-rock inclusions and contacts indicate that the Giles intrusions in the west Musgrave region were emplaced at the stratigraphic level of the Mummawarrawarra Basalt (Kunmarnara Group). The low metamorphic grade (greenschist facies) of the basalts indicates an upper crustal extensional environment of intrusion. Constraints on the crystallization age of the Giles intrusions are the minimum depositional age of the Kunmarnara Group and a direct U–Pb zircon age of 1076 ± 4 Ma from a layered Giles intrusion gabbro (GSWA 194762, CL Kirkland, written communication, 2013).

Primarily in the eastern part of the west Musgrave region (Fig. 2), massive gabbro (G2) cuts the layered Giles intrusions and typically shows abundant and widespread evidence of co-mingling with leucogranitic magmas. The leucogranite intrudes as dykes and also forms larger pluton-scale bodies in basement rocks (e.g. South Hill, Tollu pluton; Fig. 2). The leucogranite typically includes clinopyroxene-, hornblende-, and biotite-bearing equigranular to porphyritic quartz syenites, syenogranites, and lesser monzogranites, and locally shows well-developed rapakivi textures. This bimodal magmatism was accompanied by deformation (shearing and west-northwest folding adjacent to major shear zones), with age constraints on magmatism and deformation lying between 1078 ± 3 and 1074 ± 3 Ma (Howard et al., 2011b). These age constraints are virtually identical to those for the layered Giles (G1) intrusions but, where temporal field relationships can be established, G2 intrusions always post-date G1 intrusions.

South of Blackstone community, in the Blackstone Sub-basin (Fig. 2), rhyolites of the Smoke Hill Volcanics (Tollu Group) directly overlie the layered G1 Blackstone intrusion without an obvious intervening fault. Crystallization or depositional ages for the rhyolites of 1071 ± 8 Ma (GSWA 191728, Coleman, 2009), 1073 ± 7 Ma (GSWA 191706, Coleman, 2009), and 1073 ± 8 Ma (GSWA 189561, CL Kirkland, 2013, written comm., 1 February) are within analytical error of the emplacement age range of the G1 and G2 intrusions, and rhyolite compositions strongly resemble those of leucogranites associated with G2 intrusions. These ages require extensive and rapid uplift, erosion, and exhumation of the layered Giles G1 intrusions, immediately followed by felsic volcanism.

To the north of the Jameson–Blackstone components of the Jameson–Blackstone – Bell Rock G1 intrusion, remnants of Kunmarnara Group are preserved (Fig. 2), unconformably overlying high-grade basement rocks of the Wirku Metamorphics and the Wankanki and Pitjantjatjara Supersuites. These remnants of the Kunmarnara Group form the poorly defined Finlayson Sub-basin of the Bentley Basin. Immediately northeast of the Jameson G1 intrusion, andesite and dacite overlie Mummawarrawarra Basalt. Reconstructions indicate a northeast-up sense of movement along the northern margins of the Jameson–Blackstone – Bell Rock G1 intrusion (Evins et al., 2010), so this andesite and dacite volcanism represents a lower stratigraphic level than the emplacement level of the G1 intrusions, pre-dates the Smoke Hill Volcanics in the Blackstone Sub-basin, and is likely a component of the Kunmarnara Group itself.

Evidence from U–Pb zircon age dating (presented later) suggests that felsic volcanism in the Talbot Sub-basin may have commenced before emplacement of the layered Giles intrusions, possibly before c. 1080 Ma. However, the stratigraphically lower volcanosedimentary rocks were also intruded by the synvolcanic (and subvolcanic) Winburn granite[4] (Fig. 3) and the preserved stratigraphic base is now younger rhyolites deposited at c. 1070 Ma.

[4] 'Winburn granite' is an informal name.

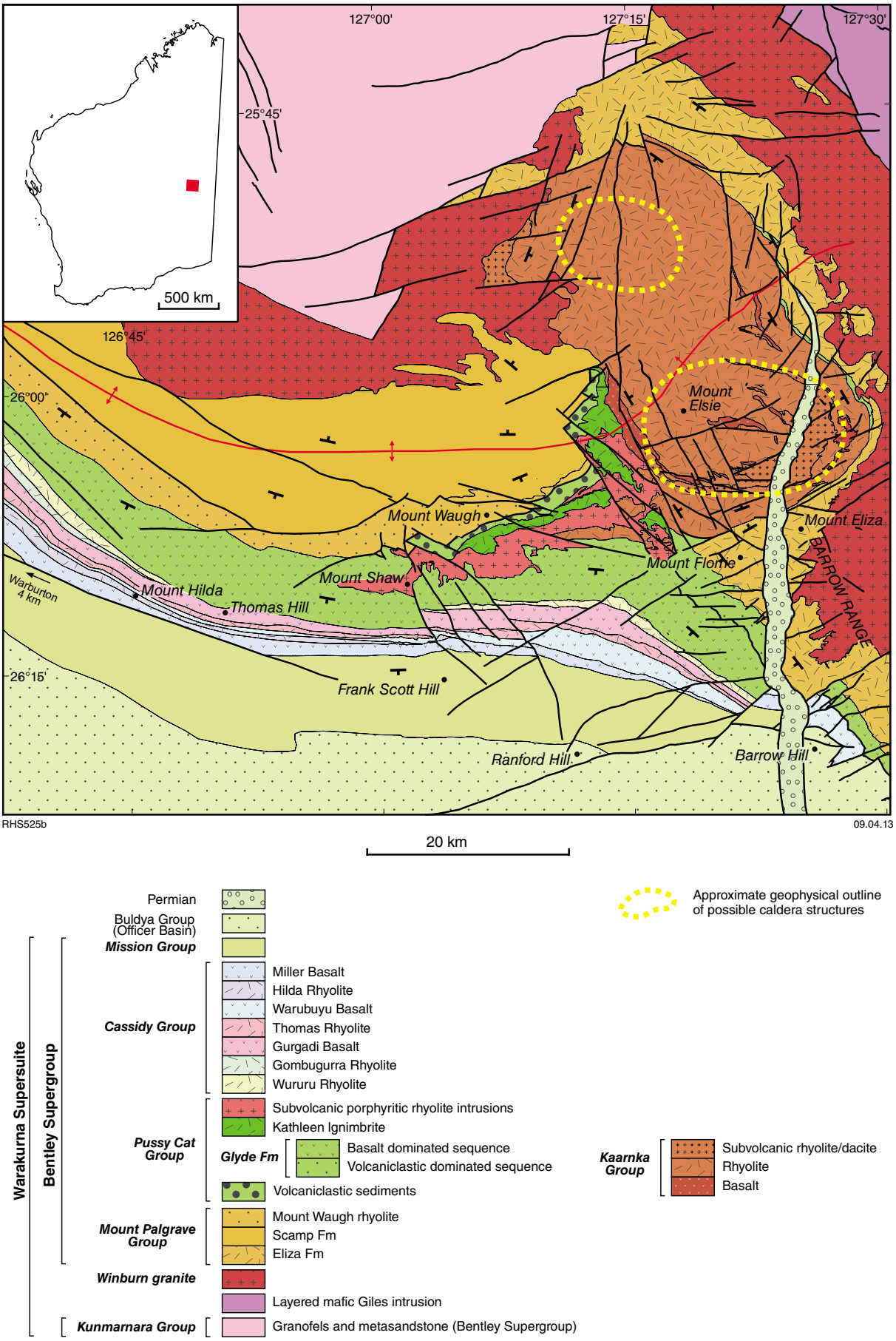

Figure 3. Detailed interpreted bedrock geology of the Talbot Sub-basin

The Talbot Sub-basin possibly represents a silicic large igneous province in its own right, and it contains the Kaarnka caldera, or caldera cluster (Fig. 3), related to the development of one or more super-volcanoes. The layered G1 Jameson intrusion is now in faulted contact with both the volcanosedimentary rocks of the Talbot Sub-basin and the Winburn granite.

A series of dolerite dykes in Western Australia are contemporaneous with and compositionally similar to the Alcurra Dolerite in the Northern Territory; these have collectively been assigned to the Warakurna Large Igneous Province (Wingate et al., 2004). In the northern part of the west Musgrave Province, these dykes have a distinctive ophitic texture with pyroxene oikocrysts up to several centimetres in diameter, and are commonly oriented east-southeast. In the Jameson area, they form northeast-trending plagioclase-phyric dykes, and to the north of Warburton they again trend to the east-southeast. In the Blackstone Sub-basin, iron-rich olivine gabbros, olivine norites, ferronorites, and ferrodiorites, compositionally equivalent to the Alcurra Dolerite (Howard et al. (2009), have intruded the Smoke Hill Volcanics. They also intrude along the margins of layered Giles intrusions, and locally host significant orthomagmatic nickel–copper mineralization at Nebo–Babel (Seat, 2008; Fig. 2). The gabbros have been dated at 1068 ± 4 Ma (Nebo–Babel; Seat, 2008) and 1067 ± 8 Ma (GSWA 194354; Kirkland et al., 2009). In the Blackstone Sub-basin (Fig. 2), the primitive (andesitic) end members of the Hogarth Formation, which overlie the Smoke Hill Volcanics, are also compositionally identical to the Alcurra Dolerite and the ferrogabbros and have the same crystallization age of 1068 ± 7 Ma (GSWA 185518; Kirkland et al., 2013b). These are the youngest rocks preserved in the Blackstone Sub-basin.

Rare and volumetrically minor mafic dykes with well-developed alkalic, oceanic island basaltic (OIB) compositions, have been identified in drillcore at the Nebo–Babel Ni–Cu deposit (Godel et al., 2011), to the east of the Talbot Sub-basin (in the Barrow Range – Cavenagh Corridor; Fig. 2), and also in outcrop, intruding the Tollu Pluton to the south of the Blackstone Sub-basin (Howard et al., 2011b). Godel et al. (2011) described these dykes as the youngest observed mafic dyke generation of the Giles Event. However, the minimum age of these rocks is not constrained, and links with the Giles Event are questionable.

Basalt compositionally similar to the Alcurra Dolerite is interleaved with rhyolite throughout the lower and middle stratigraphic regions of the Talbot Sub-basin (Fig. 3). It is mainly in the region of this sub-basin that the younger stratigraphic history of the Bentley Basin and of the Ngaanyatjarra Rift is preserved. The stratigraphy of the Talbot Sub-basin was revised by Howard et al. (2011b) as a result of recent detailed mapping; the following geological and lithological descriptions are largely a result of that work.

Talbot Sub-basin

The region to the west of Jameson Community contains the largest exposure of rocks of the Bentley Supergroup. These are within the Talbot Sub-basin (Figs 2 and 3) and show evidence of local weak, open, upright folding about east-southeast-trending axes, with an associated strong axial-planar fracture cleavage developed locally. Deformation is also locally intense close to faults and shears; elsewhere, rocks of the Talbot Sub-basin are typically undeformed. Adjacent to the Winburn granite, metamorphic grade was high enough to coarsen rhyolites into a fine- to medium-grained granofelsic texture, and in the Scamp area (Figs 2 and 3), burial of the lower stratigraphic levels has resulted in lower-amphibolite facies metamorphism. Elsewhere, the rocks are typically preserved at greenschist facies.

Within the area of the Talbot Sub-basin, Daniels (1974) proposed two geographically restricted ‘associations’ of volcanic rocks — the Palgrave Volcanic Association in the east and the Scamp Volcanic Association in the north — and related these to two separate calderas (Fig. 3). Our current stratigraphic interpretation does not recognize the Scamp caldera and requires modification of the extent of the postulated caldera in the Palgrave region. Rocks of the Palgrave Volcanic Association are now divided between two rhyolite-dominated groups (Fig. 3): the effusive and ignimbritic rocks of the Mount Palgrave Group, representing the preserved stratigraphic base of the Talbot Sub-basin, and the overlying dominantly ignimbritic rocks of the Kaarnka Group. Outcrop of the Kaarnka Group is almost entirely restricted to a discrete north-northwest-trending oval-shaped basin, up to 27 km wide and 46 km long (Fig. 3). This basin is interpreted here to define the extent of the Kaarnka caldera structure, although it corresponds only partly to the caldera structure suggested by Daniels (1974). Furthermore, it is likely that the main Kaarnka caldera structure itself comprises at least three separate calderas, forming the Kaarnka caldera cluster.

Rocks of the Scamp Volcanic Association are all assigned to the Mount Palgrave Group, correlating units from both of the former associations into a single group with a preserved outcrop strike length of more than 200 km (Fig. 3). Depositional layering within the Mount Palgrave Group generally dips shallowly (≤30º) between south (in the northern part of the sub-basin) and west (in the eastern part of the sub-basin), but is locally steep (up to 85º) adjacent to the Barrow Range anticline and adjacent to the Winburn granite. Nowhere is the stratigraphy overturned. The thickest preserved section of the Mount Palgrave Group is probably in the northeastern Talbot Sub-basin, where up to 4500 m of volcanic sequence is preserved (Table 1).

In the southwestern Talbot Sub-basin, rocks of the Pussy Cat Group directly overlie the Mount Palgrave and Kaarnka Groups and are in turn overlain by rocks of the Cassidy Group. Both the Pussy Cat and Kaarnka Groups

Table 1. Estimated stratigraphic thicknesses of units within the Talbot Sub-basin

Group	*Formation*	*Approximate maximum thickness (km)*			
		Rhyolite	*Basalt*	*Clastic rocks*	*Total*
Mount Palgrave		3.5	0.1	0.9	>4.5
Pussy Cat		0.9	2.1	0.5	3.5
Kaarnka		2.8	0.2	0.2	3.2
Cassidy	Wururu Rhyolite	0.81			0.81
	Gombugurra Rhyolite	0.11			0.11
	Gurgadi Basalt		0.5	0.1	0.6
	Thomas Rhyolite	0.36			0.36
	Warubuyu Basalt		0.2	0.1	0.3
	Hilda Rhyolite	0.54		0.05	0.59
	Miller Basalt		0.5	0.22	0.72
Mission			0.1	3.9	4.0

comprise bimodal volcanic rocks and less common sedimentary units with shallow dips (≤30º) to the south and southwest, and form continuous packages that can be traced for over 100 km. The Cassidy Group, in particular, comprises four major mafic–felsic volcanic cycles (Fig. 3) with a combined thickness of more than 3400 m (Table 1).

Both the size (extent and volume) and facies association of volcanic rocks within the Mount Palgrave, Kaarnka, and Cassidy Groups (i.e. the lower Talbot Sub-basin rocks) are unusual. Many of the felsic volcanic units of these stratigraphic groups have volumes that reflect super-volcano eruptions (≥450 km^3; e.g. Sparks et al., 2005). Magma compositions (see Geochemistry) are water-poor, but rich in F, alkalis, and FeO, reflecting very high eruptive temperatures (>900°C), as confirmed here by Zr-saturation thermometry (see Geochemistry – Talbot Sub-basin). These high eruption temperatures are evident in outcrop from well-developed and continuous flow banding (in highly felsic rocks), including extensive evidence of rheomorphism (Fig. 4), and high-temperature contact metamorphic assemblages in interflow sedimentary units. In terms of eruptive temperature, magma compositions, and volcanic textures, Miocene volcanic rocks in the central Snake River Plain area of northwestern America provide a close analogue for the lower Talbot Sub-basin volcanic rocks. The former have been assigned a rare and specific category of large-scale volcanism termed Snake River (SR)-type volcanism (Branney et al., 2008). The following facies characteristics of SR-type volcanism, as outlined by Branney et al. (2008), are relevant to the volcanic rocks of the lower Talbot Sub-basin:

- large-volume, lithic-poor rhyolitic ignimbrites with scarce pumice lapilli
- extensive, parallel-laminated, medium- to coarse-grained ashfall deposits

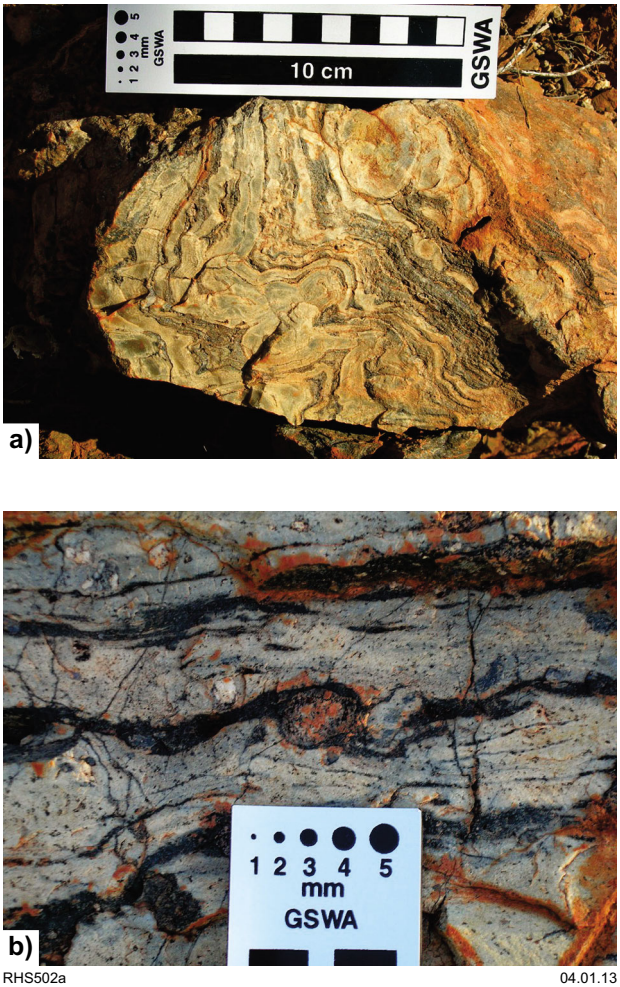

Figure 4. Outcrop photographs of rhyolites of the Talbot Sub-basin: a) flow banding; b) eutaxitic rheomorphic flow banding

- unusually extensive, large-volume rhyolite lavas
- unusually intense welding, rheomorphism, and widespread development of lava-like facies in ignimbrites
- a bimodal association between rhyolite and numerous coalescing, low-profile basalt lava shields
- evidence of emplacement in lacustrine–alluvial environments.

The Mission Group conformably overlies the Cassidy Group and represents the youngest preserved stratigraphic interval of the Bentley Supergroup. It can be subdivided into a sedimentary lower part (Gamminah Conglomerate, Frank Scott Formation, and Lilian Formation), and an upper basalt-dominated part (Milesia Formation). No evidence of felsic volcanism has yet been found. The Mission Group is conformably to unconformably overlain by the Townsend Quartzite. Daniels (1974) reported a total thickness for the Mission Group of about 4000 m.

The thickest preserved continuous stratigraphic column of the Bentley Supergroup within the Talbot Sub-basin is about 12 km (taken in a north–south direction in the region of Mount Waugh). However, the combined maximum stratigraphic thickness of individual units is estimated to be about 18.6 km (Table 1), although this is never reached in any given region. Of this 18.6 km, basaltic magmas represent about 3.7 km, and felsic magmas about 9 km, giving a total preserved maximum thickness of igneous stratigraphy of approximately 12.7 km.

Along the exposed eastern and northern margins of the Talbot Sub-basin, various phases of the Winburn granite either intrude or are overlain by generally west- to south-dipping rhyolitic lavas, subvolcanic intrusive rocks, and pyroclastic rocks of the Mount Palgrave Group (Fig. 3). Thus, the Winburn granite forms a regionally extensive composite subvolcanic sheet close to the base of the Talbot Sub-basin. The exposed contact relationships between the granite and volcanic rocks indicate active uplift and erosion.

The Winburn granite comprises rocks that range from fine- to medium-grained, from equigranular to porphyritic (and rapakivi-textured), and from syenogranitic to alkali-feldspar granite and quartz–alkali-feldspar syenite. Mafic minerals include variable proportions of green-brown clinopyroxene, blue-green amphibole, and (late) green biotite. Many of the granites contain <35% phenocrysts, these being rounded and strongly embayed quartz, and subhedral complexly rimmed (e.g. complex rapakivi texture of plagioclase rimmed by K-feldspar rimmed by plagioclase Fig. 5) and commonly embayed feldspar (Fig. 5). The phenocrysts are separated by a distinctive granophyric groundmass (Fig. 5). Several samples of Winburn granite also show fracture-controlled late-magmatic fluorite alteration, commonly associated with crystallization of garnet (Fig. 5). The apparently vein-controlled association of fluorite and garnet is also apparent within rhyolite of the Mount Palgrave Group. Along the northern margin of the Talbot Sub-basin, the Winburn granite also includes miarolitic tourmaline-bearing granites. The evolution of some magmatic units of the Winburn granite is almost certainly genetically linked to the volcanogenic evolution of the Talbot Sub-basin, and geochemically distinct phases of the granite can be matched with geochemically distinct volcanic rocks (see Geochemistry).

At most localities, the Winburn granite and the older volcanic rocks of the Mount Palgrave and Kaarnka Groups are heavily intruded by dolerite dykes, in places swamping and isolating the country rock as rafts. Most of the dolerite can be related geochemically to the Alcurra Dolerite. Along the northern margin of the Talbot Sub-basin, the dolerite dykes trend east-southeast and together comprise up to 25% (by volume) of the sequence. Similar estimated relative volumes apply to several areas within the Kaarnka caldera structure and within the adjacent Mount Palgrave Group to the east.

In the area around Barrow Range there is a large west-trending (west-closing) anticline (Barrow Range anticline; Fig. 3), with volcanic units of the Mount Palgrave Group younging away from a core of the Winburn granite. An intense west-trending (080º–110º) fracture cleavage is locally developed throughout this region. Although there is likely a tectonic component to the development of the Barrow Range anticline, it is also possible that synmagmatic doming of the Winburn granite played a major role in its formation. About 6 km north of Mount Florrie, porphyritic microgranite with a crystallization age of 1055 ± 10 Ma (GSWA 187054, Kirkland et al., 2013c) has intruded along a west-trending fracture, and possibly provides a minimum age for development of the fracture cleavage related to the anticline. Because the preserved stratigraphic base of the Mount Palgrave Group was deposited at c. 1070 Ma, doming or folding was potentially synvolcanic, or immediately post-volcanic. This is consistent with the observation that the volcanic rocks in the Mount Florrie region appear to contain a higher proportion of stratigraphically constrained tectonic breccia (rather than autoclastic breccia) than is typical elsewhere in the Mount Palgrave Group, and may have been deposited on the flanks of an active volcanic dome.

The steeply dipping northeast-trending limb of the Barrow Range anticline lies along the northeastern margin of a ~30 km wide northwest-trending fault zone, referred to here as the Barrow Range – Cavenagh Corridor (Fig. 2). Thus, development of the anticline can also be attributed to dextral and south-side-up movement along the northwestern margin of this structural corridor. The timing of faulting has not been established. Although units in the middle to upper Bentley Supergroup (Glyde Formation and above) in the southwestern extension of the Barrow Range – Cavenagh Corridor may also have been displaced, they do not appear to have been affected to the same extent as the rocks in the Barrow Range anticline. On this basis, we suggest that at least a component of deformation within the structural corridor occurred before deposition of the upper part of the Bentley Supergroup.

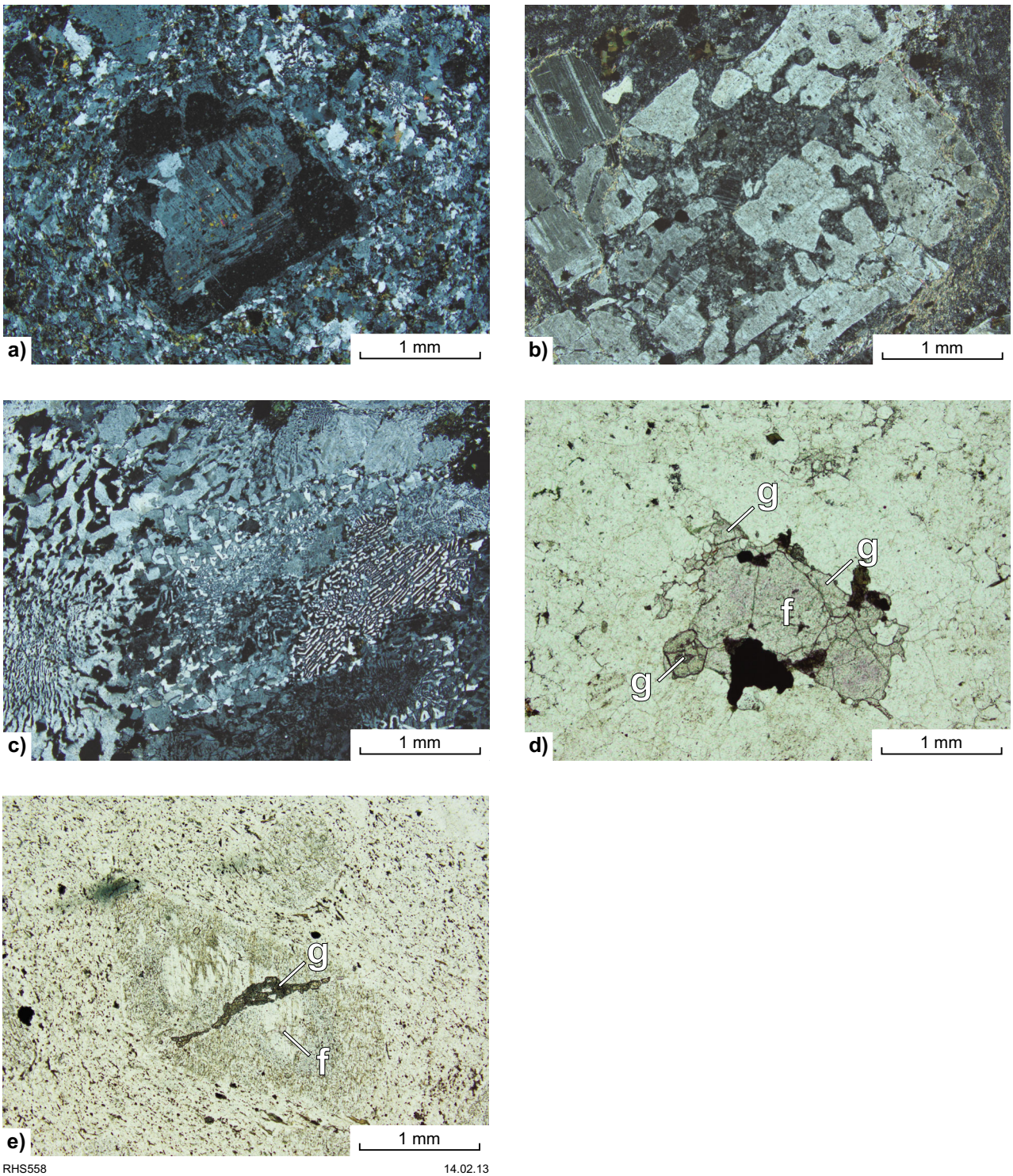

Figure 5. **Photomicrographs of rocks of the Winburn granite: a) multiply zoned and rapakivi-textured feldspar (crossed polars); b) strongly embayed and resorbed feldspar (crossed polars); c) granophyric textures (crossed polars); d) and e) common association, typically along fractures, of garnet (g) and fluorite (f) (plane-polarized light)**

Mount Palgrave Group

The Mount Palgrave Group has been subdivided into a number of depositional packages (Howard et al., 2011b). The lowermost preserved units overlying the Winburn granite form the Eliza Formation and are best exposed in the Mount Eliza – Barrow Range region (Fig. 3). These consist of aphyric to sparsely feldspar-phyric, highly vitric rhyolites and locally include voluminous and laterally continuous massive perlitic and spherulitic units (Fig. 6). Flow banding is locally well-developed and highly continuous (Fig. 6). For most of these units, there is no clear evidence of pyroclastic deposition, so these might represent lava flows. However, an unusual characteristic of SR-type volcanism is the widespread development of ignimbrites with lava-like features, and the absence of vitroclastic or eutaxitic textures (Branney et al., 2008). These lava-like facies can dominate entire ignimbrite sheets and are indistinguishable from true lavas except in cases where critical field relationships are well exposed. One of the most diagnostic features of SR-type rheomorphic lava-like ignimbrites is a lack of widespread basal autobreccias (Branney et al., 2008). Such basal autobreccias are rare in the Eliza Formation. It is possible that many units within this formation are indeed rheomorphic lava-like ignimbrites.

The upper Eliza Formation also includes localized clast-rich, non-welded ignimbrite deposits, diamictitic deposits possibly representing pyroclastic lag breccias, and autoclastic breccias. Basalt and basaltic andesite lavas, and siliciclastic conglomerates, sandstones, and mudstones rich in volcanogenic detritus form very minor intercalations throughout the formation. Near intrusive contacts with the Winburn granite, the basal rhyolite units commonly have a slightly coarser crystalline appearance due to the thermal overprint and spherulitic units in particular take on a fragmental or brecciated appearance through a combination of compaction and differential recrystallization of spherulites and inter-spherulitic domains.

Rocks of the Mount Palgrave Group in the Scamp region in the northern Talbot Sub-basin are of higher metamorphic grade than those in the Mount Eliza – Barrow Range region, typically exhibiting a granofelsic texture. These rocks were described by Daniels (1974) as ‘felsite’ to distinguish them from rhyolite with a microcrystalline groundmass. Daniels (1974) also inferred the existence of northern and southern boundary faults to the Scamp region, and interpreted the area as a volcanic caldera. Our geological interpretation of the region does not recognize this caldera structure. Indeed, where

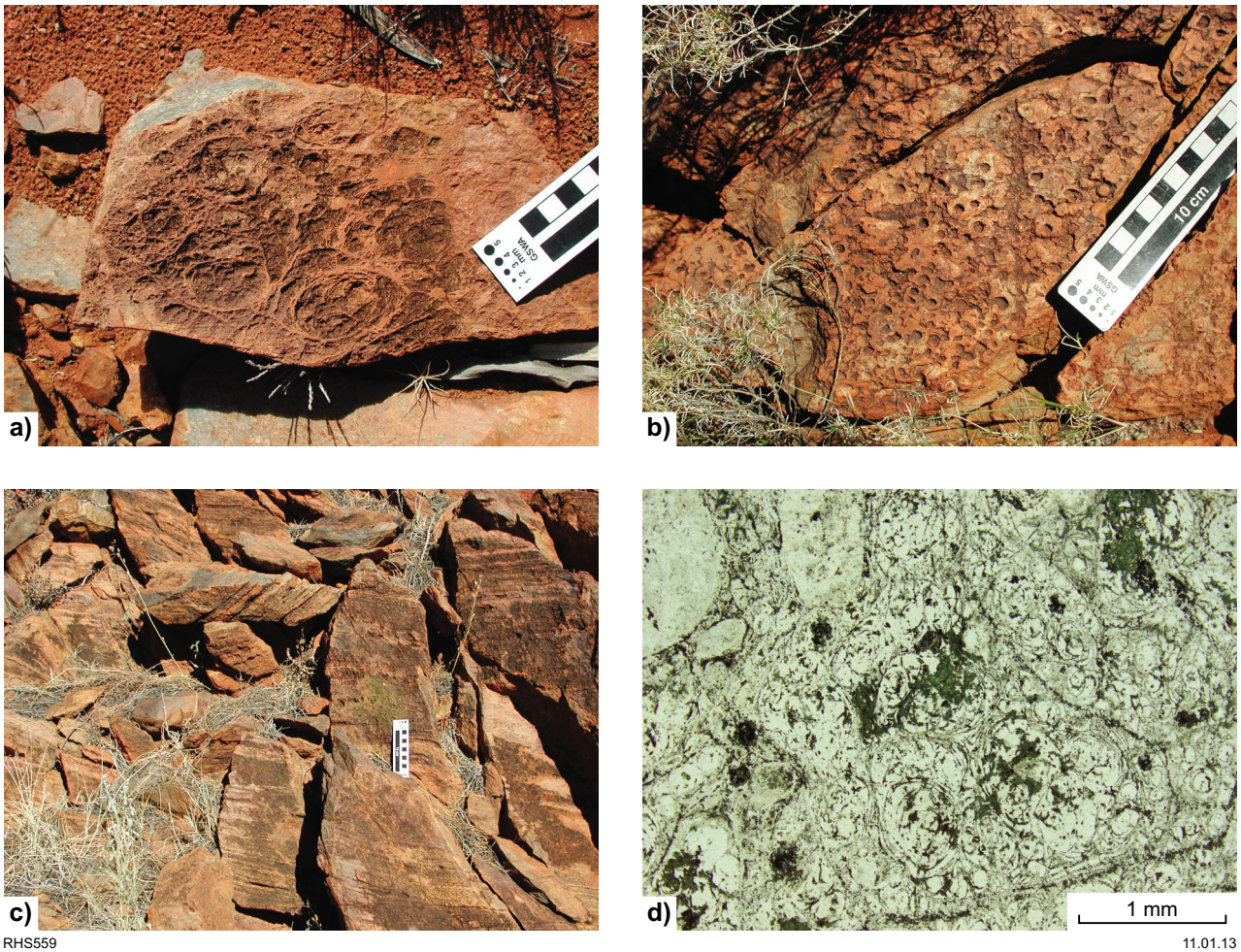

Figure 6. Outcrop photographs of rocks of the Mount Palgrave Group: a) well-developed perlite; b) spherulites; c) flow banding; d) photomicrograph showing well-developed perlite (plane-polarized light)

the granofelsic texture is less pronounced, these rocks show the same lithological range as those of the Eliza Formation, and relict flow banding and spherulites are observed in a number of places. There are, however, very slight compositional differences, and outcrop relationships in the northern Talbot Sub-basin (Scamp region) suggest that the Scamp Formation probably overlies the Eliza Formation there. One notable feature of many rhyolites (including the felsites) of the Scamp Formation is that they are garnet-bearing. The garnets vary in colour from pale pink to pale yellow. They are also highly variable in shape, ranging from idioblastic hexagonal crystals to roundish xenoblastic inclusion-rich poikiloblasts. In these rocks, garnet is commonly directly associated with fluorite and, in many cases, this association appears to be controlled by fractures (Fig. 6). It is possible that the formation of garnet in these rocks was related to late magmatic redistribution of primary fluorite-rich volatiles along late-stage fractures, resulting in localized peraluminous alteration, including precipitation of garnet. Under fluorite-rich conditions it is likely that the pressures and temperatures required for metamorphic formation of garnet were significantly reduced (Manning and Bird, 1990; Chakhmouradian et al., 2008), so garnet in these rocks might simply reflect rapid deposition of a thick pile of overlying Mount Palgrave Group rhyolites.

Outcrops of both the Eliza and Scamp Formations extend in a westerly direction for about 75 km to the area north of Warburton (Fig. 3). In the Scamp region, the southern extent of the Scamp Formation is marked by a faulted contact with rocks of the Mount Waugh rhyolite[5]. North of Warburton this faulted contact is poorly defined, and a 350-m-thick regionally continuous sequence of basalt flows separates the Scamp Formation from the Mount Waugh rhyolite.

In the western and northern Talbot Sub-basin, the Mount Waugh rhyolite forms the uppermost formation of the Mount Palgrave Group and is composed of flow-banded, poorly sorted, sparsely quartz- and feldspar-phyric rhyolite (Fig. 7). In the region north of Warburton, units with well-developed and continuous flow banding are interleaved with layers with possible fiamme and eutaxitic flow structures (Fig. 7). As for the underlying Eliza Formation, units with well-developed flow banding may represent either lavas or lava-like rheomorphic ignimbrites. The regional continuity of the Mount Waugh rhyolite and the presence of interleaved layers with features more characteristic of ignimbrites supports the view that the Mount Waugh rhyolite represents an ignimbrite, or rheomorphic ignimbrite, rather than a lava flow.

In its eastern outcrops, the Mount Waugh rhyolite includes areas in which the original rhyolite has been altered to form a schistose quartz- and muscovite-rich assemblage that locally contains stringers and pods of nodular, granoblastic kyanite and andalusite. Daniels (1974) interpreted these metamorphosed alteration zones as representative of former fumarolic activity. Their present expression is as mylonitic schists, which suggests fumarolic activity related to (or close to) major synvolcanic faulting, possibly related to caldera subsidence. Voluminous rheomorphic ignimbrite forms the Kathleen Ignimbrite that overlies the Mount Waugh rhyolite and likely reflects a caldera-forming event. Thus, the kyanite-bearing assemblage possibly records deformation related to caldera formation, development of caldera-fault related fumarolic assemblages, and rapid burial of the fumarolic assemblages during the continued accumulation of volcanic rocks of the Bentley Supergroup, reaching a pressure of at least 3.5 kbar. This pressure estimate corresponds well with an estimated thickness of about 9 km of volcanic rocks deposited over the Mount Waugh rhyolite.

The Mount Waugh rhyolite is fringed to the south by outcrops of dark-coloured micaceous mudstones, sandstones, conglomerates, and diamictites. Similarly, to the east and southeast, where the Mount Waugh rhyolite is not preserved, the Eliza Formation is overlain by a coarse diamictite, locally in deep erosive scours in the rhyolites. Angular to rounded clasts in this unit are of local derivation, predominantly or entirely from the Mount Palgrave Group. They show cuspate margins or deep irregular embayments against the dark fine-grained groundmass and commonly have wide reaction rims. Such features suggest hot deposition or interaction between mutually ductile components, suggesting that the diamictites are in fact pyroclastic breccias. This unit is particularly well-developed in the eastern Talbot Sub-basin, perhaps explaining why the Mount Waugh rhyolite is absent from that region. The diamictite unit is overlain by or, more likely, forms the base of the Kaarnka Group in the northeast of the sub-basin; elsewhere this relationship is with the Pussy Cat Group.

The observation that both the Kaarnka and Pussy Cat Groups directly overlie the Mount Palgrave Group, with their lower stratigraphic levels characterized by a similar mix of mudstone, sandstone, conglomerate, and diamictite/pyroclastic breccias layers, suggests that the basal parts of these groups share a similar stratigraphic position within the Talbot Sub-basin and may indeed be correlated. Geochemical similarities between the rhyolitic units (e.g. Kathleen Ignimbrite and quartz-porphyritic rhyolite) that overlie the diamictite/pyroclastic breccia in both groups provide further evidence for such a correlation and are discussed later (see Petrogenesis).

Kaarnka Group

The Kaarnka Group (Werner et al., 2012) outcrops within a discrete north-northwest-trending, roughly oval-shaped basin interpreted to define the extent of the Kaarnka caldera. In detail, this structure possibly represents at least three independent calderas (Fig. 3). At several localities, the ring structures that contribute to definition of caldera structures are expressed in outcrop by subvolcanic porphyritic rhyolite intrusions. Most major sequences and lithological packages can be traced throughout the basin (the main caldera structure), except for a sequence of interlayered fine- to medium-grained siliciclastic rocks and volcaniclastic rhyolitic lapilli tuffs that form the uppermost unit in the southern lobe of the basin — the southern caldera. However, some individual layers are very discontinuous, and the orientation of primary planar

[5] 'Mount Waugh rhyolite' is an informal name.

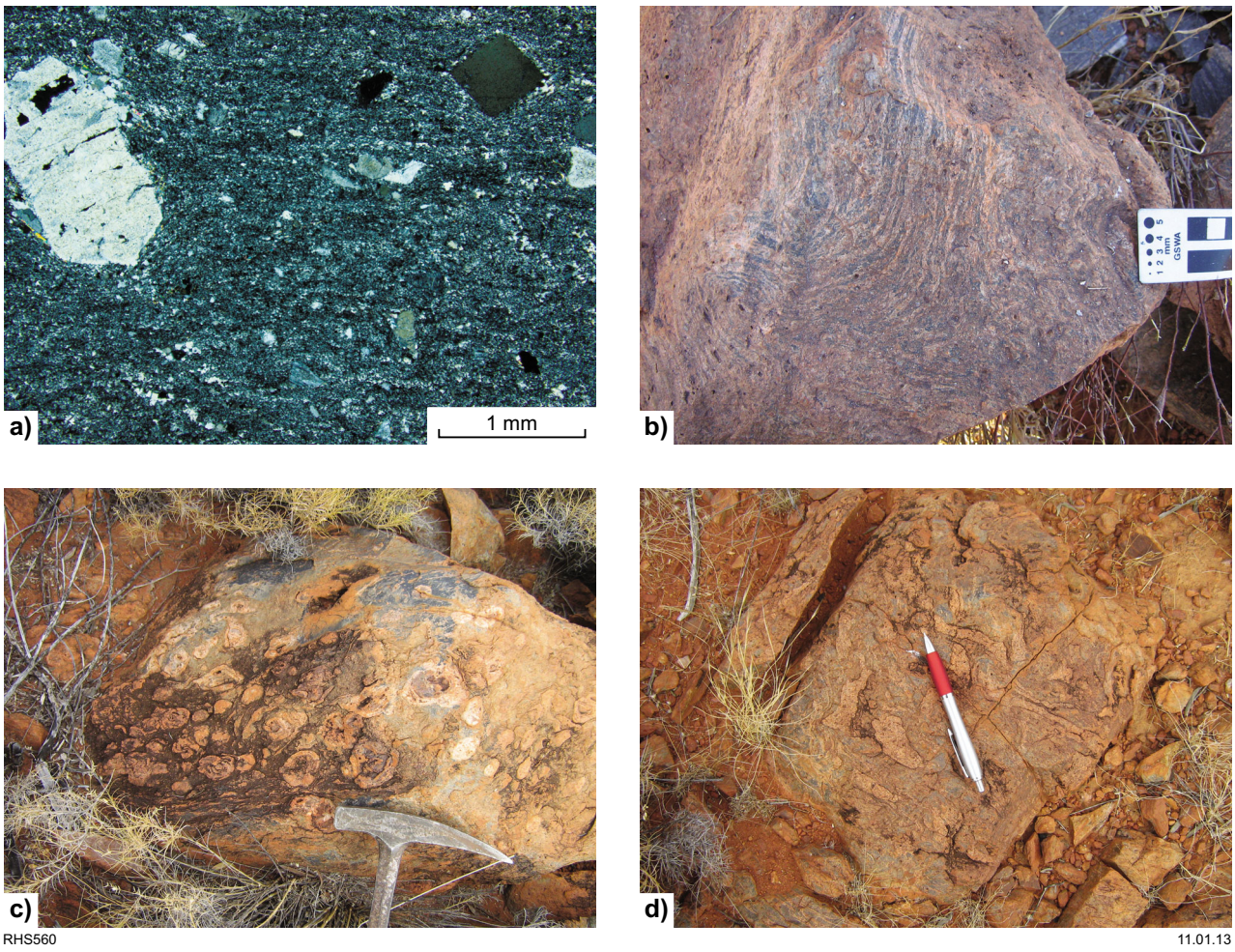

FIgure 7. Photomicrograph and outcrop photographs of rocks of the Mount Waugh rhyolite (Mount Palgrave Group): a) showing very poor sorting of some of the rocks (crossed polars); b) well-developed flow banding; c) horizons containing well-developed spherulites; and d) spherulites locally highly contorted and flattened into the plane of flow banding

structures (e.g. flow banding) varies greatly over short distances. Such chaotic architecture is not a notable feature of the volcanic sequences of either the underlying Mount Palgrave Group or the overlying Cassidy Group, and reflects extensive block rotation related to violent proximal volcanic eruptions and caldera formation. The combined stratigraphic thickness of the Kaarnka Group is estimated to be about 3.2 km.

The Kaarnka Group is characterized by massive to flow-banded feldspar- or quartz-phyric rhyolite with intercalations of crystal-rich to crystal-poor ignimbrite and lesser amounts of siliciclastic rocks (including minor interbeds containing microbial laminites), and minor basalt flows. The flow-banded rhyolite and less common dacite units — Kaarnka rhyolite (A) and rhyolite (B); discussed below under Petrography of volcanic rocks of the Talbot Sub-basin — are found at all stratigraphic levels of the group and appear to be coherent volcanic units. Many examples represent either lavas or subvolcanic sills. However, in some of these units, the abundance and size of phenocrysts varies considerably, and there are fiamme-like features and transitional contacts with bedded depositional units that suggest a pyroclastic origin.

As previously discussed, the basal unit of the Kaarnka Group is typically a diamictitic rock that most likely represents a pyroclastic breccia deposit. There are epiclastic rocks near the base of the group, but these become less common up section. They consist of dark mudstones, sandstones, and conglomerates. Bedding surfaces of the sandstones locally show wave ripples. These epiclastic rocks are typically very poorly sorted and are probably almost entirely composed of locally derived felsic–mafic volcanogenic detritus, including reworked pyroclastic material. The boundaries between the larger epiclastic horizons and overlying rhyolitic volcanic and volcaniclastic intervals are commonly gradational and are characterized by lenticular geometries characteristic of depositional bodies, for example, rhyolite intercalations several metres thick and tens of metres long within mudstone-dominated sedimentary rocks.

There is a distinctive and regionally continuous quartz-porphyritic rhyolite (Kaarnka quartz-rhyolite, hereafter)

within the lower Kaarnka Group. This rhyolite contains abundant subrounded quartz phenocrysts (up to 8 mm in size) and subhedral to euhedral feldspar phenocrysts. The grain size of both phenocrysts and the groundmass varies considerably at outcrop scale (Fig. 8) and, in rare cases, crude grain-size sorting is evident and fiamme are locally common. It is clear that this unit includes at least some pyroclastic deposits; however, lavas and very high-level sills or cryptodomes may also be present.

Feldspar- and quartz-porphyritic volcaniclastic units (mostly the Kaarnka Group crystal-rich ignimbrite) appear at lower to middle stratigraphic levels of the Kaarnka Group and dominate upper stratigraphic levels. They consist of interbedded ignimbrites, including crystal-ash and crystal-rich tuffs and are locally interlayered with flow-banded rhyolitic lavas, subvolcanic sills, or lava-like rheomorphic ignimbrites. In some places, these rocks appear to be massive, but they more commonly range from vaguely stratified to graded (fining-upward sequences) or layered crystal-rich to ash-rich tuffs (Fig. 8). Graded units can be stacked as individual cycles (1–10 m thick), each representing individual pyroclastic pulses. The crystalline component of the ignimbrite is typically dominated by subhedral to euhedral feldspar (K-feldspar > plagioclase) ranging up to 5 mm in size (in rare cases to 1 cm), but also includes abundant subhedral to rounded quartz crystals up to 5 mm in size. At one locality, the crystal tuff contains rare dark-grey, concentrically laminated accretionary lapilli (Fig. 8). Some outcrop areas are also characterized by rhyolitic breccias, including autoclastic breccias and distinctive volcaniclastic talus and debris-avalanche deposits. Basaltic lavas are also discontinuously preserved throughout this stratigraphic level and typically show well-developed peperitic contacts with bounding siliciclastic and volcaniclastic layers.

Intrusive rocks within the Mount Palgrave Group include sheets and irregular small bodies of subvolcanic porphyritic rhyolite, quartz diorite, and dolerite. The subvolcanic porphyritic rhyolite intrusions are very similar to those that intrude likely ring-fractures related to caldera formation in the Kaarnka region (subvolcanic Kaarnka porphyritic rhyolite intrusions hereafter). They also preferentially intrude mudstone-dominated intercalations and commonly carry abundant mudstone xenoliths of variable size. The subvolcanic porphyritic rhyolite intrusions define a broad northeast-trending zone linking the Winburn granite with subvolcanic porphyritic rhyolite intrusions in the Pussy Cat Group to the southwest (subvolcanic Pussy Cat porphyritic rhyolite intrusions hereafter).

Pussy Cat Group

The base of the Pussy Cat Group is not exposed in the eastern Talbot Sub-basin but is in apparent conformable contact with the underlying Mount Waugh rhyolite in the west of the sub-basin (Figs 2 and 3). The top of the Pussy Cat Group and base of the overlying Cassidy Group are defined by the first occurrence of Wururu Rhyolite. Because this unit is laterally discontinuous, the boundary between the Pussy Cat Group and the Cassidy Group is locally irregular and poorly defined. An unconformable contact between these two groups, as inferred by Daniels (1974), cannot be confirmed. Local strike differences between rocks of these groups are subtle and are most likely related to synvolcanic tectonism or emplacement of large subvolcanic porphyritic rhyolite intrusions (e.g. the subvolcanic Pussy Cat porphyritic rhyolite intrusion at Mount Shaw). The outcropping part of the Pussy Cat Group, as defined by Daniels (1974), is up to 3500 m thick. Approximately 2100 m of this represents basaltic lavas.

In its eastern outcrop area, the Pussy Cat Group is represented by the Kathleen Ignimbrite and the overlying Glyde Formation (cf. Daniels, 1974). A unit dominated by micaceous sedimentary and volcaniclastic rocks, but also including basal amygdaloidal basaltic lavas, underlies the Kathleen Ignimbrite; to the east, this unit is only thinly developed. To the west, the Kathleen Ignimbrite is absent and the sedimentary rock component of this unit is better developed. This is the stratigraphically lowest preserved unit and was originally assigned to the Glyde Formation. However, the Glyde Formation is redefined here to incorporate only the upper amygdaloidal basaltic lavas (locally containing volcaniclastic sedimentary interlayers) that overlie the Kathleen Ignimbrite.

The sedimentary and volcaniclastic unit that underlies the Kathleen Ignimbrite includes dark, massive to laminated mudstones, siltstones, and shales. There are also planar-bedded and ripple- and trough-cross-bedded arkosic to calcareous sandstones, which are poorly to well sorted. Conglomerates and very poorly sorted and matrix-supported diamictites are locally common and, particularly in the east, include pyroclastic breccias. To the west, in the area north of Warburton, there is a distinctive quartz-porphyritic rhyolite in the lower part of the lower sedimentary and volcaniclastic unit, where it overlies volcaniclastic talus and debris-avalanche deposits (Fig. 9) and crystal-rich ignimbrite. The porphyritic rhyolite contains abundant subrounded quartz phenocrysts (up to 8 mm) and subhedral to euhedral feldspar phenocrysts, which (together with the volcaniclastic talus and debris-avalanche deposits and the crystal-rich ignimbrite) closely resemble units from the Kaarnka Group.

The clastic components of the lower sedimentary and volcaniclastic unit are mainly volcanogenic detritus, represented by reworked pyroclastic rocks and erosion products of extrusive volcanic rocks. Some of the finely laminated mudstones may represent subaqueous ash-fall tuffs. Mafic source components dominate over felsic components in the finer grained fraction of the volcaniclastic and metasedimentary rocks. Minor lithofacies components include dolomitic marbles and associated calc-silicate rocks, relict evaporite horizons, and siliciclastic microbialites that are particularly common in the lower unit of the Pussy Cat Group in the western Talbot Sub-basin.

Many of the rocks of the lower sedimentary and volcaniclastic unit were deposited in a volcanically active alluvial to fluviolacustrine environment. Deposition of coarser rocks in the lower parts of the volcaniclastic

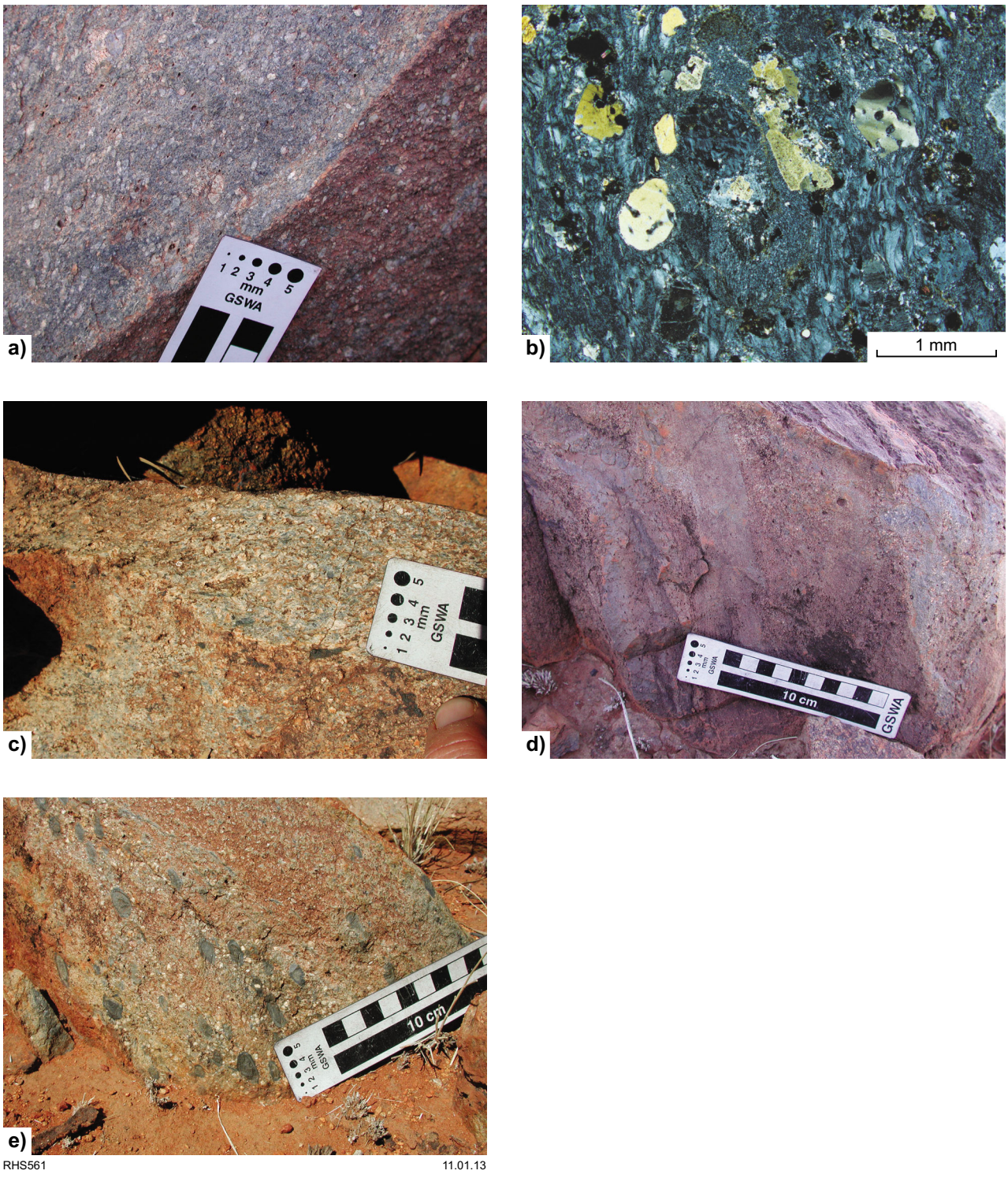

Figure 8. **Outcrop photographs and photomicrograph of rocks of the Kaarnka Group: a) poorly sorted quartz-porphyritic rhyolite; b) strongly embayed and rounded quartz phenocrysts and fragmented plagioclase crystals (crossed polars); and c) fiamme-bearing, d) stratified, and e) accretionary lapilli-bearing deposits**

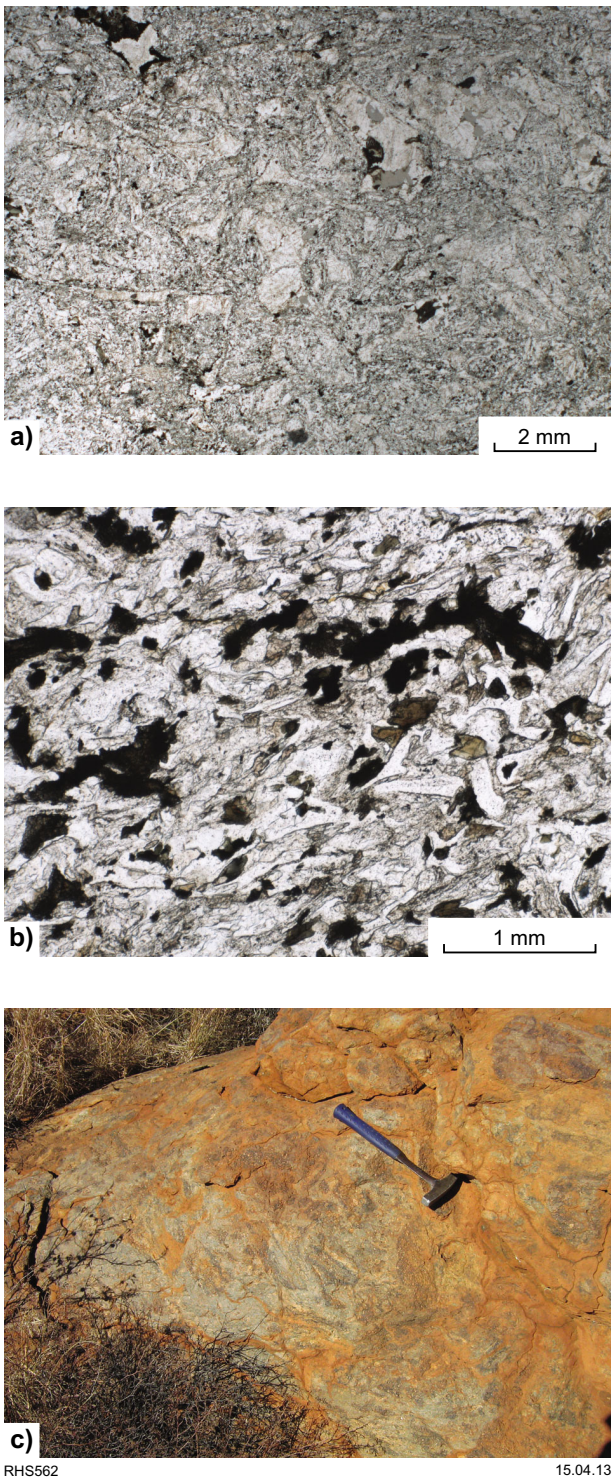

Figure 9. Photomicrographs and outcrop photograph of rocks of the Pussy Cat Group: a) and b) vitriclastic tuffs from the upper part of the Kathleen Ignimbrite, including relicts of former shards (plane-polarized light); c) coarse breccia deposit from north of Warburton

succession reflects episodic high-energy events including mud- and debris-flows, lahars, and pyroclastic events, whereas the finer grained rocks were deposited in small lakes and ponds on an alluvial plain. Desiccation cracks on mudstone bedding surfaces indicate that some of these shallow water bodies dried quickly. Higher in the sedimentary succession, very well sorted, slightly calcareous, planar-bedded to climbing-ripple cross-laminated and hummocky cross-bedded sandstones outcrop below the base of the Kathleen Ignimbrite. These indicate deposition in a more extensive, deeper, more permanent water body. Gypsum crystal moulds within mudstones and structures that appear to be enterolithic folds of former gypsum layers are associated with siliciclastic microbialites and dolomitic metalimestones; these indicate intermittent evaporitic or hypersaline conditions.

The Kathleen Ignimbrite has a maximum thickness of more than 500 m, and is composed mainly of flow-banded and lava-like rhyolite, which Daniels (1974) interpreted as a densely welded and rheomorphic ignimbrite. It is thickest in its eastern outcrop area, and shows a diverse range of lithofacies, including parts that are very rich in quartz and feldspar phenocrysts. Towards the west, both thickness and phenocryst content decreases and the rock grades into a more homogenous massive to flow-banded aphyric rhyolite, indicating that it was probably erupted from a volcanic source to the east. Evidence of a pyroclastic origin includes the irregular and patchy distribution of quartz and feldspar phenocrysts and crystal fragments, the presence of cognate quartz- and feldspar-phyric rhyolite clasts as lithic fragments, and alternating felsic and mafic ash layers in its basal part. Higher in the sequence, the Kathleen Ignimbrite grades from a strongly flow-banded rock to a eutaxitic, fiamme-textured rock that is overlain by a stratified succession of fine- to coarse-grained, commonly crystal-rich rhyolitic lapilli-ash tuffs, including relict glass shards near the top of the sequence (Fig. 9).

At its base, the Kathleen Ignimbrite contains upward-intruded clastic dykes of the sedimentary and volcaniclastic rocks that underlie the ignimbrite, indicating that the ignimbrite was deposited rapidly onto semi-consolidated water-bearing volcaniclastic sediments. Finely laminated siliceous ash tuffs in the upper, well-stratified part of the Kathleen Ignimbrite contain flame structures that strongly resemble sedimentary structures normally developed in subaqueous settings. In view of the apparently subaqueous setting of hummocky cross-bedded and climbing ripple cross-laminated sandstones that underlie the Kathleen Ignimbrite, it can be speculated that the Kathleen Ignimbrite was deposited in a large water body.

Overlying the Kathleen Ignimbrite, the Glyde Formation is dominated by basaltic lavas, some of which are massive, but more commonly they are highly amygdaloidal. Most of the basalts are aphyric, but plagioclase-phyric basalts are also present, and there are rare ropy lava surfaces. Intercalated within these lavas there are thin horizons of metasedimentary rocks, including epidote-rich cherty siltstone, quartzite, and siliceous microbialites. These

intercalations indicate the presence of running and standing water during deposition of the basaltic lavas. No pillow lavas have been found, and autoclastic metabasalt breccias are rare. East of Mount Shaw, there are possible hyaloclastite breccias in association with amygdaloidal metabasalt, quartzite, and microbial mudstone. Therefore, it appears that most of the Glyde Formation lavas were erupted and deposited subaerially, but locally the lavas entered small water bodies where they formed peperites and hyaloclastites.

Cassidy Group

The Cassidy Group is a bimodal succession of rhyolitic lava flows or lava-like rheomorphic ignimbrites (Wururu, Gombugurra, Thomas, and Hilda Rhyolites) alternating with basaltic lava flows (Gurgadi, Warubuyu, and Miller Basalts), with minor intercalations of sedimentary rocks (Figs 2 and 3). The base of the Cassidy Group is defined by the first occurrence of the Wururu Rhyolite. However, in places where the Wururu Rhyolite and the immediately underlying Gombugurra Rhyolite are not present, amygdaloidal basalts of the Glyde Formation are in contact with amygdaloidal basalts of the Gurgadi Basalt, obscuring a clear distinction between the two groups. The top of the Cassidy Group is defined as the boundary between the Miller Basalt and the overlying conglomeratic, sandy siliciclastic and calcareous rocks of the lower Mission Group. The maximum preserved thickness of the Cassidy Group exceeds 3400 m.

Most of the rhyolitic units of the Cassidy Group are lithologically very similar. They are generally dark-grey feldspar-phyric rhyolites with a very fine grained groundmass, and range from massive, to flow banded, to spherulitic. Basal autobreccias are typically not widely developed. The basal Hilda Rhyolite, however, differs in that it locally contains up to 60% subhedral to euhedral feldspar and quartz phenocrysts and is separated from the main upper body of rhyolite by about 20 m of volcaniclastic siltstones and sandstones. The lower crystal-rich and upper crystal-poor units may be sufficiently different to be considered formations in their own right.

The maximum preserved thickness of individual rhyolite units in the Cassidy Group ranges from about 110 m (Gombugurra Rhyolite) to 810 m (Wururu Rhyolite). Not all of the individual rhyolites form laterally continuous units over the entire outcrop extent of the Cassidy Group. The Wururu Rhyolite is laterally continuous in its western and eastern parts, but appears to be locally absent in the area south of Mount Shaw. The stratigraphically higher Gombugurra Rhyolite is present only in the western Talbot Sub-basin, and thins to the east in the Mount Hilda area. The Thomas Rhyolite is the most laterally continuous rhyolite unit, and can be traced over the entire extent (>90 km) of the Cassidy Group outcrop area. The stratigraphically highest Hilda Rhyolite can be traced for at least 65 km from the Warburton area eastward as a continuous unit, but thins out to the east, north of Frank Scott Hill. Despite their smaller areas of exposure, the Wururu and Gombugurra Rhyolites show remarkable lateral extent for felsic volcanic rocks. Neither shows significant development of autoclastic brecciation. The basal parts of many of the rhyolite formations show discontinuous layering or flattening, which locally resembles eutaxitic structures. The Thomas Rhyolite locally contains abundant flattened pumice, providing evidence of flow around crystals (Fig. 10). If these are indeed eutaxitic structures, some components of these formations must be rheomorphic ignimbrites. The evidence presented above to suggest that the underlying Mount Waugh rhyolite and other units of the Mount Palgrave Group are dominated by lava-like rheomorphic ignimbrite facies are equally applicable to all units of the Cassidy Group.

Between the Wururu Rhyolite and the Gombugurra Rhyolite, there is an unnamed unit of sedimentary rocks, approximately 50 m thick, composed mainly of fine-grained siltstones, with layers of sandstone and conglomerate, and very minor layers of basalt. In the western half of the area of Cassidy Group outcrop, the Gombugurra Rhyolite is overlain by fine-grained siltstones with minor amounts of sandstone, which are in turn overlain by amygdaloidal Gurgadi Basalt. In the eastern area of Cassidy Group outcrop, the Gurgadi Basalt directly overlies the Wururu Rhyolite, and is in turn overlain by the Thomas Rhyolite. Here, the Gurgadi Basalt represents a succession of amygdaloidal basaltic lavas that contain numerous thin and laterally discontinuous layers of volcaniclastic sedimentary rocks comprising cherty epidotitic mudstones, siltstones, sandstones, and conglomerates. The thickness of the Gurgadi Basalt (including sedimentary rocks) is up to 600 m.

The stratigraphic interval between the Thomas and Hilda Rhyolites is again characterized by sedimentary rocks and basaltic lavas. Within the central Talbot Sub-basin, this stratigraphic interval can be subdivided, for about 3 km along strike, into a siliciclastic sedimentary lower part and a basaltic volcanic upper part (Warubuyu Basalt). This subdivision is not possible further to the east, where the siliciclastic lower sequence is absent. However, in the eastern area, the dominantly basaltic pile is intercalated with siliciclastic rocks. This basaltic–sedimentary interval is up to 300 m thick. Sedimentary rocks include cherty epidotitic mudstones, light bluish-grey shales, brownish volcaniclastic siltstones, ripple cross-laminated sandstones, and minor conglomerate beds. A light-greenish laminated cherty, epidotitic microbialite horizon forms a conspicuous marker horizon within this stratigraphic interval, and can be traced for more than 5 km along strike. Basaltic volcanic rocks have been shallowly intruded into (and possibly extruded onto) this microbialite horizon, causing disruption, tilting, and soft-sediment deformation (faulting, folding, and slumping) of the cohesive sedimentary deposits. Partial extrusion and shallow intrusion of basalts into subaqueously deposited sediments has also led to the formation of extensive hyaloclastite breccias and peperites. These observations point to subaqueous emplacement of basalts, but true pillow structures are not evident. Similarly, the immediately overlying Hilda Rhyolite is locally under- and overlain by sedimentary rocks including finely laminated shales and fine-grained volcaniclastic siltstones and sandstones, which strongly suggest a low-

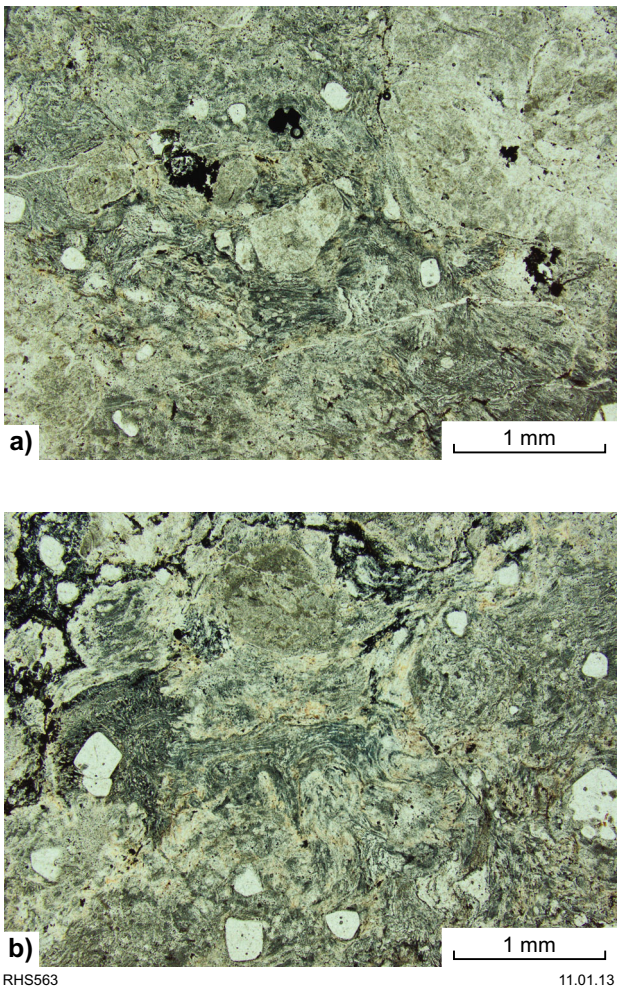

Figure 10. Photomicrographs of pumice-rich units of the Thomas Rhyolite (Cassidy Group) (both plane-polarized light)

energy subaqueous (marine or continental) depositional environment.

The Miller Basalt overlies the Hilda Rhyolite, but is commonly separated from it by a thin succession of fine-grained sedimentary rocks. For the most part, the Miller Basalt represents a repetitive succession of lava flows characterized by 10–20 m-thick basal sequences of massive basalt that grade upward into progressively more vesicular and amygdaloidal basalts. In places, there are intensively silicified or brecciated basalts at the top of such sequences, marking the tops of lava flows. The Miller Basalt is not an entirely volcanic unit; it also contains a substantial number of sedimentary layers. Near the base of the formation there are several conspicuous, orange-weathering cherty to quartzitic mudstone–sandstone layers (1–2 m thick; possibly containing redistributed rhyolitic ash) that form a laterally traceable marker within the Miller Basalt. Intercalated with the basaltic rocks of the middle of the Miller Basalt, there is a 200–250 m-thick interval characterized by several conspicuous coarsening-upward successions of volcaniclastic conglomerates and sandstones. Laterally restricted sedimentary intercalations are also common in the remaining upper part of the Miller Basalt. They comprise cherty epidotitic mudstones, fine-grained cherty microbialites, siltstones, sandstones, and minor conglomerate layers, commonly at the top of lava flows. The entire Miller Basalt succession has a thickness of about 750 m.

Mission Group

The Mission Group conformably overlies the Cassidy Group (Fig. 3) and is the youngest stratigraphic interval of the Bentley Supergroup. It can be subdivided into a sedimentary lower succession (Gamminah Conglomerate, Frank Scott Formation, and Lilian Formation) and an upper basalt-dominated succession (Milesia Formation). No evidence of felsic volcanism has yet been found in the Mission Group. It is conformably to unconformably overlain by the Townsend Quartzite. Daniels (1974) reported the total thickness of the Mission Group to be about 4000 m.

The Miller Basalt, the uppermost unit of the Cassidy Group, is overlain by siliciclastic and calcareous rocks of the Frank Scott Formation. In the Warburton Range area, the transition is characterized by 'interbanded thin basalt flows, and thin silts and dolomites' (Daniels, 1974). In that area, the Frank Scott Formation includes finely laminated siltstones, dolomitic siltstones, shales, and dolomites, as well as minor sandstones and cherts (Daniels, 1974). In the adjacent Mount Eveline area, the Miller Basalt is, in contrast, overlain by coarse clastic sedimentary rocks of the Gamminah Conglomerate, a locally restricted basal member of the Frank Scott Formation. In this area, the succession from the Gamminah Conglomerate to the overlying finer grained siliciclastic and calcareous rocks of the Frank Scott Formation, and up section into the overlying shale-dominated Lilian Formation, is a distinct fining- and deepening-upward sedimentary succession.

The Gamminah Conglomerate is a moderately coarse-grained rock containing subrounded to well-rounded pebbles and cobbles up to about 20 cm in diameter. These clasts are composed mainly of amygdaloidal basalt, felsic porphyritic volcanic rock, and milky quartz. The boundary with the underlying Miller Basalt can be sharp or transitional. Sedimentary structures are predominantly crude planar-bedding, but there is also cross-bedding. Intercalated within the conglomerates are thin sandstone layers. Towards the top of the formation, the conglomerates become finer grained and eventually grade into the sandstone–shale succession of the lower Frank Scott Formation. The sandstones are predominantly fine-grained quartzites, which weather to a reddish-brown colour, but fresh surfaces are a dark bluish-greenish grey, indicating an abundance of altered volcanic detritus. The sandstone layers commonly show parallel lamination grading into ripple cross-lamination. Low-angle, swaley trough cross-bedding is also present. Trough cross-bedding typical of a fluvial origin is almost totally absent, so the depositional environment of these quartzites is interpreted to be marine or lacustrine (Howard et al., 2011b). The sandstones most probably represent turbidites or

tempestites and their tops have been locally modified by wave- or storm-current action. The thickness of individual sandstone layers ranges from a few centimetres to about 2 m. The shales in which the sandstones are intercalated represent suspension settling of mud in an offshore, low-energy sub-wave-base setting within a large water body. Stratigraphically higher in the Frank Scott Formation, the number of sandstone layers decreases, and limestone layers (of comparable thickness) appear as intercalations within the shales. Some of the limestones show cross-bedding, are rich in intraclasts, or appear to be oolitic. North of Frank Scott Hill, a number of limestones contain metre-sized pillow-shaped stromatolites. These are commonly internally laminated and locally include small domical structures. Higher again in the succession there is a shale-dominated interval, which contains minor intercalations of fine-grained quartzitic sandstones, dolomitic limestones, and siliceous mudstones or cherts. Daniels (1974) also reported the presence of polymict conglomerate layers. Some of the more-siliceous and less-altered mudstones are black, and are probably rich in organic carbon (black shales). This part of the succession is transitional to the overlying Lilian Formation, which on Mount Eveline consists almost entirely of reddish to olive-green weathering shales. The sedimentary rocks of the Frank Scott and Lilian Formations were laid down in a deep, fairly extensive water body that existed for a substantial period of time. It is not known whether this water body represented a large lake or lake system, or was connected to the marine realm. The combined thickness of the two formations is probably in the order of 1200–1500 m.

North of the large dolerite intrusion at Frank Scott Hill, the limestone–shale succession of the upper Frank Scott Formation contains a thin, laterally traceable sheet of basalt that is slightly vesicular at its top. Also south of Frank Scott Hill, the shale-dominated outcrops contain a number of fine-grained basaltic intercalations. None of these volcanic rocks are highly vesiculated, they do not contain autoclastic breccias, and do not form peperites with the shaly host rock. Therefore, these basaltic intercalations have been interpreted as shallow intrusive sills rather than extrusive lavas (Howard et al., 2011b).

The Milesia Formation consists predominantly of basaltic volcanic rocks and has a minimum thickness of about 300 m. In the lower part of the formation, the basalts are commonly highly altered (epidotitic or hematitic), strongly amygdaloidal, or strongly quartz-mottled. Basalt breccias are also present, some of which appear to be autoclastic, whereas others are clearly peperitic in origin, with fine-grained sandstone filling the spaces between basalt clasts. The whole succession essentially represents a pile of basaltic lava flows. These lava flows contain a number of sedimentary intercalations consisting of pinkish quartzitic sandstones, and conglomerates. Some of these interlayers are laterally continuous and traceable for about 5 to 6 km, whereas others are lenticular and extend only 5 to 10 m long along strike. These interlayers are commonly between 1 and 5 m thick. About 5 km south of Frank Scott Hill, the basalts close to the southern outcrop margin of the Milesia Formation contain a laterally traceable layer of chocolate-brown, ferruginous, fine- to coarse-grained, and possibly subarkosic, sandstone. This is the first known example of continental redbed-type sedimentary rocks in the Mission Group. The uppermost Milesia Formation (and the Mission Group), which directly underlies the Townsend Quartzite of the Officer Basin, is covered by a thick wedge of eolian sand and other unconsolidated Cenozoic sediments. Two recent stratigraphic drillholes penetrated part of this stratigraphic interval (Eaton, 2010). In both wells, the upper parts of the drilled cores contain a thick interbedded sandstone–shale redbed sequence overlying extrusive basaltic rocks. One drillhole intersected an additional lower interval of redbed-type siliciclastic rocks sandwiched between basaltic intervals.

The continental redbed-type sedimentary rocks at the top of the Milesia Formation appear to provide a depositional link between the Bentley Supergroup and the Townsend Quartzite (~260 m maximum exposed thickness). Although not exposed, the boundary between the Mission Group and the Townsend Quartzite seems to be largely conformable in the western Talbot Sub-basin, but appears to become unconformable in the area between Ranford Hill and Barrow Hill. However, it is still unclear if this apparently unconformable contact is a true erosional unconformity, or is the result of younger tectonism (Daniels, 1974).

Petrography of the volcanic rocks of the Talbot Sub-basin

Rhyolitic rocks of the Talbot Sub-basin are typically very felsic and many preserve no primary mafic minerals other than magnetite. In rare cases, primary clinopyroxene is present but even then is largely altered to a late-magmatic blue-green amphibole and biotite. Fibrous or needle-like blue-green amphibole and flakes of brown-green biotite are common late-magmatic or secondary mafic minerals, both as replacement of primary mafic minerals or as a result of devitrification and alteration of groundmass. Magnetite is present as a primary phenocryst phase, forming globular grains typically rimmed by titanite. It is also found within the groundmass as a locally strong dusting of fine grains. Common accessory phases include titanite, apatite, and zircon, and, rarely, a dark-brown metamict phase tentatively identified as chevkinite.

All felsic volcanic rocks of the Talbot Sub-basin show mineralogical evidence of late- to post-magmatic volatile-fluxed alteration and autometasomatism. Rocks in the lower part of the stratigraphy, and in particular in the Scamp region, show evidence of high-temperature metamorphism. Volatile-fluxed alteration and autometasomatism can be pervasive or vein or fracture controlled. Weak pervasive alteration typically results in crystallization of epidote, chlorite, green biotite, and pyrite. Vein-controlled assemblages include green chlorite, epidote, carbonate, fluorite, muscovite, and pyrite and, primarily within rocks of the Scamp Formation and Winburn granite, brown-yellow garnet. Both alteration and metamorphism appear to have accompanied the accumulation of the stratigraphically lower parts of the Talbot Sub-basin (i.e. the Mount Palgrave and Kaarnka Groups). Here, alteration assemblages may both pre- and postdate metamorphic recrystallization. The style of

metamorphism is typically low-pressure, high-temperature metamorphism related to rapid burial beneath subsequent very hot (>900ºC; see Geochemistry – Talbot Sub-basin) and locally thick deposits. In calc-silicate rocks separating rhyolitic pyroclastic fall deposits, for example within the Kaarnka Group, the rapid burial has locally resulted in perfect preservation of intricate sedimentary structures (ripples, algal laminae) in a metamorphic assemblage comprising diopside, hydrogrossular, and fluorite. In the initially glassy rocks of the Scamp Formation, and locally also affecting some of the widespread vitric lower units of the Eliza Formation, glass-rich groundmass has recrystallized to a fine-grained granoblastic assemblage of quartz and feldspar. Metamorphism of these rocks has resulted in growth of blue-green amphibole and brown-green biotite, either as part of the granoblastic assemblage or as a retrograde phase forming oriented to random needles or flakes. Brown-yellow garnet is a rare but widespread metamorphic mineral in the Scamp Formation, where it ranges from small anhedral to euhedral phenocrysts and poikiloblasts. However, in many cases it is unclear if crystallization of garnet is purely a metamorphic feature or is a combined result of vein-controlled alteration followed by, or accompanying, metamorphism.

Most rhyolites of the Mount Palgrave Group are aphanitic rocks containing <5% phenocrysts, although rare examples contain up to 10% phenocrysts. The phenocrysts do not usually exceed ~3 mm in size but may be up to 5 mm. Perthite is commonly the dominant phenocryst phase, followed by plagioclase and, rarely, quartz and lithic fragments. Some aggregates of feldspar crystals are present. Phenocrysts range from anhedral, angular, or strongly rounded to euhedral, and many show strong dissolution embayments. For most rocks of the Eliza Formation, the groundmass is typically a felsitic intergrowth of feldspar and quartz and is strongly dusted with magnetite. Rounded to ovoid spherulites are common and range from <1 mm to several millimetres in size. In some cases, these are seeded by rounded quartz grains. Devitrified groundmass glass also contains acicular green biotite and blue-green amphibole (locally up to 15% of the groundmass). These minerals also locally define perlite fractures or flow banding. Although some rocks of the Scamp Formation have a felsitic groundmass, in most cases the groundmass has been recrystallized to become granoblastic. Spherulites, perlite cracks, and evidence for flow banding have seldom survived this recrystallization, which has commonly also increased the proportion of blue-green amphibole in the groundmass.

Samples of the Mount Waugh rhyolite that have escaped recrystallization to a granoblastic assemblage are petrographically very different from other rocks of the Mount Palgrave Group. They contain up to 15% phenocrysts, mainly comprising a very poorly sorted assemblage of angular to subrounded to euhedral perthite crystals, quartz crystals, and lithic fragments (in order of decreasing abundance). A very poorly-sorted, seriate-textured, groundmass is lightly dusted with magnetite. Slight variations in grain-size and a preferred alignment of groundmass biotite and amphibole define a locally prominent flow fabric that moulds around phenocrysts. Field evidence shows that samples of the Mount Waugh rhyolite are locally fiamme-rich.

The Kathleen Ignimbrite has been described in detail by Daniels (1974) who showed that some sections of the upper stratigraphy include glass shards and clear evidence of rheomorphism. Petrographic examination of samples of the Kathleen Ignimbrite showed that they range from phenocryst rich (up to 50%) to phenocryst-poor. Phenocrysts are typically angular, although rare euhedral crystals also occur. The phenocrysts are dominated by perthite and quartz and aggregates of these, with locally abundant lithic fragments. Plagioclase phenocrysts are rare. The phenocryst population is poorly sorted, but crystals larger than 1 cm are rare. The groundmass is very poorly sorted and seriate textured with small variations in grain size, and exhibits a preferred alignment of brown biotite to define a locally prominent flow fabric. Fine (<1 mm) spherulites are locally abundant.

The Kaarnka Group quartz rhyolite ranges from fine to medium grained and is generally very poorly sorted, with no indication in thin section or outcrop of clear grain size grading. Phenocrysts and lithic fragments are up to 8 mm in size and form up to 50% of the rock. They are angular to rounded and subhedral and commonly show strong dissolution embayments. The phenocrysts are dominated by either plagioclase or perthite, and quartz is generally common, particularly as drop-shaped crystals. Feldspar–quartz aggregates are locally common. Rare clots of green biotite are possibly relict clinopyroxene crystals. Magnetite forms phenocrysts up to 1 mm in size, typically surrounded by titanite. The groundmass is dusted with magnetite and ranges in texture from felsitic, to radiating masses of unresolvable mineralogy, to an extremely fine grained but very poorly sorted assemblage of quartz, feldspar, green to green-brown biotite, and blue-green amphibole. Very small (<2 mm) spherulites are locally abundant. Layers and discontinuous lenses are biotite-rich and show well-developed flow foliation around phenocrysts. There are devitrified and welded pumice fragments (fiamme).

The crystal-rich ignimbrite of the Kaarnka Group exhibits highly variable grain size and less variable sorting. It ranges from fine to coarse grained, but is most commonly a very weakly graded to massive, poorly sorted, medium-grained, groundmass-supported crystal tuff. The maximum abundance of phenocrysts or clasts is about 60% and, in some samples, the maximum grain size is up to 6 mm. Other samples contain relatively few phenocrysts or clasts. These abundances represent end-member examples of crystal-rich and (much less common) crystal-poor ignimbrite. Some samples show conspicuous grain-size grading at both hand-specimen and outcrop scale. Phenocrysts form a very poorly sorted population (seriate) of mainly angular and fragmental crystals with rarer subhedral grains and subrounded quartz. Perthite crystals are dominant over quartz, and there are fewer lithic fragments and plagioclase crystals. The groundmass is very fine to fine grained and poorly sorted with a light to moderate dusting of magnetite, and includes up to 5% brown biotite. Biotite also forms interstitial clots that are possibly altered pumice fragments.

The Kaarnka Group rhyolite can be subdivided geochemically (see Geochemistry) into two units: Kaarnka rhyolite (A) and (B). Kaarnka rhyolite (A) rocks are typically fine grained but have a seriate to porphyritic texture (i.e. are poorly sorted), with phenocrysts ranging up to 3 mm in size. Phenocrysts form between 10 and 30% of the rock, either plagioclase or perthite may be dominant, and there are rare strongly embayed quartz crystals and irregular magnetite crystals. These phenocrysts also range from subangular and subrounded to euhedral. Mafic clots are relict clinopyroxene, although wispy biotite-rich clots are more likely fiamme. A fine-grained felsitic groundmass is commonly strongly dusted with magnetite and contains up to 20% combined blue-green amphibole > green biotite as needles and flakes strongly aligned into flow foliation that wraps around phenocrysts. Small spherulites (<1 mm in size) are locally abundant.

Kaarnka rhyolite (B) rocks are generally similar to the Kaarnka rhyolite (A) rocks, with a fine-grained seriate to porphyritic texture. Phenocrysts form a very poorly sorted population, up to 6 mm in size, and may form up to 30% of the rock as angular, subrounded to (rarely) euhedral crystals. The dominant mineralogy of the phenocryst population varies widely from plagioclase- to perthite-dominant, although an assemblage of perthite, quartz, plagioclase, and lithic fragments (in decreasing order of abundance) appears to be most common. Feldspar crystals and aggregates showing complex and multiple rim or overgrowth patterns (including rapakivi textures) are common. In some perthite crystals and feldspar–quartz aggregates, fluorite and garnet fill early fractures that do not penetrate the flow-banded groundmass (e.g. Fig. 5). These features are most likely inherited from source chambers, and strongly resemble features seen within the Winburn granite. Rare phenocrysts of blue-green amphibole are either anhedral or subhedral and are poikilitic. Magnetite forms subhedral phenocrysts. The groundmass is typically felsitic with up to 10% in the form of needles and flakes of blue-green amphibole and green and brown biotite strongly aligned in a flow foliation that wraps around phenocrysts. Magnetite forms a moderate dusting of the groundmass, but in some samples these very fine crystals form up to 10% of the groundmass. Abundant spherulites (~1 mm in size) show varying degrees of flattening. Wispy clots of biotite probably represent fiamme. Some samples have been metamorphosed and the felsitic groundmass has recrystallized to a fine-grained granoblastic texture.

Subvolcanic porphyritic rhyolite intrusions into the uppermost Pussy Cat Group contain between 30 and 70% subhedral to euhedral phenocrysts up to 10 mm in size. These phenocrysts are dominantly perthite and complexly rimmed or zoned feldspar (e.g. rapakivi feldpsars) with fewer quartz, plagioclase, and feldspar–quartz aggregates, in descending order of abundance. All phases locally have strong dissolution embayments and complex feldspar crystals have internal embayments. Quartz phenocrysts are commonly subrounded to drop shaped. The groundmass or interstitial portions vary from a seriate and felsitic texture to well-developed granophyric texture to granoblastic texture. Green-brown biotite flakes and blue-green amphibole needles are common components of the groundmass, and are concentrated mainly along grain boundaries. The groundmass also includes subrounded clots of biotite that are likely pseudomorphs after clinopyroxene.

Rhyolites of the Cassidy Group (Wururu, Gombugurra, Thomas, and Hilda Rhyolites) share similar petrographic ranges. They are typically strongly vitric rocks with <15% phenocrysts. Phenocrysts are up to 6 mm in size and include perthite, plagioclase, feldspar aggregates, and quartz, in order of decreasing abundance. They range from angular to subrounded, but also include euhedral crystals; strong dissolution embayments are common. Rare subhedral clots of green amphibole likely represent pseudomorphs after clinopyroxene. The groundmass is typically heavily dusted with magnetite and has a felsitic texture, locally includes abundant spherulites (~1 mm) and, in some case, well-developed perlite fracturing. Blue-green amphibole needles and green-brown biotite flakes are locally abundant and strongly aligned with a prominent flow foliation that wraps around phenocrysts. In some rocks (particularly well demonstrated in the Thomas Rhyolite) the groundmass is very poorly sorted, and biotite-rich areas define pumice fragments that are flattened, bent, and moulded around phenocrysts.

Geochronology of the Bentley Supergroup

Forty new samples from the Warakurna Supersuite in the west Musgrave Province have been analysed for U–Pb in zircon by sensitive high-resolution ion microprobe (SHRIMP; Appendix). The total range of mean ages is c. 1080 to 1045 Ma and is similar to the range of c. 1090 to 1040 Ma for magmatic activity related to the Tjauwata Group in the Bloods Range region of the Northern Territory (Edgoose et al., 2004). The probability plot of U–Pb dates for all samples from the west Musgrave Province (Fig. 11) indicates that the processes during which zircon was crystallized peaked between c. 1075 and 1065 Ma. This interval included emplacement of the giant layered Giles (G1) intrusions and the massive (G2) gabbros, and brackets the age of the main magmatic episode related to the Warakurna LIP (e.g. 1078–1070 Ma as suggested by Wingate et al., 2004). However, processes leading to zircon crystallization (in most cases demonstrably magmatism) within the west Musgrave Province (at least) operated without a perceptible hiatus for at least 30 m.y. after 1070 Ma, and likely for a considerable time prior to it. For example, volcanic rocks of the Bentley Basin commonly yield zircon U–Pb ages that span the interval between the c. 1120 Ma end of the Musgrave Orogeny and the beginning of the Giles Event (Fig. 12). This range supports the suggestion (Smithies et al., 2010, 2011) that significant tectonothermal activity was a feature of the Musgrave Province almost continuously from the c. 1220 Ma beginning of the Musgrave Orogeny to the end of magmatism related to deposition of the Bentley Supergroup (c. 1040 Ma).

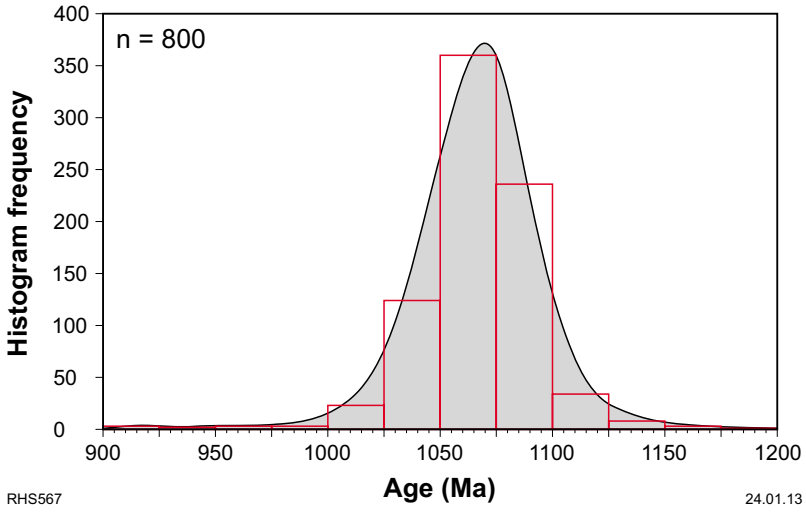

Figure 11. Combined probability density plot and histogram of 207-corrected $^{238}U/^{206}Pb^*$ (Pb^* = radiogenic Pb) zircon ages for samples of the Warakurna Supersuite (including volcanic and volcaniclastic rocks of the Bentley Supergroup)

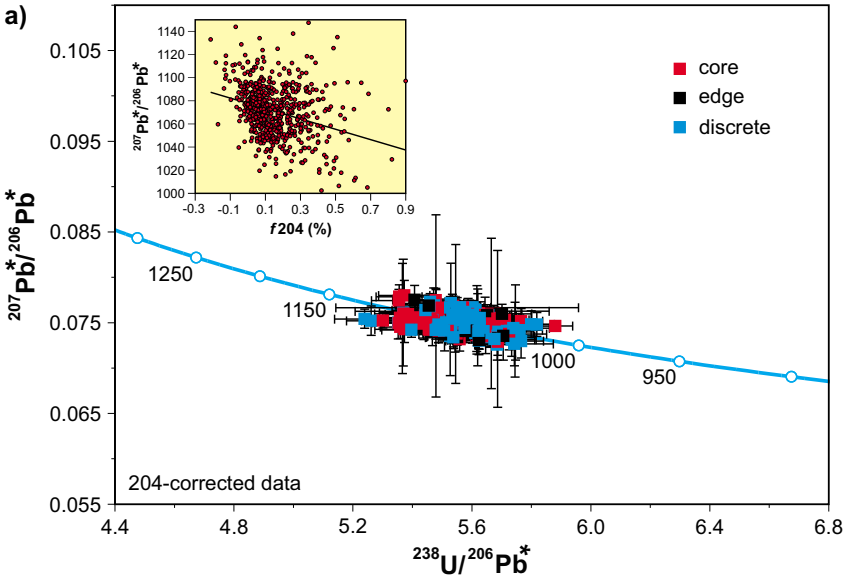

Figure 12. SHRIMP U–Pb analytical data for zircons from felsic volcanic rocks of the Talbot Sub-basin coloured according to analytical location — on a crystal core, edge, or with no discernible textural feature (discrete): a) Data corrected for common Pb using ^{204}Pb; b) data not corrected for common Pb. The inset in a) shows the correlation between 204-corrected $^{207}Pb^*/^{206}Pb^*$ age and the common-Pb correction ($f204$ is the proportion of common Pb in total ^{206}Pb). Error bars are 1 sigma.

Both prolonged zircon growth with re-entrainment in a magma and ancient radiogenic-Pb loss can result in similar patterns on a concordia diagram. However, the alpha-radiation dosage, calculated based on age and U and Th concentrations, can be used to predict the extent of structural damage in a crystal and hence the likelihood of ancient radiogenic-Pb loss (Murakami et al., 1991). These authors defined zircons with $<3 \times 10^{-15}$ alpha events as crystalline, $>3 \times 10^{-15}$ to $<8 \times 10^{-15}$ events as intermediate, and $>8 \times 10^{-15}$ events as metamict. Of 319 analyses of zircons from felsic rocks of the Talbot Sub-basin, only six can be classified as highly metamict, and 32 as intermediate, with the remaining majority classified as crystalline. No clear relationship exists between U, Th, or alpha dose and age, and we conclude that the dispersion of U–Pb data along the concordia curve (e.g. Fig. 12) does not reflect ancient radiogenic-Pb loss.

Several U–Pb dates have been obtained from leucogranite dykes, veins, and plutons of the Warakurna Supersuite in the region between the Talbot Sub-basin and the South Australian border. Analyses of typically euhedral, idiomorphically zoned zircons in these granites yielded results with little or no excess dispersion, which can confidently be interpreted as crystallization ages of single magmatic components. Sun et al. (1996) obtained a U–Pb zircon age (all mean ages are quoted with 95% uncertainties) of 1078 ± 3 Ma for a granophyric leucogranite. An age of 1078 ± 5 Ma (Glikson et al., 1996), obtained from an outcrop originally mapped by Daniels (1974) as rhyolite and attributed to the Smoke Hill Rhyolite, more likely reflects the crystallization age of the leucogranite that exclusively forms that outcrop (Smithies et al., 2009). A leucogranite at Amy Giles Hill, showing well-developed mixing and co-mingling textures with G2 gabbro (Howard et al., 2007), has been dated at 1074 ± 3 Ma (Bodorkos and Wingate, 2008). In the West Hinckley Range, locally mingled G2 gabbro and leucogranite form a kilometre-scale fold with a steep northwest-trending axial plane, intruded by syndeformational leucogranite (including synmagmatic mylonites; Howard et al., 2007) dated at 1075 ± 7 Ma (Kirkland et al., 2008e). Synmylonitic leucogranite, pooled into boudin necks in a northwest-trending mylonite immediately south of Charnockite Flats, has been dated at 1075 ± 2 Ma (Kirkland et al., 2008f). These data effectively define a very short interval, between 1078 ± 3 and 1074 ± 3 Ma, which involved comagmatic intrusion of massive G2 gabbro and leucogranites, and northwest-trending folding and shearing.

Similarly, U–Pb dating of euhedral, idiomorphically zoned zircons in volcanic rocks of the Tollu Group, in the Blackstone Sub-basin, yielded well-grouped results that can be interpreted as ages of crystallization, and potentially of volcanic deposition, of single magmatic components. Three samples from the Smoke Hill Volcanics yielded crystallization ages of 1071 ± 8 Ma (GSWA 191728, Coleman, 2009), 1073 ± 7 Ma (GSWA 191706, Coleman, 2009), and 1073 ± 8 Ma (GSWA 189561, CL Kirkland, written communication, 2013). Notably, these ages are all within analytical uncertainty of the crystallization ages of the Warakurna Supersuite leucogranites. A single sample of the overlying Hogarth Formation yielded a crystallization age of 1068 ± 7 Ma (GSWA 185518, Kirkland et al., 2013b).

In contrast to U–Pb results from leucogranites and volcanic rocks in the east, zircon age data from the volcanic rocks of the Talbot Sub-basin itself are more difficult to interpret due to geological processes favouring polycyclic disequilibrium crystallization and the dissolution of zircon and (re-)entrainment of numerous zircons of different ages. Many samples from the Talbot Sub-basin exhibit a correlation between $^{207}Pb^*/^{206}Pb^*$ dates (Pb* = radiogenic Pb), corrected for common or initial Pb using measured ^{204}Pb, and the correction itself, indicating that common-Pb corrections using ^{204}Pb are inaccurate for some or all of these analyses. Owing to this correlation, and to avoid introducing any bias when comparing U–Pb results from different samples, we chose to consistently use the 207-correction method (e.g. Gibson and Ireland, 1996). The 207-correction assumes that the radiogenic composition is concordant, and the $^{238}U/^{206}Pb^*$ ratio is determined by extrapolating the measured $^{207}Pb/^{206}Pb$ ratio to concordia along a trajectory defined by the appropriate choice of common-Pb composition (Stacey and Kramers, 1975). Nevertheless, because the data include only near-concordant analyses (strongly discordant analyses or those representing mixtures were excluded), neither the form of the common-Pb correction nor its application results in significant differences to the calculated ages. In some cases, the 207-corrected dates quoted here may differ very slightly from those cited in the GSWA Geochronology Record Series, where the 204-correction, rather than 207-correction, may have been used.

Several regions within the Talbot Sub-basin provide outcrop sections that are continuous over large parts of the stratigraphy, and geological constraints on the relative ages of volcanic deposition and subvolcanic intrusion for all units of the sub-basin are quite clear. Geopetal (i.e. 'younging' or 'way-up') indicators are well developed, contact relationships are unambiguous, and geochemical data provide no evidence for structurally repeated sections. Samples dated are representative of 12 felsic magmatic episodes, or distinct stratigraphic levels (L1–L12). Many of these felsic magmatic episodes were separated by discrete mafic magmatic events. The order of felsic magmatic deposition or intrusion, from oldest to youngest is:

- oldest components of the Winburn granite (L1)
- Mount Palgrave Group: Eliza Formation (base and upper, L2–3), Scamp Formation (L4), and Mount Waugh rhyolite (L5)
- lower part of the Pussy Cat Group, early subvolcanic Pussy Cat porphyritic rhyolite intrusions, Kathleen ignimbrite and quartz rhyolite at the base of the Kaarnka Group (Kaarnka quartz-rhyolite, L6)
- main part of the Kaarnka Group and upper part of the Pussy Cat Group (L7)
- subvolcanic porphyritic rhyolite intrusions in the upper Pussy Cat Group (overlying the Kathleen Ignimbrite) and in the Kaarnka Group (subvolcanic Kaarnka and Pussy Cat porphyritic rhyolite intrusions, L8)

- Cassidy Group: Wururu (L9), Gombugurra, Thomas (L10), and Hilda Rhyolites (L11)
- Upper part of the Kaarnka Group (L12).

Plotting relative age (stratigraphic level, Table 2) against mean isotopic age produces a crude upwards-younging trend (Fig. 13). The mean age of 1067 ± 10 Ma for the stratigraphically lowest (L2) volcanic rocks (excluding the intrusive Winburn granite, L1) is significantly older than the mean age of 1045 ± 8 Ma for the highest (L12) volcanic units. Several stratigraphic levels are represented by multiple samples and show a considerable range of mean ages (e.g. L8; 1081 ± 9 to 1063 ± 11 Ma). In addition, subvolcanic porphyritic rhyolite intrusions below the Kathleen Ignimbrite (e.g. GSWA 195001) have peperitic contacts with an intervening thin layer of siliciclastic rocks that show soft-sediment contact relationships with the ignimbrite itself (i.e. the porphyritic rhyolites, volcaniclastic rocks, and ignimbrite are contemporaneous – L6). The mean U–Pb zircon age of this subvolcanic porphyritic rhyolite intrusion (1060 ± 10 Ma), as well as the mean U–Pb zircon age of samples from the stratigraphically lower Mount Palgrave Group (e.g. L5, 1061 ± 11 Ma, GSWA 195230; L4, 1059 ± 6 Ma, GSWA 195678, and 1061 ± 8 Ma, mean of all three samples at L4; L3, 1062 ± 8 Ma, GSWA 195116, and 1066 ± 11 Ma, mean of two samples at L3), are younger than — and in some case beyond analytical error of — the mean U–Pb zircon age (e.g. 1081 ± 9 Ma, 1074 ± 7 Ma) of subvolcanic Pussy Cat porphyritic rhyolite intrusions intruded above the Kathleen Ignimbrite. Such relationships indicate that the mean U–Pb age, for at least some units, does not reflect the timing of the final (eruptive) magmatic crystallization episode.

Plotting relative age against the youngest (rather than the mean) date from each stratigraphic level (Fig. 13) produces only a slightly stronger upwards-younging trend. The date obtained from the youngest zircon is generally within 2-sigma uncertainty of the weighted mean age of all zircons from the same sample. If only the youngest individual date from each sample is considered, it appears that those from three of the four subvolcanic Kaarnka and Pussy Cat porphyritic rhyolite intrusions at L8 are indeed younger than those from most of the stratigraphically lower units. Thus, all zircons in the subvolcanic Kaarnka and Pussy Cat porphyritic rhyolite intrusions that are older than the 1058 ± 7 Ma age of the youngest stratigraphically lower depositional unit (e.g. L4 Scamp Formation rhyolite, GSWA 195678) must be either inherited grains, or antecrysts. The presence of such zircons appears to be a feature of most (probably all) felsic volcanic units of the Talbot Sub-basin, and the zircons in units from L3, 4, 6, 7, 9 and, in particular, in the subvolcanic Kaarnka and Pussy Cat porphyritic rhyolite intrusions and the Hilda Rhyolite (L11), are dominated by these crystals.

Values of MSWD (mean square of weighted deviates; York, 1966) can be used as a measure of internal consistency of the U–Pb age data. In simple terms, an MSWD of 1 suggests that dispersion can be explained by analytical uncertainties alone, and that if geologically related variation is present, it cannot be resolved within the precision of the individual analyses. Values <1 suggest that analytical uncertainties have been over-estimated, and values >1 can indicate either underestimated analytical uncertainties or another source of uncertainty (typically related to geological complexity) is reflected in the data. However, the actual MSWD value depends on the number of data (Wendt and Carl, 1991; Fig. 14, Table 2). Plotting the MSWD values of weighted mean ages of felsic volcanic rocks from the Talbot Sub-basin (Table 2) on Figure 14 indicates that many of these samples have MSWDs significantly greater than would be expected for a single magmatic zircon population (i.e. with a single crystallization age). This is consistent with the suggestion above that the zircon populations in many of these rocks include abundant inherited grains, or antecrysts.

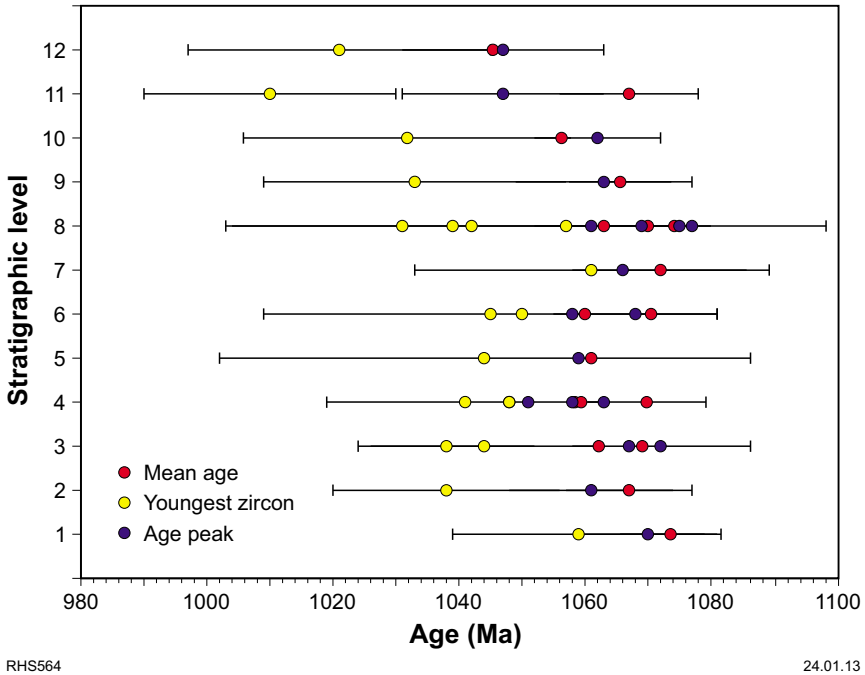

Figure 13. Stratigraphic level (L1–L12) versus U–Pb age for felsic rocks of the Talbot Sub-basin. Red circles indicate the weighted mean 207-corrected $^{238}U/^{208}Pb^*$ age for each sample; yellow circles indicate the 207-corrected $^{238}U/^{208}Pb^*$ date for the youngest zircon; and blue circles indicate the youngest age peak (coherent age component based on at least three analyses). Some stratigraphic levels include multiple samples (refer to Table 2). The difference between the red and yellow circles gives an indication of the proportion of antecrysts within the system. Error bars are at the 2-sigma level.

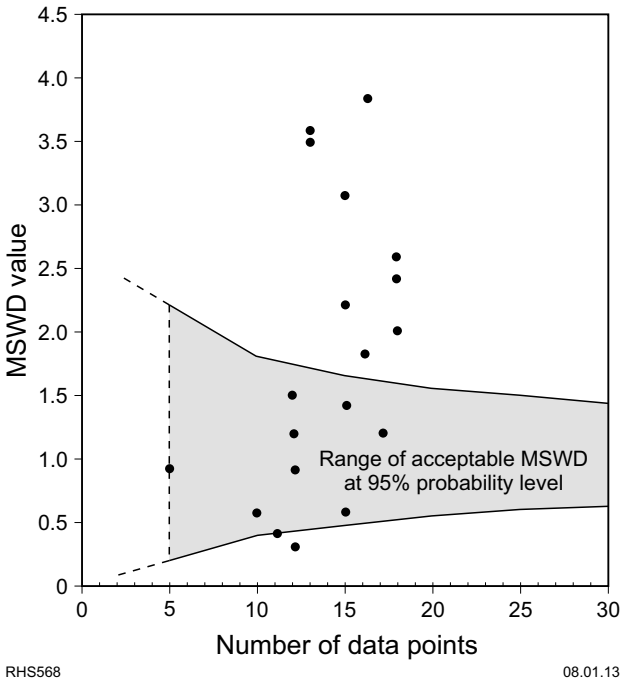

Figure 14. MSWD values (black circles) for weighted mean 207-corrected $^{238}U/^{208}Pb^*$ ages for samples from the Talbot Sub-basin. The range of acceptable MSWD values (shaded area, where the dispersion in the data can be accounted for by analytical uncertainty alone) is after Wendt and Carl (1991). MSWDs for 9 of 19 samples are beyond the range of acceptable values, and are interpreted to reflect the presence of antecrysts within the sampled zircons.

The textures of zircons from volcanic rocks of the Talbot Sub-basin also strongly support the suggestion that many of those zircons have a long and complex crystallization history; similar conclusions are reached based on textures and compositional truncations in plagioclase crystals. Cathodoluminescence images of zircons (Fig. 15) from all of these samples show patterns that reflect complex compositional zonation and textural discordance, including multigeneration core–rim relationships, and deep embayments implying periods of zircon solubility and subsequent overgrowth. Normal oscillatory zoning is also common, and reflects systematic changes in pressure, temperature, and magma composition during zircon crystallization. However, compositional discordance (core–rim relationships and embayments) likely reflects more abrupt and significant changes in magma composition (e.g. mixing, chamber recharge) or pressure–temperature conditions (e.g. mixing, eruption, remobilization or remelting), resulting in zircon dissolution and later redeposition. In the case of volcanic rocks of the Talbot Sub-basin, the complex zircon patterns, and the spread in individual and mean U–Pb zircon ages, indicate multiple zircon dissolution and redeposition events.

The likelihood of abundant inherited zircons or antecrysts renders the weighted mean U–Pb zircon age of each sample an unreliable estimate of its magmatic crystallization age or the age of eruption. This might be particularly true for samples where determined MWSD values are not ~1. However, it might also be true for most of the samples with MSWD values >0.6 or <1.5. Most of these samples yielded the oldest mean ages for stratigraphic levels L8 and below, and all lie within the narrow age interval from 1081 to 1071 Ma. Other samples at the same stratigraphic level show younger mean ages. A plausible explanation for this age distribution is that the source (or source chamber) for those magmas was greatly dominated by material that earlier crystallized within the 1081–1071 Ma age range, and that zircon grains or rims formed at the actual time of eruption were either very rare and/or difficult to analyse (i.e. thin rims).

To estimate the influence of inherited zircons or antecrysts within age components from each stratigraphic level, we also considered the youngest coherent age component (based on at least three analyses) from each sample (Table 2, Fig. 13). This approach suggests that the oldest preserved felsic volcanic rocks of the Talbot Sub-basin had been erupted by at least c. 1077 Ma and that felsic volcanism ended at c. 1047 Ma — a crystallization or depositional duration of about 30 m.y. However, the presence of rhyolite rafts and xenoliths in the Winburn granite, which is distant from the preserved base of the Mount Palgrave Group, indicates that the true base of the rhyolite sequence has not been directly sampled. In addition, the majority of samples (13 of 19) yielded individual zircon dates that are significantly younger (as young as 1010 Ma) than the minimum age peak.

The basement to the Talbot Sub-basin comprises Mesoproterozoic rocks with ages >1150 Ma, with the majority having ages >1300 Ma. The complete absence within the volcanic rocks of zircons with ages >1115 Ma indicates that these magmas have acquired zircons only from the volcanic system itself (including magma chambers). Geochemical data (presented in the next section) indicate that the less-evolved magmas were not saturated with Zr. However, available country-rock and basement components have Nd-isotopic compositions that are significantly less radiogenic than the felsic volcanic rocks; hence, the main reason for the absence of country-rock and basement zircons is that these components simply were not sampled to any significant extent by the magmas.

Furthermore, oxygen isotope signatures ($\delta^{18}O_{VSMOW}$) are similar for all zircons in the volcanic rocks, ranging between 1.4 and 3.6‰. Such values are different to those of zircons in basement rocks in the region (e.g. 5.0 to 7.9‰; Kirkland et al., 2013), and, together with the zircon age data, indicate prolonged periods of zircon growth within the upper crust, under the influence of oceanic or meteoric water (GSWA and University of Western Australia, unpublished data). This, together with the continuous range of zircon ages <1115 Ma, indicates that all zircons within the felsic volcanic rocks are directly related to one or more large and prolonged volcanic systems that were isolated from older crustal

Table 2. Youngest and mean 207-corrected $^{238}U/^{206}Pb$ and youngest peak dates for zircons in rocks from the Talbot Sub-basin[a]

Sample	*Group/Formation*	*Stratigraphic level*	*Youngest single age (Ma)[b]*	*Error (2 sigma)*	*Mean age (Ma)[c]*	*Error (2 sigma)*	*MSWD[d]*	*n*	*Youngest peak[e]*	*No. of analyses in peak*
174662	Winburn granite	1	1059	20	1074	8	1.5	12	1070	11
194800	Eliza Formation	2	1038	18	1067	10	2.6	18	1061	13
195114	Eliza Formation	3	1038	14	1069	8	2.2	15	1072	14
195116	Eliza Formation	3	1044	18	1062	8	2.0	18	1067	13
195115	Scamp Formation	4	1048	18	1070	9	3.5	13	1063	9
195673	Scamp Formation	4	1041	22	1058	8	1.8	16	1051	13
195678	Scamp Formation	4	1048	18	1059	6	0.6	15	1058	15
195230	Mount Waugh rhyolite	5	1044	42	1061	11	0.3	12	1059	11
195001	Lower subvolcanic Pussy Cat porphyritic rhyolite intrusion	6	1045	36	1060	10	0.4	11	1058	11
195723	Kathleen Ignimbrite	6	1050	18	1071	6	1.4	15	1068	13
189580	Kaarnka Group	7	1061	28	1072	14	0.9	5	1066	5
194637	Subvolcanic Kaarnka porphyritic rhyolite intrusion	8	1042	38	1063	11	0.6	10	1061	10
195031	Upper subvolcanic Pussy Cat porphyritic rhyolite intrusion	8	1057	40	1081	9	0.9	12	1077	11
195058	Upper subvolcanic Pussy Cat porphyritic rhyolite intrusion	8	1039	36	1074	7	1.1	25	1075	23
195231	Upper subvolcanic Pussy Cat porphyritic rhyolite intrusion	8	1031	26	1070	11	3.1	15	1069	11
174690	Wururu Rhyolite	9	1033	24	1066	8	2.4	18	1063	14
174691	Thomas Rhyolite	10	1032	26	1056	9	1.2	12	1062	10
185407	Hilda Rhyolite	11	1010	20	1067	11	3.8	16	1047	16
185415	Upper Kaarnka Group	12	1021	24	1045	8	1.2	17	1047	16

NOTES:

(a) All results are derived from 207-correction of U–Pb data in the GSWA geochronology Record series available at <www.dmp.wa.gov.au/geochron/>.

(b) Youngest age refers to the youngest date from an individual crystal.

(c) Mean age refers to the weighted mean date calcuated using all analyses from a sample that are <5% disconcordant, have <1% $f207$, and are not mixtures.

(d) MSWD and n refer to the mean age.

(e) Peak defined as a maximum in age probability that comprises age-probability contributions (at 2-sigma) from 3 or more analyses.

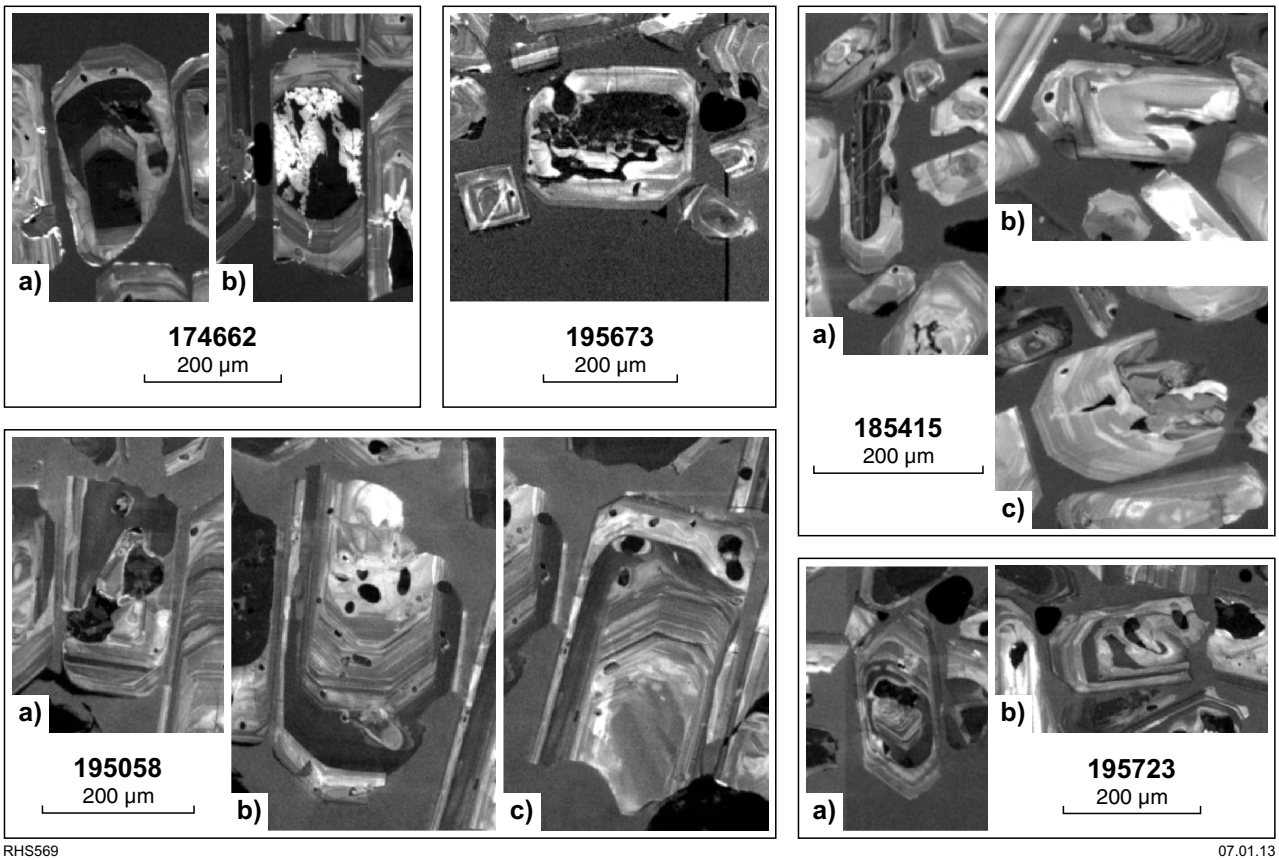

Figure 15. Cathodoluminescence images of zircons from five samples of Warakurna Supersuite felsic volcanic rocks in the west Musgrave Province. Crystals were sectioned at approximately half-grain thickness. GSWA 174662 (a and b): 1074 Ma Winburn granite. a) Zircons show clear evidence of high-U antecrysts, which have undergone variable degrees of dissolution and subsequent overgrowth by oscillatory-zoned zircon (the two components yielded near-identical ages); b) high-U antecryst core with partial replacement by low-U zircon. GSWA 195673: 1058 Ma Scamp Formation, Mount Palgrave Group. Zircons are oscillatory zoned and contain high-U cores (antecrysts) with discordant textural relationships to the rims. GSWA 185415 (a, b, and c): 1045 Ma upper Kaarnka Group. Antecrysts show convoluted boundaries between rims and high-U zoned cores. GSWA 195058 (a, b, and c): 1074 Ma upper subvolcanic Pussy Cat porphyritic rhyolite intrusion. Variable contacts between antecrystic cores and zoned overgrowths range from a) convoluted to b) essentially planar, though with a substantial change in elemental composition, to c) displaying only minor reabsorption of antecrystic core. GSWA 195723 (a and b): 1071 Ma Kathleen Ignimbrite. Convoluted, U-rich antecrystic cores, interpreted to have undergone substantial dissolution prior to growth of new magmatic zircon.

components. Throughout the felsic volcanic history of the Talbot Sub-basin, individual magma batches thermally and mechanically reprocessed earlier unerupted components within the root(s) of the volcanic system(s) — likely including the Winburn granite — contributing to the complex multistage growth of individual zircons. Thus, these zircons can be regarded as antecrysts (rather than inherited crystals) and the true duration of the recycling of cognate components can almost certainly be extended well beyond our conservative about 30 m.y. estimate, as suggested above. The maximum duration of felsic magmatism within the Talbot Sub-basin is about 100 m.y., between the ages of 1116 ± 28 Ma (1σ) for the oldest potential antecryst, and 1010 ± 20 Ma (1σ) for the youngest dated zircon.

For the purpose of this Report, we define 'volcanic system' or 'volcanic chamber system' to include both the volcanic rocks and their variably solidified mid- to upper-crustal chambers. The system is effectively closed to country-rock inheritance and produces a geochronologically continuous record of volcanic and plutonic rocks within a geographically restricted and geologically constrained area.

Although the Mount Palgrave and Kaarnka Groups almost certainly represent several individual eruptive cycles, there is no field evidence that the felsic volcanic units of the Cassidy Group each represent more than one major depositional cycle. However, it is clear that volcanic activity in the Talbot Sub-basin was not strictly

continuous throughout this >30 m.y. period. The repetitive felsic–mafic cycles (at least six in total) and the presence of siliciclastic units between cycles, indicates that volcanic activity was episodic. Nevertheless, the duration of non-eruptive periods cannot be resolved by current dating methods. Moreover, felsic volcanism occurred repetitively, in the same area, and repetitively recycled common, cognate chamber material throughout that period. In these ways, the rhyolites of the Talbot Sub-basin can be regarded as a single very long-lived magmatic system.

Volcanic eruptions are geologically instantaneous events. Collections of eruptive events, representing the duration of volcanic activity attributable to a single volcano or to a particular period or cycle of volcanic activity, are typically measured at the thousand-year scale (e.g. Schmitt et al., 2010; Storm et al., 2011, 2012; Eppich et al., 2012; Stelten and Cooper, 2012), irrespective of tectonic setting. Regional felsic volcanism related to specific tectonic settings may occur in punctuated cycles over periods of up to 50 m.y. (e.g. Bryan et al., 2000, 2008; Bonnichsen et al., 2008; Wolff et al., 2005), and this duration has been suggested as a maximum in the definition of a large igneous province (e.g. Bryan and Ernst, 2008). However, occurrences of this duration are rare, and volcanism is either of regional extent orders of magnitude greater than that of the Talbot Sub-basin and Bentley Basin, or shows a systematic age-progressive migration in the focus of magmatism. The Whitsunday Volcanic Province in eastern Australia, for example, covers an area of $>5 \times 10^5$ km^2, and the Chron Aike Province of South America and Antarctica covers an area of $>3 \times 10^6$ km^2 (Bryan et al., 2000; Pankhurst et al., 2000). Nevertheless, even the minimum estimated duration of volcanism in the Talbot Sub-basin is up to two orders of magnitude longer than volcanism in most geographically restricted regions of felsic magmatism (e.g. Cathey and Nash, 2004).

Geochemistry

Introduction

The felsic rocks of the Warakurna Supersuite, including the subvolcanic intrusive rocks and extrusive and effusive rocks of the Bentley Supergroup, can be divided into at least 25 geochemical groups. These include several geographically isolated subgroups within the Mount Palgrave Group, which possibly reflect distinct eruptive volumes of slightly different composition. However, to reduce data clutter and simplify interpretation of the geochemical data, all individual stratigraphic units within the Mount Palgrave Group (except the Mount Waugh rhyolite) are portrayed by a common symbol in compositional variation diagrams for the Warakurna Supersuite (Figs 16 to 20). Average geochemical analyses are presented in Table 3 and all data and analytical details can be obtained from the WACHEM database <geochem.dmp.wa.gov.au/geochem/>.

In terms of mineralogical classification, the intrusive rocks of the Warakurna Supersuite range from monzogranite to alkali-feldspar granite and alkali-feldspar syenite. Because the felsic volcanic rocks of the Bentley Supergroup typically contain a significant proportion of devitrified glass, modal mineralogical classifications cannot be applied. According to chemical classifications based on variations in SiO_2 and total alkali (K_2O + Na_2O) contents, most of the volcanic rocks are rhyolites. Some of the Kaarnka Group units are trachytes, and lavas of the Hogarth Formation range from basaltic andesite to dacite, trachyte, and rhyolite (Fig. 16). However, the application of this classification scheme to at least some of the geochemical groups might be questionable because there is evidence for mobility of alkali elements. This is most obvious for the highly vitric units, suggesting that the mobility is related to the devitrification process. Consequently, there is a wide range in concentrations of alkalis for very small variations in concentrations of relatively fluid-immobile trace elements such as Nb and Th (Fig. 17). In a similar way, the concentrations of many trace elements show small variations over wide ranges of silica content, suggesting mobility related to silicification. However, other trace element concentrations (e.g. Th, Zr, Nb, Y) show well-developed correlations with silica content, which can be positive or negative (Fig. 19). Silica alteration is, therefore, not a significant factor.

Using the Winchester and Floyd (1977) classification based on variations of the concentrations of the less-fluid-mobile trace elements (Fig. 16) avoids the potential effects of alkali mobility and classifies many of the volcanic rocks as comendites and pantellerites, with fewer rhyolites and rare trachytes (Zr/Ti vs SiO_2; Fig. 16c), or as rhyolites and less common comendites and pantellerites, with rare rhyodacite and dacite (Zr/Ti vs Nb/Y; Fig. 16b). Many of the rocks classified as comendites and pantellerites in Figure 16c are classified as rhyolites in Figure 16b, and vice versa. Comendites and pantellerites represent a specific classification of peralkaline rocks. Notwithstanding the evidence for mobility of alkali elements, there is no evidence that these rocks are of peralkaline affinity (maximum agpaitic coefficient is 0.97). They do not crystallize any strongly peralkaline minerals and there is no regionally correlated peralkaline magmatism. Their geochemical variations, mineralogy, and lithological associations are much more typical of bimodal tholeiitic basalt–potassic rhyolite associations than with the typically more alkaline sodic alkalic associations of Nekvasil et al. (2004). Accordingly, the felsic volcanic rocks of the Bentley Supergroup are referred to here in general terms as rhyolites. Almost all of the geochemical groups are low-silica rhyolite (i.e. <75% SiO_2). However, the Kathleen Ignimbrite and many of the rocks of the Mount Waugh rhyolite can be classified as high-silica rhyolite.

In the terminology of Frost et al. (2001), all of the Talbot Sub-basin granites and volcanic rocks are ferroan (Fig. 16d) and most (at least 18 of >20 geochemical groups) are alkaline-calcic (Fig. 16e); the remainder range from calc-alkaline to alkaline-calcic. All of the rocks belong to a high-K series and all plot in the within-plate field on traditional tectonic discrimination diagrams (e.g. Nb vs Y, Pearce et al., 1984; Fig. 16f), with enriched and ferroan compositions typical of A-type magmas (e.g. Frost et al., 2001). The rocks cover a silica range from 60 to 78.3 wt%,

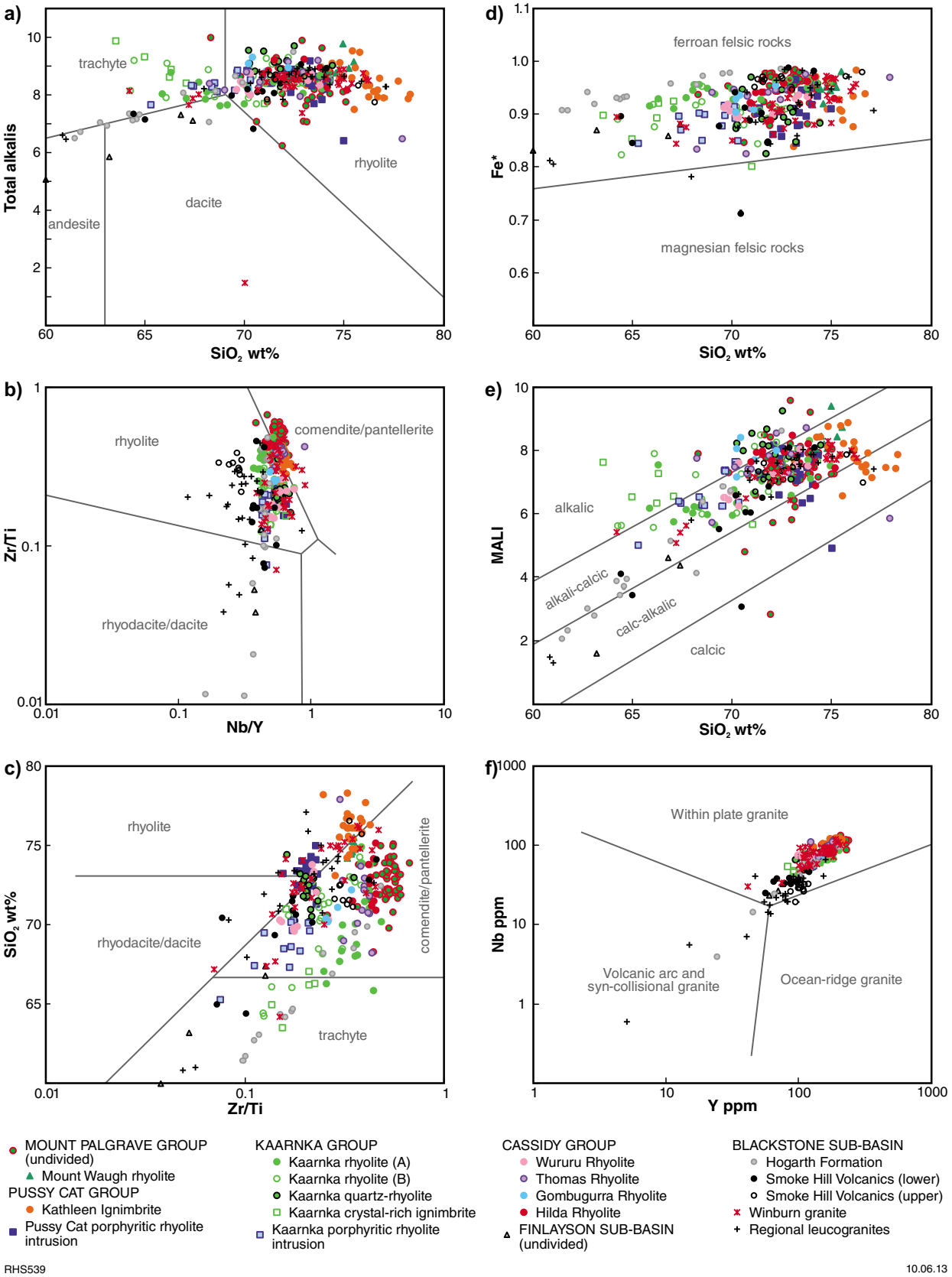

Figure 16. Various geochemical classification diagrams (after Winchester and Floyd, 1977; Frost et al., 2001; Pearce et al., 1984) for felsic rocks of the Warakurna Supersuite. Fe* = FeO/(FeO + MgO) with total Fe expressed as FeO; MALI (modified alkali-lime index) = $Na_2O + K_2O - CaO$.

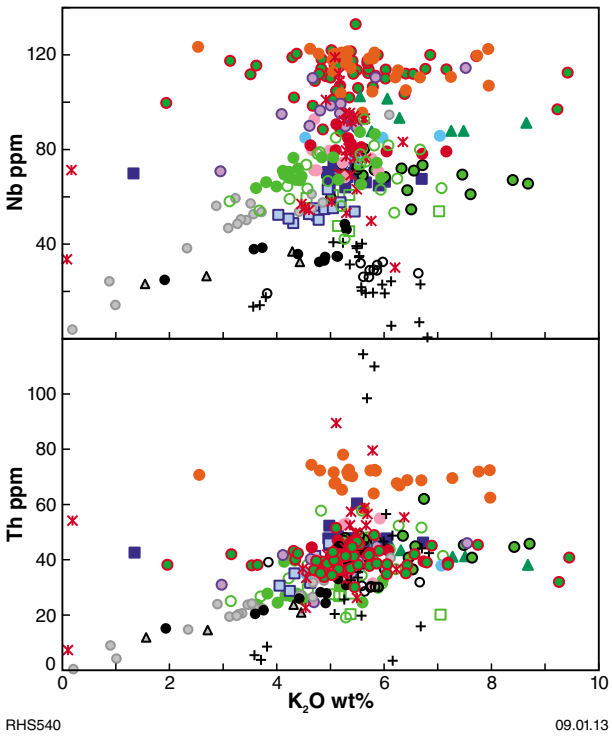

Figure 17. Compositional variation diagrams showing K_2O versus Nb and Th for felsic rocks of the Warakurna Supersuite (symbols as in Fig. 16). Note that for many of the more vitric units (e.g. Mount Palgrave Group and Kathleen Ignimbrite) there is a complete lack of correlation between fluid-mobile elements (e.g. K) and fluid-immobile elements (e.g. Nb and Th).

although individual units show a much narrower range (Fig. 18). For the population in general, and for individual units, increasing SiO_2 content is correlated with decreasing concentrations of TiO_2, Al_2O_3, Fe_2O_3, MgO, CaO, P_2O_5, Ba, and Sr, and increasing concentrations of K_2O, Th, U, and Rb, whereas concentrations of $Na2_O$ remain constant (with a large degree of scatter) or decrease slightly (Figs 18 and 19). Concentrations of Zr and Hf show a general increase up to silica contents of ~70 wt%, corresponding to Zr concentrations of ~500 to 1100 ppm and Hf concentrations of 15 to 30 ppm (Fig. 19). Above 70 wt% SiO_2, concentrations of Zr and Hf decrease significantly for the entire group and for most individual units. Concentrations of Nb, (Ta), and light rare earth elements (LREE) for the entire population show a progressive increase with increasing silica content. However, with increasing silica contents above 70 wt%, Nb (Ta) and LREE concentrations for individual units either remain constant or decrease. Concentrations of middle rare earth elements (MREE) and heavy rare earth elements (HREE) typically remain constant or increase very slightly at silica contents below 70 wt%, but typically decrease at higher silica contents.

The felsic volcanic rocks of the Talbot Sub-basin form part of a classic bimodal association, being interlayered with locally voluminous lenses and flows of basalt and basaltic andesite. These mafic lavas exhibit tholeiitic geochemical trends. Only one unit (the Hogarth Formation of the Blackstone Sub-basin) contains lavas that appear to bridge the compositional gap between basalts and rhyolites. In general, the rocks of the Talbot Sub-basin show close compositional similarities with bimodal volcanic rocks of the Snake River Plain – Yellowstone – High Lava Plains region of western North America. These represent examples of continental rift- and hotspot-related bimodal, tholeiitic basalt to high-K rhyolite associations (e.g. Christiansen and McCurry, 2008).

Blackstone Sub-basin

Lower and upper Smoke Hill Volcanics

Compared to the lower Smoke Hill Volcanics, the upper Smoke Hill Volcanics show a much narrower range of silica concentrations that extends to higher values (71.13 – 76.55 wt% cf. 64.41 – 74.12 wt%), and at equivalent silica contents typically have higher Fe_2O_3 and K_2O contents and lower Al_2O_3 and Na_2O contents. Concentrations of HFSE overlap extensively. However, the upper Smoke Hill Volcanics tend to show slight HREE enrichment, which decreases with increasing silica content, in contrast to a slight increase within the lower Smoke Hill Volcanics. Concentrations of Zr and Hf are also slightly higher in the upper Smoke Hill Volcanics, and decrease with increasing silica content for both lower and upper units. Concentrations of Nb and Ta tend to be lower in the upper Smoke Hill Volcanics than in the lower Smoke Hill Volcanics, leading to distinctly higher La/Nb ratios (3.2 – 4.4 cf. 1.9 – 2.9) and lower Nb/Y ratios (0.3 – 0.2 cf. 0.36 – 0.55; Figs 19 and 20). However, neither Nb nor Ta shows any systematic variations in concentration with either increasing silica content or decreasing Fe_2O_3 content. The upper Smoke Hill Volcanics are also more enriched in Ba (up to 1890 ppm) than other units of the Bentley Supergroup and show significant decreases in Ba concentrations with increasing silica content.

In terms of major element contents, the lower and upper Smoke Hill Volcanics, collectively, overlap extensively the wide range for all other volcanic rocks of the Bentley Supergroup. Possible exceptions include CaO and P_2O_5 contents, both of which appear to be slightly enriched in the lower and upper Smoke Hill Volcanics, at any given silica content. Collectively, the lower and upper Smoke Hill Volcanics are slightly depleted in Th, U, and LREE and significantly depleted in Nb, Ta, and HREE compared to most or all other volcanic rocks of the Bentley Supergroup.

Hogarth Formation

In contrast to all other igneous units of the Bentley Supergroup, rocks of the Hogarth Formation show an extended silica range, from 52.43 to 72.46 wt%, albeit with a gap between 55.55 and 61.45 wt% SiO_2 (Fig. 21). Throughout the extended silica range, geochemical

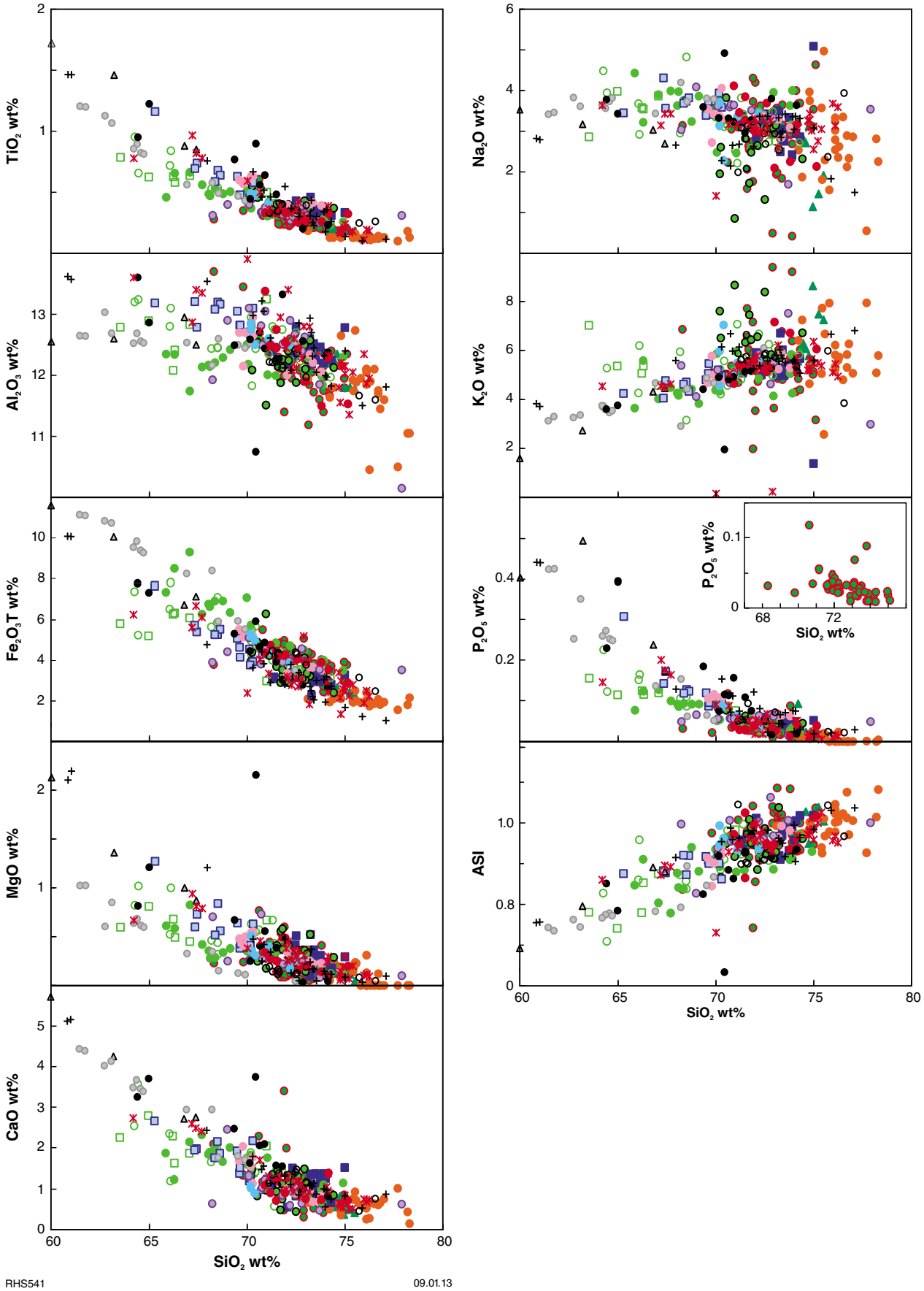

Figure 18. Major element compositional variation diagrams for felsic rocks of the Warakurna Supersuite (ASI refers to Aluminium Saturation Index; symbols as in Fig. 16)

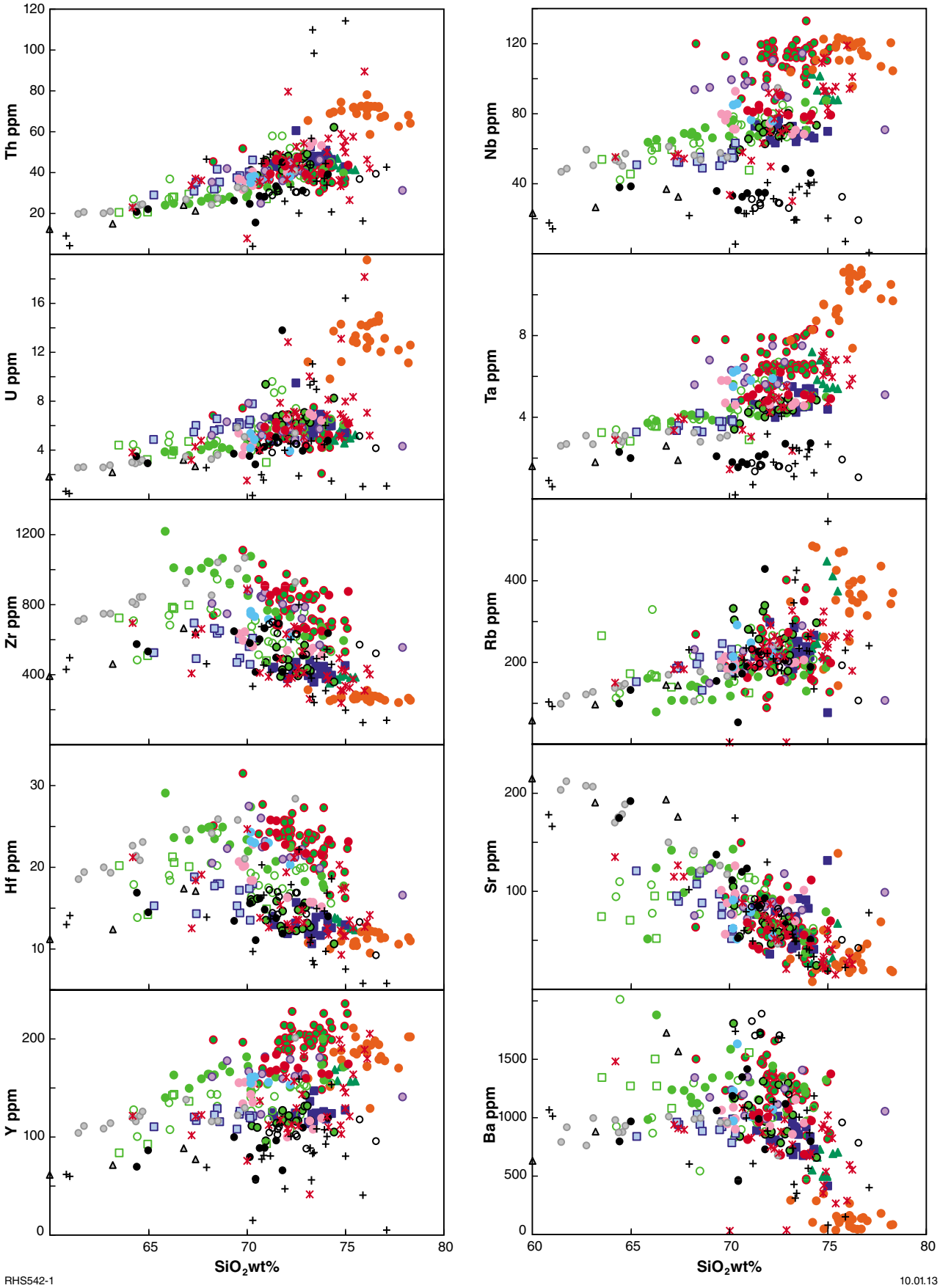

Figure 19. Selected trace element composition and trace element ratio variation diagrams for felsic rocks of the Warakurna Supersuite (symbols as in Fig. 16)

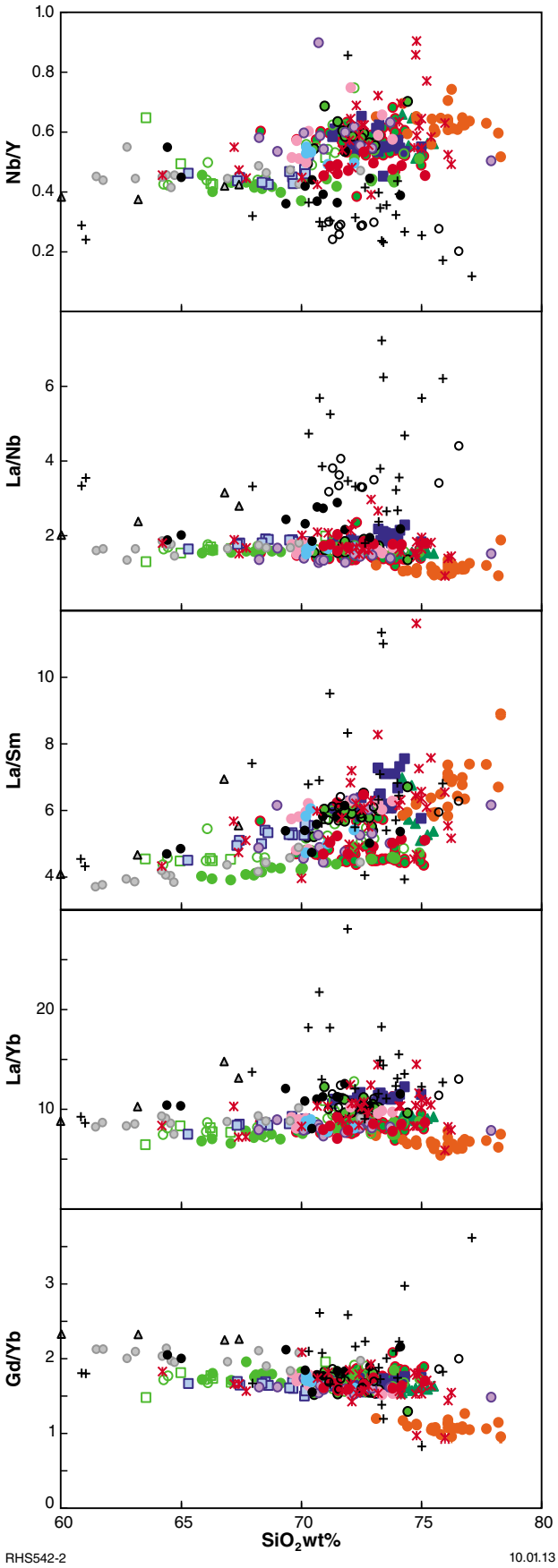

Figure 19. continued

trends are continuous for all major and incompatible trace elements. At above ~65 wt% SiO_2, rocks of the Hogarth Formation overlap the range for other units of the Bentley Supergroup for all major elements except CaO and P_2O_5, which are enriched, and MgO, which is depleted, in the Hogarth Formation (Figs 18 and 21). Continuous increases in Zr (341–1066 ppm) and Hf concentrations with increasing silica content distinguish the Hogarth Formation from most other units of the Bentley Supergroup, although this may simply reflect the less-evolved (silica-rich) compositions of the Hogarth Formation (i.e. they did not reach zircon saturation). Trends for Na_2O, K_2O, and large-ion lithophile elements (LILE) are tightly constrained compared to the many other units of the Bentley Supergroup and reflect a significantly lower degree of element mobility. This is most likely related to the (low) proportion of glass that initially crystallized in these rocks.

Finlayson Sub-basin

Four analyses of andesite and dacite collected immediately northeast of the Jameson G1 intrusion within the Finlayson Sub-basin, range in silica content from 60.0 to 67.4 wt%. They show similar major and trace element trends to those of the Hogarth Formation, but at higher concentrations of TiO_2 and MgO, and lower concentrations of Fe_2O_3, Na_2O, K_2O, and all incompatible trace elements.

Geochemical trends in felsic volcanic rocks outside the Talbot Sub-basin

Blackstone and Finlayson Sub-basins

Compared with the felsic volcanic rocks of the Talbot Sub-basin, those of the Blackstone and Finlayson Sub-basins typically have more extended silica ranges that include a large proportion of lower silica contents (<68 wt%). Exceptions include the rocks of the upper Smoke Hill Volcanics (Blackstone Sub-basin), which have a narrow range of high silica contents (>70 wt%) and rocks of the Kaarnka Group (Talbot Sub-basin), which extend to low silica contents similar to the range for the Hogarth Formation. The rocks of the Blackstone and Finlayson Sub-basins are also notably depleted in Nb, Ta, and HREE concentrations and, at any given silica content, generally also range to lower concentrations of LREE, Th, and U, but have similar to higher concentrations of Zr and Hf than the felsic volcanic rocks of the Talbot Sub-basin. Rocks of the Hogarth Formation, however, again overlap the range for the Kaarnka Group of the Talbot Sub-basin. At lower silica contents, between 60 and 70 wt% SiO_2, the rocks of the Blackstone and Finlayson Sub-basins (including the Hogarth Formation) also have notably higher concentrations of Sr than those of the Kaarnka Group.

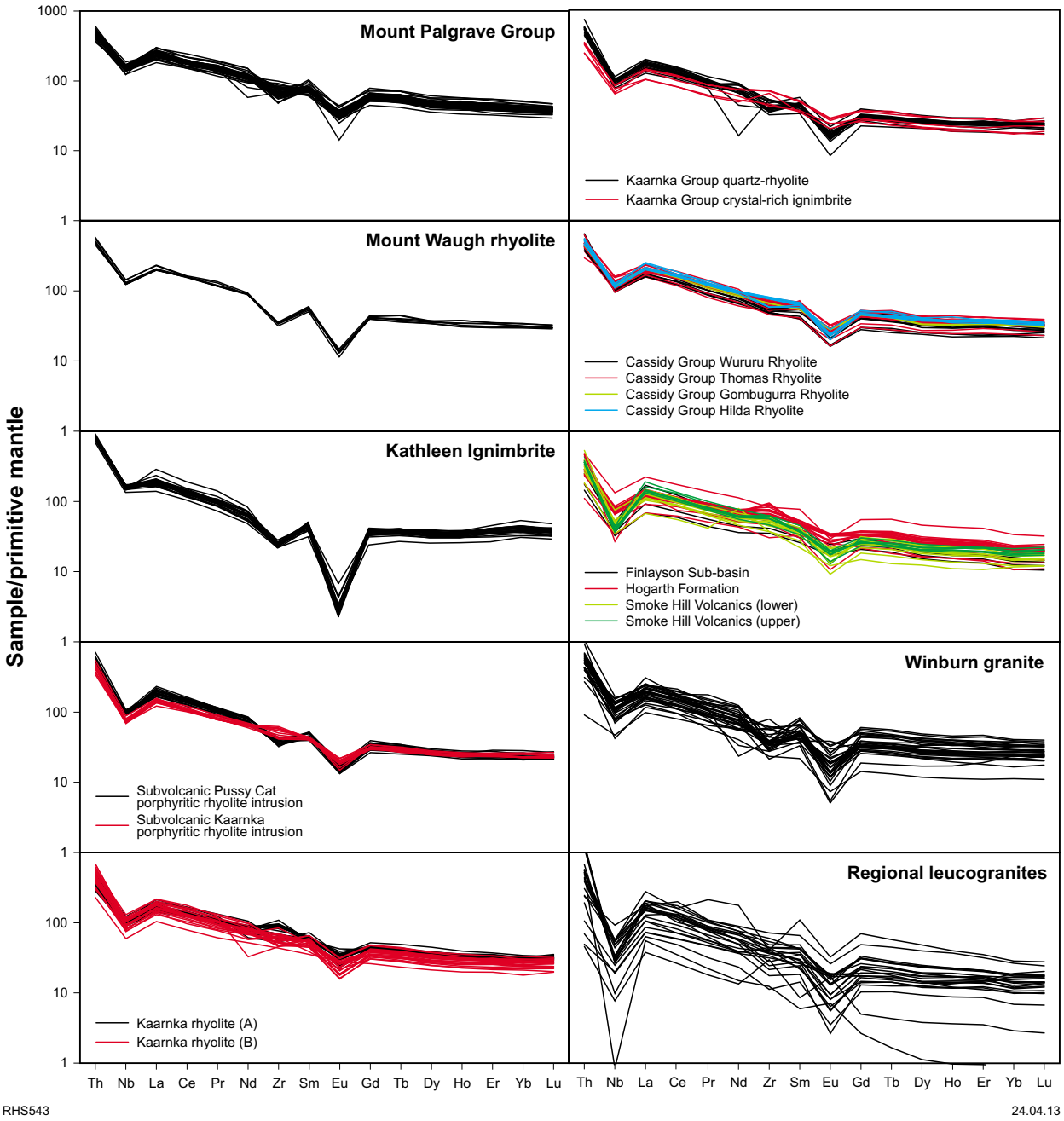

Figure 20. Primitive mantle-normalized incompatible trace element spider diagrams for felsic rocks of the Warakurna Supersuite (normalizations are from Sun and McDonough, 1989)

Table 3. Average geochemical compositions of felsic rocks of the Warakurna Supersuite

	Mount Palgrave Group – Eliza Fm (n = 29)			*Mount Palgrave Group – Scamp Fm (n = 25)*			*Mount Palgrave Group – Mount Waugh rhyolite (n = 7)*		
	Av.	*Min.*	*Max.*	*Av.*	*Min.*	*Max.*	*Av.*	*Min.*	*Max.*
wt%									
SiO_2	72.36	69.80	73.90	73.39	68.30	75.10	74.82	74.20	75.51
TiO_2	0.26	0.21	0.37	0.22	0.17	0.35	0.18	0.18	0.19
Al_2O_3	12.22	11.85	13.45	12.07	11.40	13.70	12.05	11.78	12.35
Fe_2O_3T	4.15	2.45	5.52	3.80	2.93	4.81	2.48	2.27	2.74
MnO	0.10	0.04	0.17	0.08	0.02	0.31	0.03	0.02	0.05
MgO	0.16	0.05	0.45	0.21	0.09	0.60	0.12	0.04	0.21
CaO	1.07	0.48	1.99	0.95	0.31	3.40	0.58	0.37	0.82
Na_2O	3.03	1.75	4.19	2.94	0.40	4.63	2.33	1.12	3.23
K_2O	5.32	3.51	7.16	5.61	1.94	9.42	6.72	5.55	8.65
P_2O_5	0.03	0.01	0.06	0.02	0.01	0.09	0.03	0.02	0.09
LOI	0.65	0.01	2.62	0.16	-0.65	0.62	0.33	0.20	0.42
SO_3	0.01	-0.01	0.08	0.01	-0.01	0.03	0.07	0.01	0.11
Mg#	6.80	2.78	16.66	9.37	5.11	19.81	8.28	3.45	13.52
Fe*	0.96	0.90	0.98	0.94	0.88	0.97	0.95	0.92	0.98
ASI	0.96	0.86	1.04	0.96	0.74	1.08	0.99	0.95	1.04
MALI	7.28	5.72	8.42	7.59	2.84	9.58	8.47	8.03	9.40
ppm									
F	1621	539	2233	1789	443	2676	2359	2020	2798
As	3.3	-0.5	16.0	7.4	4.9	15.0	5.6	-0.5	16.0
Cr	1.1	-1.0	12.0	7.1	4.0	15.0	3.3	-1.0	12.0
Ni	4.7	-1.0	29.0	5.4	3.0	10.0	1.9	-1.0	5.0
V	2.3	-1.0	20.0	5.7	-1.0	21.0	2.0	-1.0	8.0
Sc	3.8	1.4	5.6	2.3	1.0	4.0	1.6	1.0	2.0
Cu	0.6	-5.0	11.3	0.9	-1.0	3.0	3.2	-1.0	7.0
Zn	138.9	14.0	681.0	88.7	5.0	244.0	63.1	13.0	150.0
Sn	13.7	9.9	19.0	13.7	6.0	22.0	12.3	9.5	15.0
Cs	0.6	0.21	2.20	0.5	0.21	2.38	0.7	0.31	1.47
Ba	1251.9	468.00	1655.00	1167.6	704.00	1720.00	614.1	497.00	723.00
Rb	210.9	114.50	309.30	219.8	89.70	401.00	313.8	214.90	447.20
Sr	73.0	36.30	312.45	50.1	16.10	108.50	32.1	22.40	67.30
Pb	26.3	7.60	53.00	19.9	4.00	51.00	16.0	8.94	26.00
Th	41.1	36.55	51.80	39.4	30.46	45.70	43.4	38.47	49.10
U	5.6	3.85	7.46	5.4	2.12	7.52	5.2	4.60	6.00
Ga	30.0	23.70	40.50	32.1	25.60	36.00	25.9	23.20	30.20
Nb	112.0	87.70	133.00	112.9	97.00	122.00	93.2	87.70	102.50
Ta	6.3	4.70	7.90	7.2	6.10	8.30	6.0	5.40	7.20
Zr	835.9	550.0	1110.0	676.5	533.0	781.0	382.4	353.0	400.0
Hf	24.7	21.40	31.50	21.5	16.26	25.50	13.1	12.35	13.85
Y	197.7	165.00	228.00	198.0	148.00	236.00	162.6	155.50	173.00
La	162.5	137.00	207.00	170.3	151.19	205.63	142.6	134.35	159.00
Ce	333.4	268.00	386.00	335.5	283.00	433.00	280.4	274.48	289.00
Pr	41.6	35.00	49.90	42.9	37.00	53.80	33.6	31.98	37.20
Nd	155.0	78.33	189.50	160.5	138.50	205.00	121.4	118.60	126.00
Sm	34.4	28.40	40.40	34.6	27.30	46.00	24.6	22.30	26.51
Eu	5.6	2.39	7.46	5.5	4.18	6.91	2.3	1.91	2.49
Gd	35.3	30.30	44.20	35.8	30.90	46.90	24.7	23.54	26.40
Tb	6.0	5.23	7.67	6.2	5.38	7.74	4.3	3.86	4.85
Dy	34.8	28.80	41.90	36.1	30.40	45.20	26.3	25.08	27.65
Ho	7.4	6.25	9.37	7.5	6.48	9.39	5.6	5.00	6.20
Er	20.8	18.05	26.30	20.8	16.60	26.20	15.7	14.27	16.90
Yb	20.3	17.75	25.50	20.0	16.30	24.90	15.6	14.51	16.90
Lu	2.9	2.46	3.49	2.9	2.42	3.47	2.2	2.12	2.42
T°C (zir)	947	910	976	923	895	958	870	858	878

NOTES: Mg#, magnesium number; Fe* = FeO/(FeO + MgO) with total Fe expressed as FeO; ASI, Aluminium Saturation Index (= mol ratio of Al_2O_3/K_2O+Na_2O+CaO); MALI, modified alkali-lime index (= $Na_2O + K_2O – CaO$); T°C (zir), zircon saturation temperature

Table 3. continued

	Kathleen Ignimbrite (n = 25)			*Subvolcanic Pussy Cat porphyritic rhyolite (n = 19)*			*Kaarnka rhyolite (A) (n = 20)*		
	Av.	*Min.*	*Max.*	*Av.*	*Min.*	*Max.*	*Av.*	*Min.*	*Max.*
wt%									
SiO_2	76.00	73.11	78.30	73.17	71.29	74.99	70.19	65.86	74.91
TiO_2	0.13	0.10	0.19	0.34	0.30	0.46	0.42	0.26	0.66
Al_2O_3	11.77	10.45	12.74	12.40	12.18	12.80	12.19	11.74	12.75
Fe_2O_3T	2.01	1.56	2.51	3.06	2.26	3.41	5.80	3.51	9.30
MnO	0.03	0.01	0.07	0.06	0.03	0.11	0.13	0.03	0.38
MgO	0.18	0.03	0.37	0.29	0.10	0.52	0.34	0.13	0.83
CaO	0.60	0.15	1.02	1.10	0.56	1.51	1.58	0.66	2.32
Na_2O	2.73	0.53	4.97	3.17	2.41	5.08	3.53	2.45	4.42
K_2O	5.76	2.53	7.95	5.18	1.33	6.70	4.69	3.61	5.95
P_2O_5	0.01	0.00	0.03	0.05	0.04	0.06	0.07	0.02	0.13
LOI	1.19	-0.02	3.19	1.13	0.06	2.93	1.24	-0.19	2.99
SO_3	0.01	-0.01	0.03	0.03	0.01	0.11	0.08	0.01	0.27
Mg#	13.62	2.97	25.60	15.56	6.00	24.67	9.96	5.90	14.94
Fe*	0.92	0.84	0.98	0.91	0.84	0.97	0.94	0.91	0.97
ASI	1.00	0.93	1.08	0.97	0.91	1.02	0.89	0.78	0.95
MALI	7.89	6.56	8.88	7.25	4.91	8.17	6.64	5.65	8.31
ppm									
F	3278	317	5457	1900	895	2944	1556	328	2998
As	3.9	-0.5	10.0	3.8	-0.5	13.0	2.2	-0.5	7.0
Cr	7.0	-1.0	10.0	10.2	3.0	26.0	3.4	-1.0	11.0
Ni	3.7	2.0	8.0	4.7	1.0	8.0	2.8	-1.0	7.0
V	6.8	-1.0	13.0	11.9	5.0	25.0	6.8	-1.0	20.0
Sc	1.6	-1.0	2.0	3.9	2.0	5.0	6.9	3.0	11.0
Cu	4.7	-1.0	34.0	5.3	-1.0	13.0	8.8	-1.0	61.0
Zn	54.3	11.0	219.0	67.9	24.0	107.0	159.3	18.0	975.0
Sn	21.2	4.0	127.5	9.7	5.9	15.8	8.2	4.7	13.1
Cs	0.9	0.35	3.15	1.2	0.41	5.22	0.8	0.13	3.03
Ba	134.4	36.00	349.00	805.0	417.00	1030.00	1255.0	966.50	1879.00
Rb	359.5	143.90	484.70	225.1	77.50	299.60	147.4	79.30	193.40
Sr	33.8	7.80	138.70	66.2	35.90	131.40	95.6	36.80	143.00
Pb	33.5	9.00	263.00	23.5	7.96	51.47	22.8	3.99	82.12
Th	69.8	58.73	78.20	46.8	40.29	60.60	31.7	24.07	41.76
U	13.2	9.84	19.55	6.2	4.78	9.51	4.8	3.59	6.37
Ga	27.2	18.40	31.80	23.8	19.60	26.40	27.8	24.70	32.30
Nb	114.8	95.60	123.40	69.1	63.30	77.00	71.4	63.70	87.40
Ta	9.9	7.38	11.30	4.7	3.99	5.80	4.3	3.72	5.60
Zr	272.4	242.0	315.0	421.0	359.0	485.0	879.0	597.4	1218.0
Hf	11.3	9.51	12.80	12.9	10.65	15.70	22.4	17.51	29.09
Y	183.1	128.70	211.00	122.8	113.00	146.70	163.4	139.70	200.00
La	130.8	95.71	197.50	132.1	112.51	159.00	115.9	98.20	146.48
Ce	239.8	186.30	338.00	254.7	213.00	289.00	240.0	215.04	295.13
Pr	27.2	20.17	39.20	29.1	24.64	32.08	29.1	26.57	36.55
Nd	86.6	65.51	113.50	100.6	87.66	115.40	114.3	82.79	142.75
Sm	19.8	13.92	22.60	20.4	17.50	23.18	26.7	24.44	32.08
Eu	0.5	0.38	1.14	2.7	2.23	3.20	5.5	3.87	7.13
Gd	21.3	14.32	24.80	19.6	15.76	23.40	26.4	24.05	30.87
Tb	4.0	2.90	4.43	3.3	2.71	3.73	4.4	3.97	5.31
Dy	25.2	18.78	29.18	19.4	17.55	22.15	27.0	24.64	33.11
Ho	5.6	4.22	6.30	4.0	3.54	4.58	5.5	5.11	6.46
Er	17.9	12.79	21.60	11.8	10.37	13.75	15.8	14.46	17.82
Yb	19.8	15.14	26.30	11.8	10.27	13.95	15.1	13.95	16.80
Lu	2.8	2.16	3.56	1.7	1.59	2.02	2.4	2.11	2.61
T°C (zir)	837	826	851	874	857	890	933	903	966

Table 3. continued

	Kaarnka rhyolite (B) (n = 23)			*Kaarnka quartz rhyolite (n = 18)*			*Kaarnka crystal-rich ignimbrite (n = 6)*		
	Av.	*Min.*	*Max.*	*Av.*	*Min.*	*Max.*	*Av.*	*Min.*	*Max.*
wt%									
SiO_2	70.16	64.26	74.27	72.09	70.21	74.43	66.52	63.52	71.00
TiO_2	0.48	0.24	0.95	0.38	0.25	0.55	0.63	0.50	0.79
Al_2O_3	12.56	11.83	13.24	12.25	11.51	12.85	12.71	12.08	13.25
Fe_2O_3T	4.95	3.11	7.82	3.65	2.41	6.30	5.46	2.99	6.34
MnO	0.09	0.05	0.14	0.06	0.02	0.12	0.08	0.04	0.10
MgO	0.47	0.12	1.02	0.37	0.14	0.58	0.62	0.45	0.81
CaO	1.49	0.58	3.57	1.03	0.45	1.47	2.14	1.62	2.79
Na_2O	3.31	2.20	4.82	2.59	0.84	3.82	3.39	2.56	3.97
K_2O	5.25	3.12	7.07	6.35	5.01	8.68	5.41	4.55	7.03
P_2O_5	0.08	0.02	0.23	0.06	0.03	0.10	0.12	0.08	0.16
LOI	1.05	0.04	2.88	1.38	0.35	2.53	2.75	1.28	4.00
SO_3	0.05	0.01	0.10	0.05	-0.01	0.44	0.18	0.02	0.76
Mg#	15.25	6.01	27.77	16.97	5.24	27.47	19.15	12.75	30.74
Fe*	0.91	0.82	0.97	0.90	0.82	0.97	0.88	0.80	0.92
ASI	0.91	0.71	1.00	0.94	0.87	1.04	0.84	0.74	0.98
MALI	7.07	5.56	8.49	7.90	7.05	9.25	6.66	5.66	7.63
ppm									
F	1 720	563	2 630	1 686	268	2 555	1 162	321	1 706
As	4.2	-0.5	14.0	2.1	1.0	3.9	3.2	-0.5	11.0
Cr	6.6	-1.0	18.0	3.6	-1.0	13.0	9.8	-1.0	16.0
Ni	4.8	-1.0	11.0	3.3	1.0	7.0	6.3	2.0	9.0
V	16.2	-1.0	52.0	11.4	1.0	19.0	23.3	9.0	35.0
Sc	7.3	3.0	14.0	4.9	3.0	9.0	9.0	7.0	10.0
Cu	7.0	-1.0	22.0	7.4	-1.0	80.0	2.6	-1.0	5.0
Zn	98.3	24.0	316.0	59.4	15.0	104.0	38.2	21.0	71.0
Sn	10.4	4.9	28.0	9.2	6.6	14.4	4.9	3.6	6.0
Cs	1.1	0.08	2.95	1.1	0.14	2.87	0.7	0.20	1.54
Ba	1 063.1	536.00	2 013.00	1 020.6	653.00	1 806.00	1 334.7	1 076.00	1 555.00
Rb	206.7	111.00	331.00	256.7	176.50	341.10	173.1	126.00	266.60
Sr	88.3	43.70	138.20	63.6	24.40	104.60	83.5	51.90	114.00
Pb	20.6	6.04	57.00	20.5	8.22	52.00	13.1	6.00	32.00
Th	39.4	19.51	58.00	45.7	36.83	62.25	25.6	20.52	29.49
U	6.0	3.74	9.63	6.4	4.46	9.40	3.9	3.03	4.74
Ga	26.4	23.40	29.90	23.2	19.50	26.30	25.2	21.80	27.20
Nb	69.2	42.20	92.80	68.5	54.70	80.20	54.7	45.50	60.80
Ta	4.6	2.63	6.70	4.4	3.41	4.92	3.3	2.83	3.70
Zr	639.2	486.0	944.0	477.5	360.2	593.6	681.8	482.0	801.0
Hf	18.1	13.86	24.20	14.0	10.64	16.40	18.6	14.22	21.28
Y	134.0	99.90	154.80	118.0	95.50	142.30	114.8	83.20	143.10
La	115.9	71.69	149.00	113.8	86.29	136.10	89.5	70.18	103.40
Ce	228.2	139.60	314.00	231.4	182.21	270.00	177.8	142.10	207.90
Pr	27.3	16.86	36.50	25.8	21.02	31.05	21.1	16.28	24.49
Nd	99.1	44.22	135.50	95.0	21.91	122.60	86.2	66.58	103.00
Sm	22.8	15.69	29.20	19.5	14.88	25.22	19.0	15.55	22.70
Eu	3.9	2.66	5.31	2.7	1.42	3.67	4.2	3.42	4.82
Gd	22.3	15.53	28.70	18.1	13.31	23.26	19.0	15.17	22.35
Tb	3.7	2.52	4.79	3.0	2.31	3.78	3.2	2.46	3.88
Dy	22.5	15.62	28.10	18.9	15.13	23.20	19.3	15.29	22.60
Ho	4.6	3.27	5.87	3.9	3.05	4.79	4.0	3.06	4.71
Er	13.3	9.51	16.30	11.3	8.73	13.87	11.4	8.99	13.68
Yb	13.1	8.82	16.35	11.4	8.71	12.95	11.1	8.41	12.84
Lu	2.0	1.46	2.36	1.7	1.28	2.14	1.7	1.26	2.13
T°C (zir)	903	822	930	881	860	904	888	838	918

NOTES: Mg#, magnesium number; Fe* = FeO/(FeO + MgO) with total Fe expressed as FeO; ASI, Aluminium Saturation Index (= mol ratio of Al_2O_3/K_2O+Na_2O+CaO); MALI, modified alkali-lime index (= $Na_2O + K_2O – CaO$); T°C (zir), zircon saturation temperature

Table 3. continued

	Subvolcanic Kaarnka porphyritic rhyolite (n = 12)			*Wururu Rhyolite (n = 10)*			*Thomas Rhyolite (n = 13)*		
	Av.	*Min.*	*Max.*	*Av.*	*Min.*	*Max.*	*Av.*	*Min.*	*Max.*
wt%									
SiO_2	68.74	65.29	70.30	71.25	69.60	73.79	71.81	68.24	77.90
TiO_2	0.63	0.45	1.16	0.51	0.39	0.63	0.34	0.25	0.40
Al_2O_3	12.98	12.68	13.21	12.43	12.01	12.95	12.42	10.15	13.10
Fe_2O_3T	5.09	3.78	7.66	4.57	3.36	5.53	4.13	3.53	5.12
MnO	0.08	0.05	0.10	0.09	0.05	0.12	0.08	0.03	0.14
MgO	0.62	0.38	1.27	0.41	0.23	0.55	0.30	0.08	0.73
CaO	1.82	1.20	2.66	1.33	0.69	2.03	0.99	0.48	2.45
Na_2O	3.68	3.38	4.30	3.26	2.71	4.05	3.36	1.68	4.08
K_2O	4.74	4.03	5.45	5.12	4.66	5.90	5.08	2.95	7.52
P_2O_5	0.13	0.09	0.31	0.09	0.06	0.12	0.05	0.02	0.07
LOI	1.38	0.18	2.33	0.65	0.03	2.26	1.35	0.00	5.54
SO_3	0.07	0.01	0.15	0.04	0.00	0.07	0.03	-0.01	0.09
Mg#	18.92	13.99	24.75	14.65	10.84	17.68	12.19	4.27	27.49
Fe*	0.88	0.84	0.92	0.91	0.89	0.94	0.93	0.82	0.98
ASI	0.90	0.86	0.92	0.94	0.84	0.99	0.97	0.83	1.06
MALI	6.61	5.00	7.64	7.04	6.24	8.04	7.44	5.72	8.72
ppm									
F	2016	1444	2978	441	261	868	493	-50	1831
As	3.1	0.5	12.0	2.4	-0.5	10.0	1.4	-0.5	6.0
Cr	4.6	-1.0	13.0	7.7	3.0	15.0	3.5	-1.0	10.0
Ni	4.4	-1.0	10.0	4.1	2.0	6.0	3.3	-1.0	7.0
V	22.6	7.0	50.0	21.7	14.0	31.0	8.1	2.0	22.0
Sc	7.1	5.0	12.0	4.3	4.0	5.0	4.4	3.0	6.0
Cu	5.0	-1.0	13.0	-0.6	-1.0	–	12.9	-1.0	119.0
Zn	62.6	28.0	106.0	165.8	54.0	482.0	132.8	26.0	289.0
Sn	8.4	5.9	12.5	10.6	9.0	13.0	12.9	9.0	19.0
Cs	0.8	0.24	1.80	0.7	0.31	1.28	0.7	0.25	1.73
Ba	912.9	779.00	1023.00	980.7	852.50	1149.20	1172.8	984.80	1405.00
Rb	195.4	132.40	247.20	205.0	183.50	243.60	201.1	107.50	291.00
Sr	90.3	51.80	120.80	89.5	56.20	126.00	89.9	72.00	123.50
Pb	14.5	6.86	42.00	31.9	19.13	59.00	37.1	22.84	79.55
Th	36.7	29.08	46.20	41.8	31.80	55.17	38.3	24.99	46.30
U	6.1	4.90	7.81	5.5	3.64	7.01	5.7	4.35	7.86
Ga	26.3	24.20	28.50	25.3	20.00	29.50	26.9	13.50	32.70
Nb	53.9	48.90	63.20	75.2	68.30	92.80	96.4	70.80	114.50
Ta	3.7	3.28	4.70	5.1	4.57	6.30	6.2	5.10	7.50
Zr	574.2	461.0	698.0	590.5	511.0	741.0	760.7	558.0	882.0
Hf	16.5	13.53	18.83	18.4	15.17	22.80	22.0	16.60	27.50
Y	119.1	107.50	128.50	131.7	99.40	155.50	163.3	122.60	181.60
La	98.2	83.82	108.00	124.4	108.78	148.00	138.5	108.00	166.00
Ce	191.7	179.74	216.61	246.6	217.32	278.00	283.5	208.00	334.00
Pr	22.6	21.34	25.10	27.8	23.88	34.50	32.4	22.10	38.90
Nd	87.9	80.80	93.62	103.3	87.73	120.00	123.7	82.10	143.00
Sm	18.8	17.47	19.74	21.5	17.70	24.60	26.3	17.50	32.10
Eu	3.2	2.50	3.71	3.6	2.72	4.69	4.4	3.40	5.45
Gd	18.7	17.41	20.60	22.5	16.66	27.70	27.0	20.20	31.40
Tb	3.1	2.87	3.43	3.8	2.74	5.08	4.6	3.51	5.68
Dy	19.0	18.05	20.70	22.0	17.64	27.60	27.6	20.00	32.50
Ho	4.0	3.76	4.33	4.7	3.62	6.18	5.9	4.50	7.26
Er	11.7	11.08	12.56	13.8	10.71	17.00	17.2	13.90	20.40
Yb	11.5	11.07	12.91	13.6	11.04	16.80	17.0	13.70	20.00
Lu	1.7	1.64	1.97	2.0	1.59	2.44	2.5	1.90	2.91
T°C (zir)	887	868	908	901	886	923	935	905	953

Table 3. continued

	Gombugurra Rhyolite (n = 5)			*Hilda Rhyolite (n = 10)*			*Finlayson Sub-basin dacite (n = 4)*		
	Av.	*Min.*	*Max.*	*Av.*	*Min.*	*Max.*	*Av.*	*Min.*	*Max.*
wt%									
SiO_2	70.82	70.20	72.20	72.58	70.92	75.15	64.35	60.00	67.40
TiO_2	0.43	0.30	0.49	0.31	0.26	0.33	1.23	0.85	1.72
Al_2O_3	12.64	12.50	12.85	12.33	11.50	13.38	12.65	12.50	12.95
Fe_2O_3T	4.76	3.91	5.30	4.03	2.90	4.75	8.89	6.74	11.60
MnO	0.10	0.07	0.15	0.10	0.04	0.15	0.15	0.12	0.19
MgO	0.35	0.17	0.51	0.23	0.10	0.49	1.34	0.87	2.13
CaO	1.02	0.90	1.13	0.93	0.72	1.38	3.90	2.71	5.87
Na_2O	3.17	2.27	3.70	3.09	2.08	4.11	3.10	2.68	3.52
K_2O	5.71	4.53	7.04	5.64	4.63	7.16	3.24	1.55	4.43
P_2O_5	0.07	0.04	0.09	0.03	0.02	0.04	0.33	0.17	0.49
LOI	0.35	0.08	0.47	0.34	0.12	0.60	0.58	0.51	0.64
SO_3	0.02	0.01	0.03	0.03	0.00	0.08	0.03	0.02	0.03
Mg#	12.43	7.93	16.01	9.81	5.13	18.35	22.48	19.42	26.67
Fe*	0.93	0.90	0.95	0.94	0.89	0.97	0.86	0.83	0.88
ASI	0.95	0.93	0.99	0.96	0.86	1.02	0.81	0.69	0.89
MALI	7.87	7.16	8.41	7.81	6.89	8.48	2.44	-0.81	4.60
ppm									
F	–	–	–	784	54	1 440	–	–	–
As	–	–	–	2.2	-0.5	14.0	–	–	–
Cr	8.4	6.0	9.0	6.6	-1.0	14.0	24.0	22.0	26.0
Ni	5.0	5.0	5.0	2.0	-1.0	5.0	12.3	10.0	14.0
V	15.2	6.0	31.0	21.6	-1.0	109.0	50.5	22.0	102.0
Sc	–	–	–	2.8	1.0	4.0	–	–	–
Cu	–	–	–	1.7	-1.0	6.0	20.0	0.0	50.0
Zn	228.0	70.0	499.0	145.8	0.0	243.0	86.5	30.0	151.0
Sn	13.4	12.0	15.0	11.3	7.9	15.0	5.5	4.0	9.0
Cs	0.6	0.44	0.80	0.6	0.40	0.96	0.3	0.09	0.60
Ba	1 178.4	967.00	1 630.00	957.8	673.00	1 371.60	1 197.0	623.00	1 725.00
Rb	233.9	189.50	293.00	216.7	156.00	352.00	111.4	58.10	145.50
Sr	67.6	51.30	91.00	68.7	41.10	111.50	193.8	176.00	215.00
Pb	41.2	33.00	52.00	31.2	21.00	38.00	28.0	19.00	35.00
Th	37.3	35.10	38.20	43.4	39.20	47.30	18.2	12.30	24.10
U	4.7	3.96	5.39	5.5	4.26	6.29	2.5	1.86	3.23
Ga	28.9	26.40	32.20	30.4	24.20	36.30	24.0	22.50	25.20
Nb	81.6	75.90	85.80	81.8	78.20	90.70	29.8	23.20	36.90
Ta	5.9	5.50	6.30	5.3	4.81	6.20	2.0	1.60	2.60
Zr	717.2	617.0	765.0	795.1	652.0	908.0	542.5	393.0	668.0
Hf	22.8	20.30	24.30	23.3	21.50	25.80	14.5	11.20	17.40
Y	156.9	153.00	161.00	170.2	159.50	184.00	74.0	60.60	87.90
La	134.6	127.00	148.50	145.9	132.00	173.00	79.4	46.90	116.50
Ce	278.2	269.00	291.00	297.2	280.95	331.00	157.5	105.00	218.00
Pr	30.9	29.80	32.20	34.2	32.60	38.40	17.9	12.20	23.00
Nd	117.4	113.00	121.00	128.3	118.50	134.00	68.0	48.80	85.70
Sm	25.0	23.80	27.30	27.8	25.20	30.19	14.6	11.50	16.75
Eu	4.4	3.89	4.78	3.9	3.36	4.71	3.4	2.87	4.08
Gd	26.9	25.40	27.80	28.6	26.98	31.20	15.0	12.35	17.65
Tb	4.6	4.44	4.85	4.9	4.45	5.49	2.4	2.05	2.70
Dy	25.2	24.30	27.20	29.0	27.41	30.30	13.0	11.25	14.20
Ho	5.5	5.29	5.70	6.2	5.74	6.96	2.6	2.28	2.92
Er	16.4	15.95	16.80	17.9	16.47	18.85	7.5	6.35	8.35
Yb	16.0	15.45	16.55	17.5	16.37	18.75	6.6	5.32	7.87
Lu	2.3	2.24	2.39	2.5	2.38	2.64	0.9	0.78	1.07
T°C (zir)	925	908	937	940	906	967	854	787	899

NOTES: Mg#, magnesium number; Fe* = FeO/(FeO + MgO) with total Fe expressed as FeO; ASI, Aluminium Saturation Index (= mol ratio of Al_2O_3/K_2O+Na_2O+CaO); MALI, modified alkali-lime index (= $Na_2O + K_2O – CaO$); T°C (zir), zircon saturation temperature

Table 3. continued

	Tollu Group – Hogarth Fm. (n = 18)			*Tollu Group – Smoke Hill Rhyolite (lower) (n = 11)*			*Tollu Group – Smoke Hill Rhyolite (upper) (n = 10)*		
	Av.	*Min.*	*Max.*	*Av.*	*Min.*	*Max.*	*Av.*	*Min.*	*Max.*
wt%									
SiO_2	62.50	46.25	72.46	70.11	64.42	74.12	72.75	71.14	76.55
TiO_2	1.07	0.32	2.74	0.62	0.20	1.22	0.34	0.25	0.41
Al_2O_3	12.71	12.17	14.56	12.54	10.75	13.60	12.11	11.60	12.42
Fe_2O_3T	10.00	3.52	16.48	4.80	2.64	7.78	3.99	2.49	4.49
MnO	0.18	0.05	0.27	0.10	0.04	0.18	0.09	0.03	0.11
MgO	1.44	0.05	8.42	0.64	0.03	2.16	0.13	0.05	0.19
CaO	4.34	0.87	11.70	2.17	0.84	3.75	1.17	0.46	1.46
Na_2O	3.39	1.30	4.19	3.56	2.95	4.92	2.79	1.98	3.93
K_2O	3.28	0.19	6.10	4.46	1.91	5.30	5.66	3.82	6.64
P_2O_5	0.27	0.02	0.70	0.14	0.02	0.39	0.05	0.02	0.09
LOI	1.04	0.02	4.20	0.95	-0.26	2.01	0.73	-0.18	2.75
SO_3	0.04	0.01	0.32	0.02	0.02	0.05	0.03	0.02	0.07
Mg#	15.18	2.52	57.30	17.51	2.15	41.84	6.03	3.61	9.09
Fe*	0.90	0.57	0.99	0.89	0.71	0.99	0.97	0.95	0.98
ASI	0.76	0.60	0.91	0.86	0.63	0.97	0.95	0.90	1.05
MALI	2.34	-10.21	8.62	5.85	3.08	8.10	7.28	6.70	7.87
ppm									
F	826	103	1 534	912	90	2 120	1 116	391	1 892
As	-0.3	-0.5	1.3	-0.3	-0.5	1.9	-0.4	-0.5	1.0
Cr	57.2	-2.0	633.0	31.3	1.0	77.0	26.7	-1.0	54.0
Ni	22.3	2.0	237.0	9.0	3.0	30.0	5.6	1.0	8.0
V	47.5	-3.0	413.0	19.4	-3.0	94.0	1.5	-3.0	9.0
Sc	16.4	-2.0	44.0	8.9	2.0	16.0	5.8	2.0	10.4
Cu	41.8	6.0	201.0	33.4	5.0	84.0	6.0	1.0	11.0
Zn	172.1	70.0	384.0	88.2	36.0	126.0	115.9	82.0	137.0
Sn	6.2	0.6	9.5	5.3	3.9	7.4	4.2	2.4	5.6
Cs	0.8	-0.03	1.52	1.0	0.18	3.65	1.1	0.51	1.73
Ba	799.8	131.60	1 048.00	983.8	459.00	1 413.00	1516.0	779.00	1 890.00
Rb	124.8	3.20	245.60	186.2	53.70	428.10	196.6	107.30	233.70
Sr	174.4	46.50	257.10	109.7	50.70	192.00	75.8	42.30	92.10
Pb	21.3	1.49	41.90	32.4	9.00	47.15	50.3	32.83	98.60
Th	21.7	0.87	41.00	28.7	15.55	45.19	32.1	28.88	39.44
U	3.0	0.12	5.87	4.8	2.87	13.81	4.6	3.84	5.18
Ga	27.4	16.90	40.20	21.4	16.70	25.90	18.8	11.90	23.50
Nb	48.8	3.90	94.70	36.5	24.90	48.50	28.2	19.20	32.50
Ta	2.7	0.15	4.90	2.1	1.55	2.73	1.6	1.06	1.93
Zr	738.4	84.0	1066.0	554.9	417.0	668.0	631.1	518.0	704.0
Hf	19.1	1.91	28.40	14.3	11.09	16.90	15.0	9.25	17.24
Y	110.0	24.40	201.00	86.8	56.60	119.00	103.4	87.50	117.40
La	81.4	7.71	152.30	83.4	46.35	101.00	100.6	84.63	130.00
Ce	171.2	16.91	307.90	165.9	98.02	200.12	192.5	132.60	238.00
Pr	21.6	2.29	38.26	19.4	11.48	23.74	22.4	18.33	27.48
Nd	87.1	10.67	152.40	79.9	62.11	107.60	84.0	68.65	104.00
Sm	20.0	2.83	34.31	15.6	9.79	18.87	16.7	13.45	20.24
Eu	4.8	1.05	5.84	2.7	1.55	3.69	2.8	1.80	3.34
Gd	19.2	3.40	32.73	14.5	8.86	18.83	15.7	12.92	18.02
Tb	3.4	0.54	6.02	2.4	1.40	3.14	2.6	1.96	3.02
Dy	18.8	3.53	33.93	14.3	9.11	17.95	15.9	11.96	18.12
Ho	4.0	0.73	7.09	3.0	1.82	3.76	3.4	2.53	3.81
Er	11.0	2.04	19.92	8.3	5.13	10.63	9.7	6.99	10.65
Yb	9.4	1.88	16.65	7.6	5.74	9.22	9.1	6.49	10.47
Lu	1.4	0.28	2.37	1.2	0.89	1.38	1.4	0.99	1.65
T°C (zir)	858	609	954	878	798	915	913	888	938

Table 3. continued

	Winburn granite (n = 32)			*Regional leucogranite (n = 23)*		
	Av.	*Min.*	*Max.*	*Av.*	*Min.*	*Max.*
wt%						
SiO_2	72.69	64.21	76.24	71.30	59.14	77.10
TiO_2	0.35	0.11	0.97	0.50	0.10	1.55
Al_2O_3	12.47	11.36	13.91	12.60	11.51	13.81
Fe_2O_3T	3.34	1.35	6.69	3.80	1.03	10.40
MnO	0.06	0.01	0.13	0.06	0.01	0.16
MgO	0.31	0.06	0.94	0.50	0.03	2.31
CaO	1.39	0.51	9.16	1.67	0.53	5.57
Na_2O	3.22	1.39	7.20	2.82	1.48	3.41
K_2O	4.98	0.09	6.35	5.52	3.56	6.81
P_2O_5	0.05	0.01	0.20	0.12	0.02	0.48
LOI	1.14	-0.11	3.48	1.05	-0.10	2.71
SO_3	0.01	0.00	0.07	0.05	0.01	0.23
Mg#	14.40	4.88	24.85	15.35	2.72	33.34
Fe*	0.91	0.84	0.97	0.90	0.78	0.98
ASI	0.95	0.73	1.03	0.93	0.74	1.04
MALI	6.82	-7.68	8.30	6.67	0.77	8.06
ppm						
F	2567	124	4451	1598	-50	6088
As	3.2	-0.5	17.0	-0.4	-0.5	0.7
Cr	2.8	-1.0	8.0	10.9	-1.0	37.0
Ni	4.9	2.0	8.0	8.0	-2.0	28.0
V	12.2	-1.0	54.0	28.3	-3.0	156.0
Sc	4.5	1.0	12.0	5.6	-2.0	21.0
Cu	4.7	-1.0	15.0	11.2	-1.0	35.0
Zn	73.4	3.0	140.0	71.3	7.0	118.0
Sn	10.0	2.6	20.0	4.9	0.7	20.3
Cs	1.2	0.12	2.86	1.0	0.06	4.57
Ba	764.9	30.40	1479.00	825.3	79.10	1738.00
Rb	224.5	4.00	328.20	243.3	91.70	545.10
Sr	72.7	15.00	500.70	76.2	18.60	181.50
Pb	26.8	2.13	76.00	41.7	20.87	74.43
Th	44.8	7.74	89.58	41.0	3.90	114.40
U	6.9	1.55	18.16	4.5	0.33	16.43
Ga	25.5	19.10	33.00	20.2	14.70	23.60
Nb	76.9	30.10	119.00	25.9	0.60	65.80
Ta	5.1	1.45	7.20	1.4	-0.10	4.05
Zr	445.0	239.0	890.0	414.7	127.0	803.0
Hf	14.8	9.29	24.69	12.9	5.80	22.18
Y	133.4	41.70	205.20	78.4	5.10	158.70
La	132.0	67.75	212.00	97.1	26.04	191.20
Ce	259.3	141.61	376.90	191.3	46.70	355.20
Pr	29.8	16.02	48.60	21.1	5.00	58.96
Nd	105.3	31.81	168.00	78.3	18.22	240.40
Sm	22.4	9.68	36.70	15.3	2.66	48.73
Eu	3.0	0.85	6.48	2.2	0.45	5.48
Gd	21.8	8.47	36.00	13.8	1.59	41.86
Tb	3.7	1.42	6.05	2.2	0.18	6.24
Dy	22.5	8.68	35.90	13.3	0.83	35.73
Ho	4.8	1.85	7.50	2.8	0.16	6.59
Er	13.6	5.30	22.50	7.7	0.46	16.95
Yb	13.6	5.55	20.00	7.1	0.44	14.10
Lu	2.0	0.81	2.95	1.1	0.07	2.06
T°C (zir)	872	824	925	856	776	945

NOTES: Mg#, magnesium number; Fe* = FeO/(FeO + MgO) with total Fe expressed as FeO; ASI, Aluminium Saturation Index (= mol ratio of Al_2O_3/K_2O+Na_2O+CaO); MALI, modified alkali-lime index (= $Na_2O + K_2O – CaO$); T°C (zir), zircon saturation temperature

Warakurna Supersuite

Leucogranite dykes of the Warakurna Supersuite are widespread and locally abundant in the region to the east of the Talbot Sub-basin. These leucogranites (regional leucogranites in Fig. 16) have no compositional equivalent in the Talbot Sub-basin, but are compositionally very similar to the Smoke Hill Volcanics, and share the same early magmatic age (c. 1078–1070 Ma). Hence, early felsic magmatism east of the Talbot Sub-basin has no compositional equivalent in the Talbot Sub-basin.

Talbot Sub-basin

Mount Palgrave Group

The range of silica contents for rocks of the Mount Palgrave Group is 68.3 – 75.5 wt%. These units are amongst the most vitric units within the Talbot Sub-basin and are likely to be relatively more susceptible to alteration related to devitrification. As previously mentioned, there is clear evidence for mobility of K_2O and Na_2O when these are plotted against the relatively immobile trace element Th (Fig. 17). However, systematic variations of several major element contents (e.g. Fe_2O_3, TiO, and CaO) suggest that silica mobility has not been extreme.

The three formations of the Mount Palgrave Group (Fig. 3) can be geochemically subdivided into four units with successively narrower ranges of silica content (Fig. 18). From stratigraphically lowest to highest these are: the lower Eliza Formation (68.3–72.9 wt% SiO_2), the upper Eliza Formation (71.1–73.9 wt% SiO_2), the Scamp Formation (72.9–75.1 wt% SiO_2), and the Mount Waugh rhyolite (74.2–75.5 wt% SiO_2). The upper Eliza Formation and Scamp Formation can be further subdivided, although several of the constituent units are either very rare (e.g. Mount Palgrave amygdaloidal rhyolite) or are slight compositional variants of limited geographical extent, possibly reflecting distinct eruptive volumes (e.g. units within the Scamp Formation). However, as previously mentioned, the Mount Palgrave Group has not been subdivided based on geochemical analysis (except the Mount Waugh rhyolite) for the purposes of this Report. Nevertheless, an overall trend to slightly more silicic magmatism with decreasing age is evident. This trend correlates with very broad decreases in concentrations of TiO_2, Fe_2O_3, and CaO, at given silica contents, and is generally consistent with the rocks becoming more evolved with decreasing age. However, for most HFSE and REE (including the typically highly incompatible elements Th, Nb, and Ta), concentrations for most individual units of the Mount Palgrave Group tend to be widely scattered, mostly without any clear trend (Fig. 19).

Although the rhyolites of the Mount Waugh rhyolite form the high-silica end of the apparent evolutionary trend for the Mount Palgrave Group, these rhyolites have distinctly lower concentrations of Nb, Ta, and HREE than all other rocks of the Mount Palgrave Group (Fig. 19). They also show distinct decreases in concentrations of Th, Nb, and HREE with increasing silica (or decreasing Fe_2O_3) content.

Cassidy Group

The compositional fields for rocks of the Cassidy Group overlap extensively those of the rhyolites of the Mount Palgrave Group for most major and trace elements. However, rhyolites of the Cassidy Group generally tend to have lower silica contents, and lower concentrations of Zr, Hf, Nb, Ta, and REE. Rhyolites of the Mount Waugh rhyolite (discussed above) are atypical of the Mount Palgrave Group in this respect, having trace element concentrations closer to those of rhyolites from the Cassidy Group.

Individual rhyolite formations within the Cassidy Group are geochemically distinct in terms of trace element concentrations. The rhyolites typically form parallel, or stacked, arrays and, with increasing silica content, show trends of increasing concentrations of Th, decreasing concentrations of Zr, Hf, Sr, and Eu, and constant to slightly decreasing concentrations of Nb, Ta, and REE (Fig. 19).

Kaarnka Group

The Kaarnka Group shows an wide range of silica content from 63.5 to 74.9 wt% (Fig. 18), but almost half of the rocks have silica contents <68 wt%, which is lower than those of all of the other felsic volcanic units of the Talbot Sub-basin. Five compositional units are identified. Unlike the Mount Palgrave and Cassidy Groups, where compositional units typically form discrete stratigraphic entities (i.e. formations), the compositional units of the Kaarnka Group individually dominate specific stratigraphic levels, but typically are also interbedded with, or intrude, each other. Within the Kaarnka Group, quartz-rhyolite is generally the most silica-rich unit and its range of silica content overlaps the lower half of the range for the Mount Palgrave Group. Rocks of the Kaarnka Group rhyolite (A) and rhyolite (B) span almost the entire silica range of the group, whereas the subvolcanic Kaarnka porphyritic rhyolite intrusions and the Kaarnka Group crystal-rich ignimbrites are restricted largely to silica contents <70 wt%.

As for the Cassidy Group, individual units of the Kaarnka Group have trace element trends that form more or less parallel, or stacked, arrays when plotted against silica content. Individual trends parallel those of the group in general and, as silica content increases, so do concentrations of Th, U, Nb, Ta, Y, and LREE, whereas concentrations of Zr, Hf, Eu and Sr decrease and concentrations of M–HREE remain relatively constant or increase slightly.

Rhyolite (A), in particular, and to a lesser extent rhyolite (B), typically have higher concentrations of Zr, Hf, Nb, Ta, and REE than the quartz-rhyolite and subvolcanic Kaarnka porphyritic rhyolite intrusions at equivalent silica content. Both the silica-poor, crystal-rich ignimbrites and rhyolite

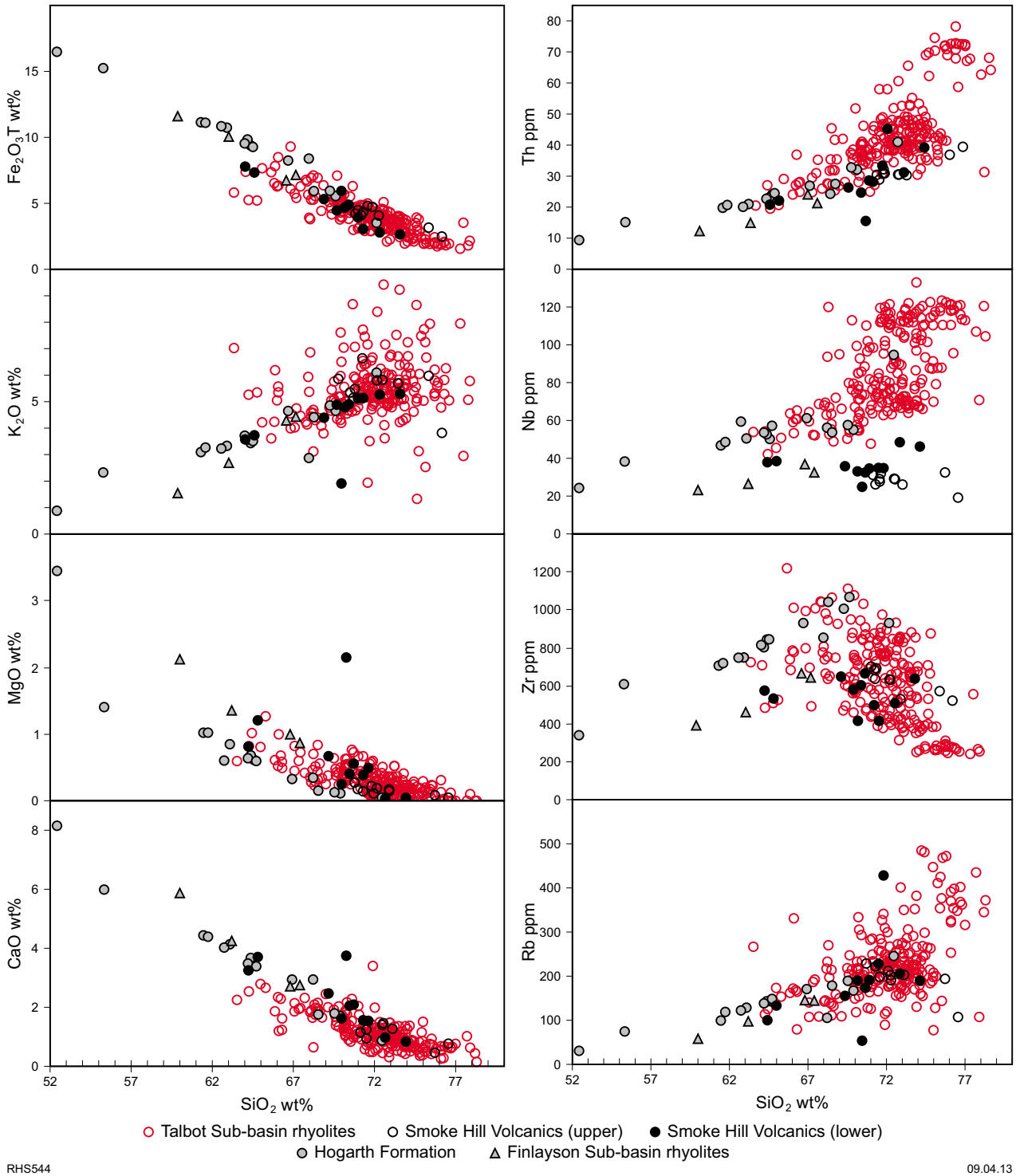

Figure 21. Selected major and trace element contents versus SiO_2 content for rocks of the Hogarth Formation

(B) have very variable trace element concentrations; the crystal-rich ignimbrites cannot be geochemically distinguished from the lower-silica members of rhyolite (B). The compositional variability suggests that both of these might be composite units (i.e. include members of other units), although this is not apparent petrographically. Nevertheless, it is likely that the majority of rocks grouped into these units are directly related to each other, and that the crystal-rich ignimbrites are simply crystal-rich equivalents of rhyolite (B).

Interestingly, the quartz-rhyolite unit consistently lies at the high-silica content end of the range of the silica-poor, subvolcanic Kaarnka porphyritic rhyolite intrusions, and also shows near-complete compositional overlap with the subvolcanic Pussy Cat porphyritic rhyolite intrusions (Figs 18 and 19). Thus, most of the subvolcanic porphyritic rhyolite intrusions throughout the entire geographical and stratigraphic range are compositionally similar, and may be directly related genetically. Additionally, the field encompassing the subvolcanic Kaarnka porphyritic rhyolite intrusions, Kaarnka quartz-rhyolite, and the subvolcanic Pussy Cat porphyritic rhyolite intrusions overlaps that of the main population of granites in the Winburn granite. Several of the granite analyses appear to bridge the compositional gap between this field and the field of the Kathleen Ignimbrite. It is also apparent that a small number of samples of rhyolite (B) consistently overlap the high-silica end of the range for the quartz-rhyolite and subvolcanic Kaarnka porphyritic rhyolite intrusions. Interestingly, these samples lie at the stratigraphic base of the Kaarnka Group, which is poorly exposed in that region, and it is possible that they actually belong to the quartz-rhyolite unit.

Kathleen Ignimbrite

The Kathleen Ignimbrite is a geographically restricted but high-volume ignimbrite with variable, but typically low, crystal content (mainly K-feldspar). Contact relationships indicate little if any significant difference in magmatic age between the ignimbrite and the overlying and underlying subvolcanic Pussy Cat porphyritic rhyolite intrusions despite apparent differences in mean U–Pb zircon age (see Geochronology of the Bentley Supergroup). The ignimbrite is highly siliceous (73.1 – 78.3 wt% SiO_2) and extensive scatter of LILE element concentrations suggests significant element mobility, likely also including silicification. The rocks are characterized by enrichments in Th (to 78 ppm), U (to 19.5 ppm), Nb (to 123 ppm), Ta (to 11.3 ppm), HREE, and Rb, and depletions in Zr, Hf, Ba, Sr, and Eu. In several compositional variation diagrams, the ignimbrite forms an extension of the trend defined by the subvolcanic Kaarnka and Pussy Cat porphyritic rhyolite intrusions, with the gap between these two fields partially filled by samples from the Winburn granite (Fig. 19). In many case, the trend that these combined fields define is distinct from that defined by the combined field for rocks of the Mount Palgrave and Cassidy Groups (e.g. Hf vs SiO_2; Fig. 19). The difference between these two major trends is perhaps best shown by a plot of Th vs Nb (Fig. 22), where the subvolcanic porphyritic rhyolite intrusions, Kathleen Ignimbrite, and most samples of the Winburn granite define a distinct high-Th/Nb trend.

Winburn granite

The compositional range of the Winburn granite overlaps extensively the range of the volcanic rocks. Based on matching distinct compositional groups of granites with volcanic units, it appears that the majority of granites are related to the subvolcanic Kaarnka and Pussy Cat porphyritic rhyolite intrusions, although two other granite groups more closely resemble volcanic units within the Mount Palgrave Group, and single analyses match both the Kathleen Ignimbrite and Mount Waugh rhyolite. These compositional data confirm the suggestion based on age data, cross-cutting field relationships, and lithological variations, that the Winburn granite is a composite granite complex.

Nd-isotopic compositions

All isotopic data discussed here and analytical details can be obtained from the WACHEM database <geochem.dmp.wa.gov.au/geochem/>. Initial Nd-isotopic compositions have been calculated based on best estimates of the crystallization ages of the volcanic rocks (see Geochronology of the Bentley Supergroup). The range of $\varepsilon_{Nd(t)}$ values (+1.24 to –5.20) indicates a juvenile source and define two groups (Figs 23 and 24). Group 1 contains the most samples and includes analyses from all felsic units of the Talbot Sub-basin, and the Hogarth Formation of the Blackstone Sub-basin. These data show a very tightly constrained Nd-isotopic range with $\varepsilon_{Nd(t)}$ values between +1.24 and –0.96, reflecting compositions that are considerably more radiogenic than any known country rock or basement component of the Musgrave Province. Group 2 includes all samples from the Smoke Hill Volcanics of the Blackstone Sub-basin, all samples from the Finlayson Sub-basin, and all leucogranites to the east of the Talbot Sub-basin. This group shows the widest compositional range and the least radiogenic compositions, with $\varepsilon_{Nd(t)}$ values ranging from +0.04 to –5.20.

Petrogenesis

Introduction

A combination of compositional variation patterns, isotopic compositions, geographic range, and lithological associations allows the felsic rocks of the Warakurna Supersuite (Bentley Basin and sub-basins) to be divided into the following seven main types, each probably reflecting a common range of petrogenetic processes:

- the Hogarth Formation (HF magmas)
- the Smoke Hill Volcanics (lower and upper), the dacites of the Finlayson Sub-basin, and leucogranite dykes that intrude the region to the east of the Talbot Sub-basin (the eastern magmas)

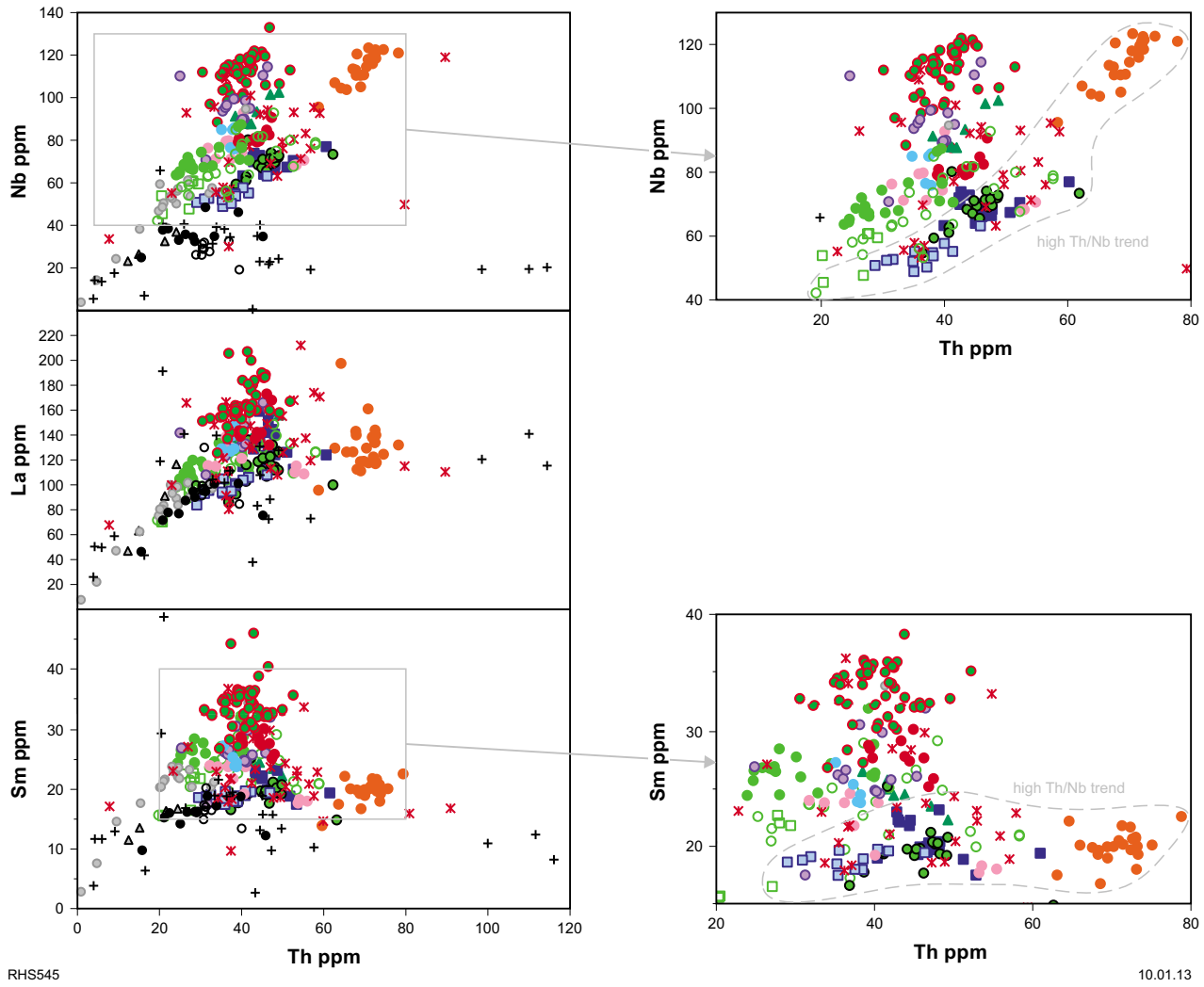

Figure 22. Variations of Th content versus Nb, La, and Sm contents for felsic rocks of the Warakurna Supersuite (symbols as in Fig. 16)

- compositionally restricted rhyolite units of the Eliza and Scamp Formations (Mount Palgrave Group) and of the Cassidy Group
- compositionally extended rhyolite (A), rhyolite (B), and crystal-rich ignimbrite units of the Kaarnka Group
- the Mount Waugh rhyolite
- subvolcanic Kaarnka and Pussy Cat porphyritic rhyolite intrusions and the Kaarnka quartz-rhyolite
- the Kathleen Ignimbrite.

Compositional variations within and between these groups is likely dominated by upper crustal processes that act on the felsic magmas themselves, rather than on their source regions or parental magmas. Lines of evidence that support this suggestion include the lack of isotopic evidence for basement assimilation and of inherited zircon age populations, and the oxygen isotopic signature of zircon within the rhyolites of the Talbot Sub-basin (see Geochronology of the Bentley Supergroup). In the section below, potential source compositions and magma genesis processes are considered. This is followed by a discussion of the potential upper crustal processes of magma modification that distinguish or relate to the seven magma types.

Source regions and parental magma genesis

Felsic magmas that are metaluminous, ferroan, potassic, and anhydrous in intracontinental settings (rifts, hot spots) are commonly associated with comagmatic mafic tholeiitic magmas, representing a classic bimodal magmatic association. In the Talbot Sub-basin, tholeiitic basalt forms ~35% of the outcropping bimodal sequence. However, the relative contributions that crustal and mantle source regions make to intracontinental felsic magmas

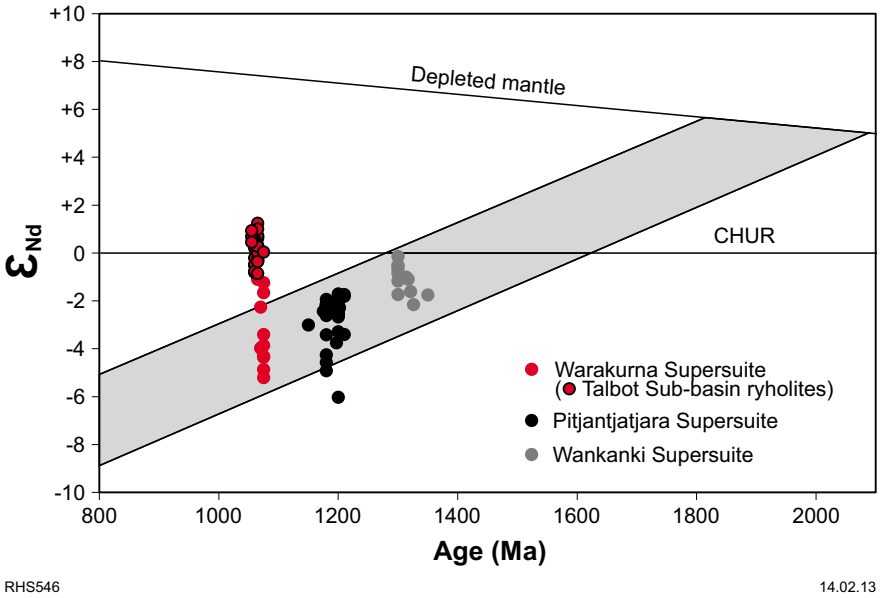

Figure 23. Nd-isotopic evolution diagram comparing felsic rocks of the Warakurna Supersuite with older rocks of the west Musgrave Province. Grey field defines the isotopic evolution of pre-Warakurna Supersuite felsic crust in the Musgrave Province.

varies between the two extremes (e.g. Anderson, 1983; Haapala and Rämö, 1990; Whitaker et al., 2007; Streck and Grunder, 2008). Evaluating the roles of these specific sources asks questions about how continental crust forms and evolves in intracontinental regions. In cases where a significant mantle component can be identified, an additional question is whether the felsic rocks reflect the culmination of a liquid line of descent (e.g. Whitaker et al., 2007; Streck and Grunder, 2008) or are derived from mafic lower crust that underwent low-degree partial melting immediately after emplacement (e.g. Frost and Frost, 1997). The suggestion that metaluminous, ferroan, felsic magmatism is the result of partial melting of lower crust, including juvenile mafic crust, is favoured by the observations that intermediate members are very rarely associated with these magmas (i.e. a truly bimodal association) or that mafic magmas are commonly not present in high enough abundances to represent viable parental magmas through a liquid line of descent (e.g. Whitaker et al., 2007). However, in calc-alkaline systems, a primary reason for a lack of intermediate compositions is that the large compositional changes across the intermediate compositional range reflect small temperature intervals (e.g. Grove and Donnelly-Nolan, 1986), so intermediate magma is naturally poorly represented, and this has been shown to be equally applicable to a tholeiitic liquid line of descent (e.g. Turner and Rushmer, 2009).

The Nd-isotopic data for volcanic rocks of the various sub-basins of the Bentley Basin provide significant constraints on the compositions of source components. The two groups defined based on Nd-isotopic composition show several distinct trends (Fig. 24). Analyses from both groups cover a wide range of silica contents (Group 1, 52.4–76.3 wt%; Group 2, 60.0–76.5 wt%), but although Group 1 shows no correlation between $\varepsilon_{Nd(t)}$ and SiO_2, rocks from Group 2 become generally less radiogenic with increasing silica content. Similarly, Group 1 defines a very narrow range of La/Nb (1.0–2.1) and La/Sm (3.2–6.3) ratios, whereas rocks from Group 2 show a much wider range (La/Nb 1.9–7.2; La/Sm 4.1–11.3) with ratios increasing with decreasing $\varepsilon_{Nd(t)}$. La/Nb ratios are used here as a proxy for crustal material because crust is known to typically have La/Nb ratios much greater than the mantle value of ~1.1 (mid-ocean ridge basalt (MORB); Sun and McDonough, 1989), and igneous processes acting within the crust have little effect on this ratio, except in extreme cases.

Group 1 have Nd-isotopic compositions approximating bulk Earth — chondritic uniform reservoir (CHUR) — and are significantly more radiogenic than any pre-existing crust in the west Musgrave Province (Fig. 23). Hence, they are dominated by a juvenile component that was added to the crust after the end of the Musgrave Orogeny. Sheraton and Sun (1995) drew a similar conclusion, noting that some rhyolites of the Bentley Supergroup showed low La/Nb ratios and Nd-isotopic compositions more radiogenic than all basement components known at that stage. They suggested that these rhyolites may be the result of direct fractional crystallization of basalts, but could not identify any locally available mafic rocks with the appropriate Nd-isotopic compositions, noting that the Mummawarrawarra Basalt (basalt to basaltic andesite) of the basal Kunmarnara Group was not radiogenic enough.

Group 1 may reflect an undepleted (asthenospheric?) mantle source. A more likely scenario is that the juvenile component in these rocks was derived from a relatively depleted mantle source and that Group 1 itself reflects addition of a non-radiogenic crustal component. The

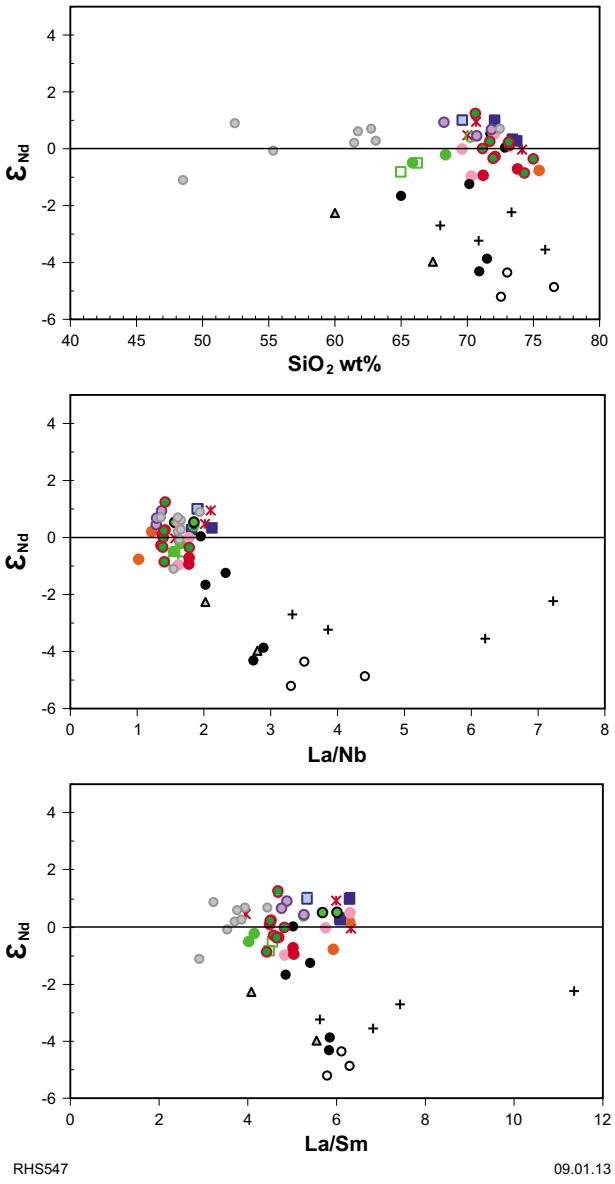

Figure 24. Nd-isotopic variations versus SiO_2 content and La/Nb and La/Sm ratios for felsic rocks of the Warakurna Supersuite (symbols as in Fig. 16)

lack of any correlation between $\varepsilon_{Nd(t)}$ and SiO_2, La/Nb, or La/Sm for Group 1 (Fig. 24) requires that any crustal addition happened at the isotopically juvenile source, or very soon after parental melt production, and that the system then remained closed to any further addition of non-radiogenic material.

Group 2 represents the eastern magmas defined above. The most radiogenic compositions correspond to the least geochemically evolved samples (Fig. 24). These also have compositions similar to bulk Earth and to most of the felsic rocks from the Talbot Sub-basin, and are thus likewise dominated by a juvenile component that was added to the crust since the end of the Musgrave Orogeny. The simplest suggestion here is that the juvenile component in Groups 1 and 2 was the same, or very similar. The observed trends for Group 2, however, indicate that compositional evolution of these rocks was accompanied by progressive incorporation of non-radiogenic, high La/Nb, high La/Sm crustal material. The least radiogenic compositions for Group 2 correspond with time integrated $\varepsilon_{Nd(t)}$ values for known locally exposed crustal sources such as rocks of the Wankanki and Pitjantjatjara Supersuites. Hence, the main difference in Nd-isotopic compositions between Groups 1 and 2 probably reflects the way a mantle-derived mafic magma, or a magma representing a partial melt of such a juvenile component, interacted with non-radiogenic crust.

To further investigate potential links with mantle source regions, the felsic rocks of the Bentley Basin are compared with comagmatic basalts in terms of their isotopic compositions and La/Nb ratios (Fig. 25). Basaltic magmas that are comagmatic with these felsic rocks include the basalts of the Talbot Sub-basin and the dolerites of the regional Alcurra Dolerite suite. The latter have already been shown to have a strong compositional and isotopic overlap with the HF magmas (Howard et al., 2009). In addition, many of the basalt units of the Talbot Sub-basin appear to owe their slightly different compositional characteristics to variable crustal contamination of Alcurra-like magmas (Howard et al., 2009). Thus, on diagrams showing $\varepsilon_{Nd(t)}$ and SiO_2 vs La/Nb, the majority of these basaltic rocks form a rather tight cluster. Because Alcurra Dolerite refers to magmas of specific age (c. 1068 Ma; Howard et al., 2009) within the magmatic age range of the Bentley Basin, this larger group with be informally referred to here as Alcurra-like magmas. The Mummawarrawarra Basalt typically shows outcrop evidence of significant contamination from the underlying basement and from sandstones of the MacDougall Formation (e.g. Evins et al., 2010; Fig. 25). These basalts and basaltic andesites have low $\varepsilon_{Nd(t)}$ values, as noted by Sheraton and Sun (1995), and deviate significantly in composition from the Alcurra-like magmas, forming $\varepsilon_{Nd(t)}$ vs La/Nb trends similar to the eastern magmas. However, not only does the $\varepsilon_{Nd(t)}$ and La/Nb range for the Alcurra-like magmas encompass the range for the comagmatic Talbot Sub-basin rhyolites and the HF magmas, but those rhyolites lie at the less 'crustal' end (i.e. higher $\varepsilon_{Nd(t)}$, lower La/Nb) of that range. This provides very good evidence that the rhyolites and the Alcurra-like magmas are truly cogenetic. It also indicates that the crustal component detected within the rhyolites was probably added to the basaltic parental stage of rhyolite petrogenesis and was sufficiently small that mafic magmas showing considerably more crustal contamination than any of the Talbot Sub-basin rhyolites remained fundamentally basaltic.

Hence, the rhyolites of the Talbot Sub-basin and the HF magmas of the Blackstone Sub-basin provide a clear case of metaluminous, ferroan, felsic magmatism greatly dominated by a mantle-derived source, or parental melt, component. In this respect, these rocks differ from many other high-volume metaluminous, ferroan, hot and dry rhyolite centres, such as those of the Snake River Plains – Yellowstone system, which do appear to require a

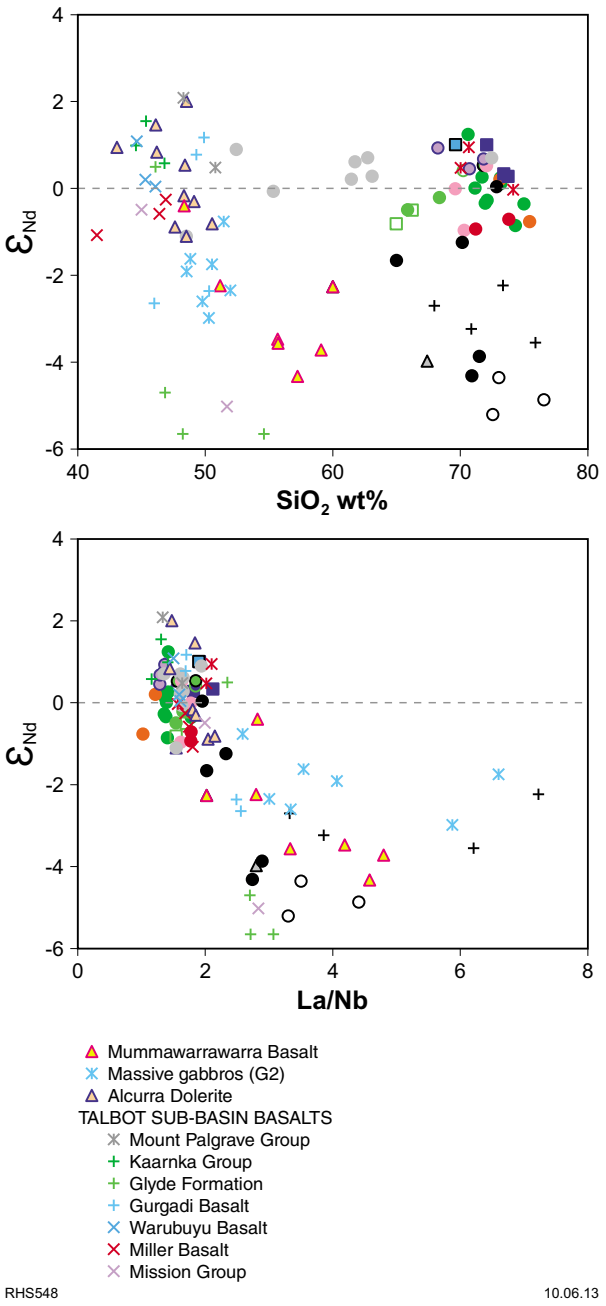

Figure 25. Nd-isotopic variations versus SiO_2 content and La/Nb ratio comparing felsic and mafic rocks of the Warakurna Supersuite (symbols as in Fig. 16 with additional symbols as shown)

significant crustal input. The Smoke Hill Volcanics of the Blackstone Sub-basin and dacites of the Finlayson Sub-basin (eastern magmas) appear more similar to these crustally influenced magmas (but see Eastern magmas).

The question of whether the rhyolites of the Talbot Sub-basin were derived through low-degree partial melting of Alcurra-type rocks at lower crustal depths or are the culmination of a liquid line of descent from Alcurra-type magmas in mid- to upper crustal chambers is difficult to assess because both processes can lead to compositionally similar felsic products. In addition, the compositional gap separating Talbot Sub-basin basalt from rhyolite, at least in terms of silica content, is so large (typically >11wt% SiO_2) that very few additional realistic inferences can be made in terms of their relationship based on geochemistry. However, given the huge volume of felsic magmatism associated with the Talbot Sub-basin (see Discussion – Processes and physical conditions), the extraordinary volume of mafic magma required to produce the rhyolites through a liquid line of descent probably negates this process, at least as the main petrogenetic mechanism in the mid- to upper crust. If fractional crystallization was a significant process, it was likely at lower crustal levels. A preferred alternative is that extensive lower crustal intra- and under-plating of Alcurra-type magmas resulted in a zone of partially melted mafic rocks, and incompletely crystallized Alcurra-type magmas; hence, both fractional crystallization and partial melting contributed to the production of felsic magmas (e.g. Annen et al., 2006; Solano et al., 2012). In any case, the lack of zircon age inheritance suggests that the felsic magmas of the Talbot Sub-basin were emplaced to the subvolcanic level at a stage when they were still undersaturated with respect to zircon. Because Zr appears to have behaved as a compatible trace element in all of these rhyolites (Fig. 19), magma migration was probably not as rhyolite. It is possible that magmas of dacitic composition rose from lower crustal Alcurra-type source regions, and left mid- to upper crustal chambers as rhyolite.

However, the extended range of silica content (52.43 – 72.46 wt%) and the continuity of major and trace element trends distinguish the HF magmas from all rhyolites of the Talbot Sub-basin. For these magmas at least, a continuous liquid line of descent is strongly implicated.

Hogarth Formation

Major element modelling was preformed using the PELE software of Boudreau (1999) to see if fractional crystallization of a primitive Alcurra Dolerite could lead to compositions similar to the HF magmas and, if so, whether the required intensive variables are realistic. PELE is a thermodynamic modelling program that computes equilibrium phase relationships (including mineral and liquid major element compositions) for igneous systems. The parental magma was assumed to be compositionally similar to the most MgO-rich (~9 wt%) samples of Alcurra Dolerite (Table 4). Model runs were isobaric but at a range of assumed pressures (4–10 kbar), initial water contents (0.2 – 0.6 wt% H_2O), and fO_2 with a quartz–

fayalite–magnetite (QFM) to QFM-2 buffer. Features common to most models include liquidus temperatures of ~1260–1280°C, an early temperature range (down to 1180°C) over which olivine alone crystallized, followed by clinopyroxene, plagioclase, and then magnetite. This is consistent with petrographic observations of the Alcurra Dolerite. Most models tend to overestimate SiO_2, Al_2O_3, and CaO and underestimate TiO_2 and Fe_2O_3 within the Alcurra Dolerite itself (Fig. 26), although many of these discrepancies might be related to cumulate olivine within the dolerite. Nevertheless, some models do predict evolved compositions consistent with dacitic HF magmas, particularly at low pressures and low initial H_2O contents. High pressure and high initial H_2O models lead to strongly Al-rich magma compositions because plagioclase is predicted to be destabilized under such conditions. Hence, likely constraints that can be obtained from these models are that if the Alcurra Dolerite and the HF magmas reflect a liquid line of descent (e.g. Howard et al., 2009), as is suggested by the Nd-isotopic data, this process must have occurred at pressures below ~6 kbar and at initial H_2O contents <0.6 wt%. Such constraints are similar to those required to explain potassic rhyolites of the Snake River Plain through extended crystallization of tholeiitic basalt (e.g. Whitaker et al., 2008).

The fractionating mineral assemblages predicted by PELE (i.e. 31% olivine, 56.5% plagioclase, 10% clinopyroxene, 2.5% magnetite) can also account for much of the trace element variation between the primitive Alcurra dolerite and a primitive (~61 wt% SiO_2) HF magma (Tables 4 and 5). However, the calculated concentration of strongly incompatible trace elements (e.g. Th, Zr, Nb, La) is typically underestimated, and these discrepancies cannot be resolved even if the elements are assumed to be perfectly incompatible. Thus, a process other than fractional crystallization must also be involved. Much of the over-enrichment in highly incompatible trace elements actually appears to occur within Alcurra Dolerite itself; these enrichments require an unlikely high degree of crystallization (~80%, compared with ~50% using PELE) to reach silica contents of only 49.0 wt%. To attribute these discrepancies to the dilution effect of cumulate olivine alone requires unreasonable amounts of cumulate olivine in the primitive Alcurra dolerites. However, $\varepsilon_{Nd(t)}$ values and SiO_2 content show a weak negative correlation for the Alcurra Dolerite (Fig. 25) and, consistent with suggestions made above, indicate that these magmas have incorporated small amounts of trace element-rich crustal material at a very early stage, prior to any putative role in the evolution of rhyolitic magmas.

The PELE models also indicate that the amounts of crystallization of a primitive Alcurra dolerite required to achieve compositions similar to a primitive or evolved (~71 wt% SiO_2) HF magma are about 82% and 88%, respectively. Despite the discrepancies noted above in terms of the degrees of crystallization calculated using PELE and trace element variations, the value from PELE for an evolved HF magma is only slightly lower than the estimate based on enrichments of strongly incompatible trace elements (~94% crystallization). This is because elements such as Th, Nb, and Zr appear to be less incompatible at SiO_2 > 60 wt% than in lower silica magmas, as shown by slight inflections in trends in Figure 19, so calculations overestimate the required degree of crystallization from 60 to 71 wt% SiO_2. Regardless, it can be realistically suggested that the HF magmas represent, on average, about 80–85% crystallization of a primitive Alcurra-type magma.

Source and origin of the Alcurra Dolerite

Godel et al. (2011) suggested that the Alcurra-type magmas were derived from a deep (>80 km) asthenospheric garnet-residual source, and acquired much of their enrichment through interaction with previously subduction-modified subcontinental lithospheric mantle. For the possibly similar geological setting of the Mesoproterozoic Midcontinental Rift of North America, Nicholson and Shirey (1990) proposed that basalts compositionally and isotopically similar to the Alcurra-type magmas were derived from an enriched mantle plume with $\varepsilon_{Nd(t)}$ values ~0 and high normalized La/Sm ratios (2 to 3). Again, excursions to strongly negative $\varepsilon_{Nd(t)}$ values were attributed to interaction with subcontinental lithospheric mantle (Shirey et al., 1994). In view of our suggestion that trace element enrichments in the Alcurra-type rocks reflect crustal contamination, the origins of the Alcurra-type magmas themselves deserve brief discussion here.

For Alcurra-type magmas, the least radiogenic sample remains significantly more radiogenic than average known older crustal components, and there is a weak negative correlation between $\varepsilon_{Nd(t)}$ and SiO_2 content. Kirkland et al. (2013) pointed out that known older crustal components of the west Musgrave Province typically have significant enrichments, particularly in HFSE, Th, and LREE, compared to global crustal averages. This means that extremely small degrees of contamination of a basaltic melt will produce significant enrichments in incompatible trace element concentrations and marked changes in Nd- and Hf-isotopic compositions, particularly if assimilation is of low-degree partial melts of crust rather than bulk assimilation. For example, less than 10% bulk contamination of average Pitjantjatjara Supersuite granite into the most primitive Alcurra Dolerite can explain the entire isotopic variation and much of the highly incompatible trace element variation within the Alcurra Dolerite. Assuming assimilation of low-degree (20%) partial melt of an average Pitjantjatjara Supersuite granite rather than bulk assimilation, the required assimilation reduces to <4% (Fig. 27). The amount is considerably lower still (<1%; Fig. 27) if we take into account the suggestion that Alcurra Dolerite samples, even at 49.0 wt% SiO_2, have undergone up to 50% crystallization (estimated in the PELE models) of the most primitive Alcurra Dolerite — which would have considerably enhanced the signal of assimilation. This amount of assimilation, however, is slightly less than that required to satisfy the isotopic variations, and might reflect a wide range of lower crustal compositions, or suggest that the process of crustal contamination within a lowest crustal underplate zone, or hot zone, was not directly linked to the crystallization state of the mafic magmas. In any

Table 4. Geochemical data used in major and trace element modelling

	Primitive Alcurra Dolerite (average of GSWA samples 190253 and 183849)	*Primitive Hogarth Formation (average of GSWA samples 185342 and 185329)*	*Average Wankanki Supersuite*	*Average Pitjantjatjara Supersuite*
wt%				
SiO_2	47.53	61.60	67.54	67.17
TiO_2	1.25	1.20	0.51	0.83
Al_2O_3	15.89	12.65	14.94	13.88
Fe_2O_3T	13.09	11.12	3.95	5.17
MgO	9.18	1.02	1.34	0.78
MnO	0.18	0.21	0.09	0.09
CaO	9.07	4.41	3.38	2.74
Na_2O	2.49	3.43	3.36	2.85
K_2O	0.69	3.18	4.01	4.99
P_2O_5	0.18	0.42	0.15	0.31
ppm				
Cr	228.0	17.0	22.7	8.8
Ni	284.5	5.0	11.4	4.8
V	190.5	6.5	56.2	33.9
Sc	20.5	16.5	10.5	11.2
Cu	93.5	49.5	9.5	6.2
Zn	96.0	195.0	48.2	94.2
F	326.0	1 020.0	614.7	1 212.6
Ba	252.0	891.5	1 098.3	1 107.8
Sr	238.3	216.3	288.6	195.3
Rb	15.8	112.3	135.6	229.8
Cs	0.1	0.8	0.5	0.8
Pb	4.0	32.5	28.0	47.9
Th	1.1	20.3	16.4	42.5
U	0.4	2.6	1.3	3.9
Ga	19.7	28.1	18.2	21.9
Nb	6.8	47.7	8.3	25.5
Ta	0.3	2.6	0.4	1.3
Zr	122.0	715.5	191.1	453.4
Hf	3.3	19.0	5.7	14.2
Y	22.8	107.2	27.7	79.6
La	11.8	77.8	41.4	112.7
Ce	26.3	173.6	80.0	232.0
Pr	3.7	21.9	8.7	26.5
Nd	15.8	89.1	31.2	98.2
Sm	4.0	20.9	5.9	18.5
Eu	1.5	5.4	1.5	2.9
Gd	4.4	19.5	4.9	15.4
Tb	0.7	3.5	0.8	2.4
Dy	4.3	18.5	4.5	13.9
Ho	0.9	4.0	0.9	2.8
Er	2.4	11.1	2.7	7.7
Yb	2.1	9.2	2.5	6.5
Lu	0.3	1.5	0.4	1.0

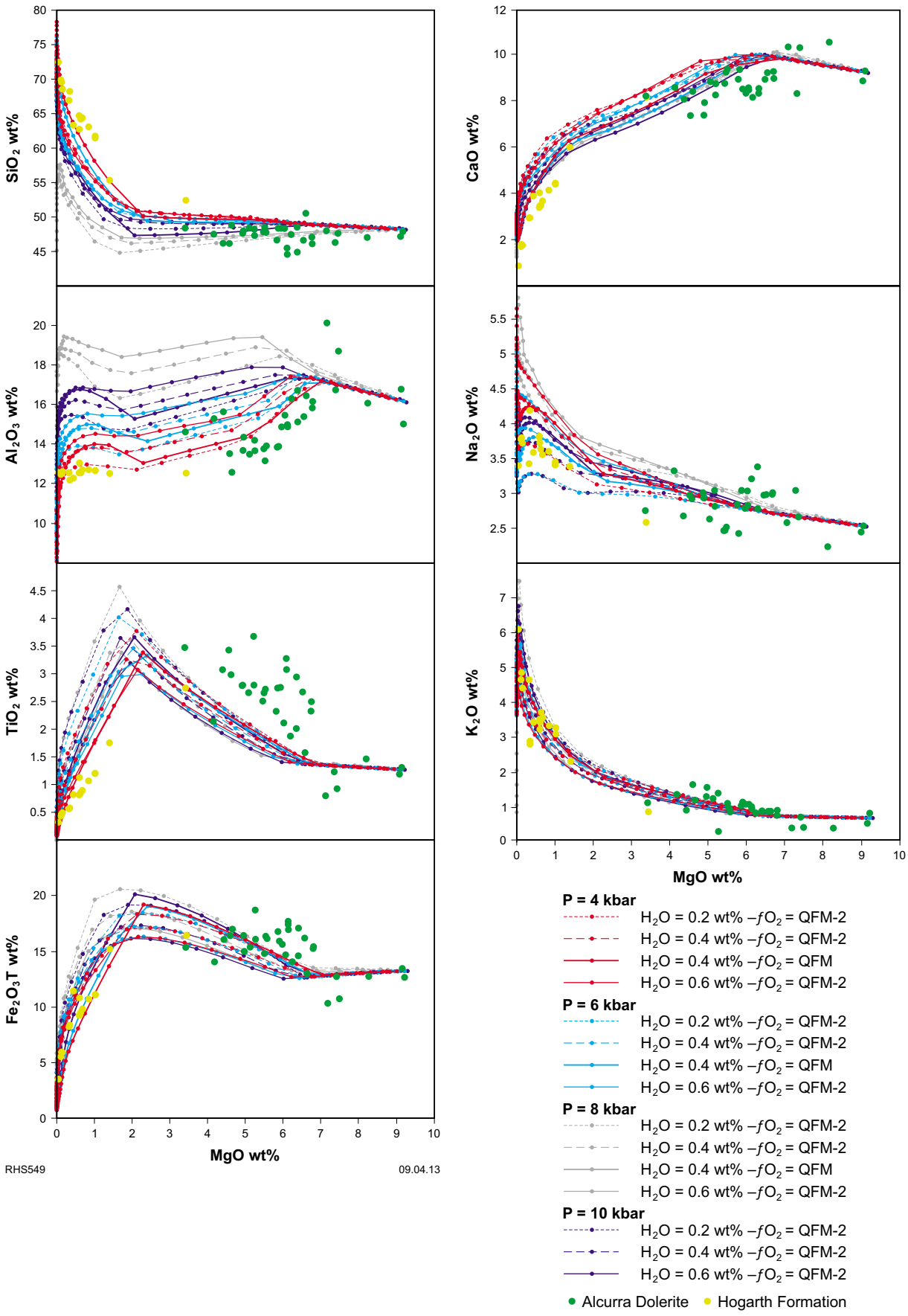

Figure 26. PELE models for the Alcurra Dolerite and Hogarth Formation. Lines show modelled magma compositional evolution under the specified conditions (pressure, wt% H_2O, and $ƒO_2$) in temperature increments of 20°C (dots on lines).

Table 5. Results of trace element modelling

Trace elements	*Primitive Alcurra Dolerite*	*Fractionating assemblage (distribution coefficients – D)[a]*					*Derived liquid composition at F = 0.18[c]*	*Expected concentrations (primitive Hogarth Fm dacite)*	*Difference*
		Olivine	Plagioclase	Clinopyroxene	Magnetite	Bulk D			
		Proportion[b]							
		0.308	0.564	0.103	0.026				
	(ppm)						(ppm)	(ppm)	(%)
Th	1.1	0	0.05	0	0	0.03	5.8	20.2	29
Zr	122	0.17	0	0.13	0.9	0.09	582.1	715.1	81
Nb	6.8	0	0.05	0.03	0.84	0.05	34.5	47.7	72
La	11.8	0	0.17	0.1	0.03	0.11	54.8	77.8	70
Gd	4.4	0	0.05	0.59	0.11	0.09	20.8	19.5	106
Yb	2.1	0.04	0.04	0.59	0.13	0.10	9.9	9.2	108
Sr	238	0	2.27	0.19	0	1.30	142.3	216.2	66
Ba	252	0	0.38	0.02	0.03	0.22	964.7	891.0	108

NOTES: (a) Average values (basalts) from GERM <www.earthref.org/GERM>
(b) From PELE model results
(c) F = proportion of melt remaining (i.e. F = 0.18 after 82% crystallization)

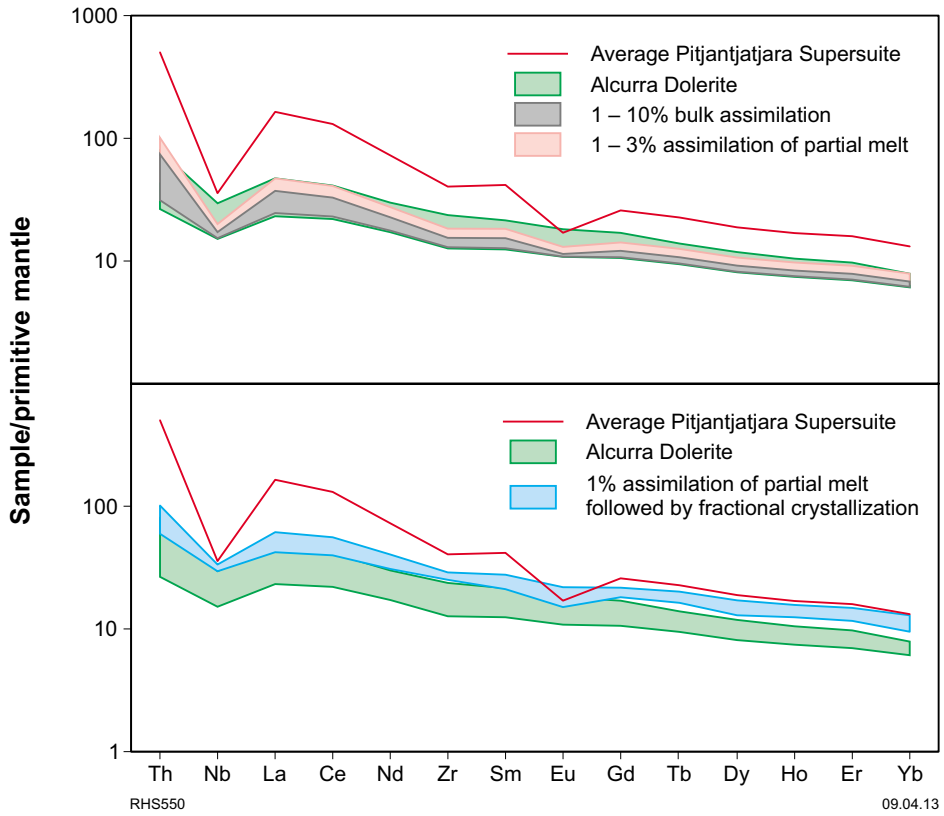

Figure 27. Trace element modelling of contamination in the Alcurra Dolerite. Fractional crystallization (lower panel) assumes ~50% crystallization of primitive Alcurra Dolerite (from PELE modelling) with a fractionating assemblage of 30% olivine, 50% plagioclase, and 20% clinopyroxene (see text for further details). Normalizations are from Sun and McDonough (1989).

case, such low degrees of contamination explain why correlations between $\varepsilon_{Nd(t)}$ and SiO_2 are only weak.

The inference that the Alcurra-type magmas are high-pressure melts (Godel et al., 2011) was based on their high La/Yb ratios. However, although the Alcurra-type rocks have La/Yb ratios between 5 and 9.7, these are not accompanied by depletions in Yb concentrations (average 3.34 ppm) with respect to MORB and are better explained by minor crustal contamination, as demonstrated here. Thus, there is no evidence for a deep mantle source, nor is there any need for interaction with enriched subcontinental lithospheric mantle. Indeed, as mentioned earlier, prolonged UHT metamorphism throughout the proceeding Musgrave Orogeny required near or complete removal of the subcontinental lithospheric mantle.

If available crustal contaminants are systematically subtracted from the most primitive Alcurra Dolerite to the point where chondritic La/Nb ratios of ~1 (Sun and McDonough, 1989) are achieved, La/Sm ratios still remain slightly above chondritic values (Fig. 28). PELE models show that at this stage olivine is the only liquidus phase, so fractional crystallization will have little effect on incompatible trace element ratios. The elevated La/Sm ratios are therefore likely to reflect primitive magma compositions. The effect on Nd-isotopic values would be to move to slightly more radiogenic compositions, but it appears unlikely that the mantle source was significantly depleted. Thus, the Alcurra-type magmas were most likely derived from melting of a slightly depleted to undepleted mantle source at relatively shallow levels (<80 km) and have undergone early and very minor (<4%) contamination with highly enriched crustal material.

Eastern magmas

Representatives of the eastern magmas are restricted to areas east of Talbot Sub-basin. Their most diagnostic features include generally high La/Nb and Th/Nb ratios (Figs 19 and 22). Increasing La/Nb ratios are strongly correlated with increasing silica content, increasing La/Sm ratios, and decreasing $\varepsilon_{Nd(t)}$, trends that are absent for all other felsic units. The most radiogenic sample is isotopically similar to the HF magmas and also has similarly low La/Nb ratios (Fig. 24). As suggested above, Nd-isotopic data suggest that parental eastern magmas were likely derived either from primitive HF magmas, or from a similar Alcurra–HF magmatic association, but subsequently evolved within a system open to progressive incorporation of non-radiogenic, high La/Nb, high La/Sm crustal material. Thus, on a range of compositional variation diagrams employing incompatible trace elements (and ratios thereof) and Nd-isotopic compositions, the eastern magmas are consistently displaced from magmas of the Talbot Sub-basin and the HF magmas, and fall within the fields of known locally exposed crustal sources such as rocks of the Wankanki and Pitjantjatjara Supersuites.

However, at equivalent values of La/Nb, SiO_2, and Th, the eastern magmas are typically significantly depleted in Nb, Ta, Zr, Hf, and HREE (Figs 19 and 29). These depletions might suggest that the mafic parental magmas became contaminated with crustal material at a late stage, but this does not explain why the concentrations of other incompatible trace elements, such as Th, U, and LREE, are similar in both the HF and eastern magmas at similar SiO_2 contents (Fig. 19). Either the crustal component or

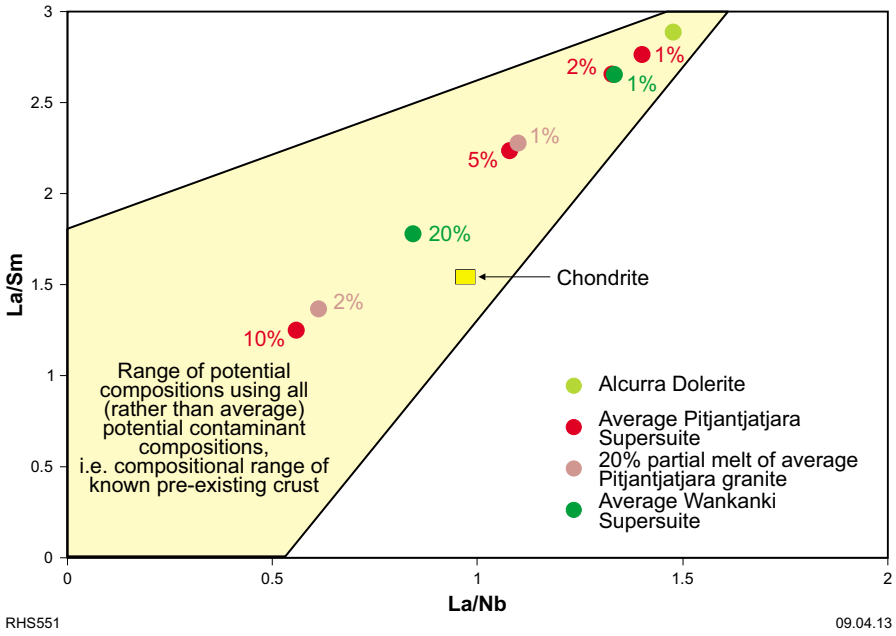

Figure 28. Trace element modelling of compositions of potential sources of the Alcurra Dolerite. The dots show the effect of removing the specified percentages of various potential contaminants from a primitive Alcurra Dolerite magma (see text for details).

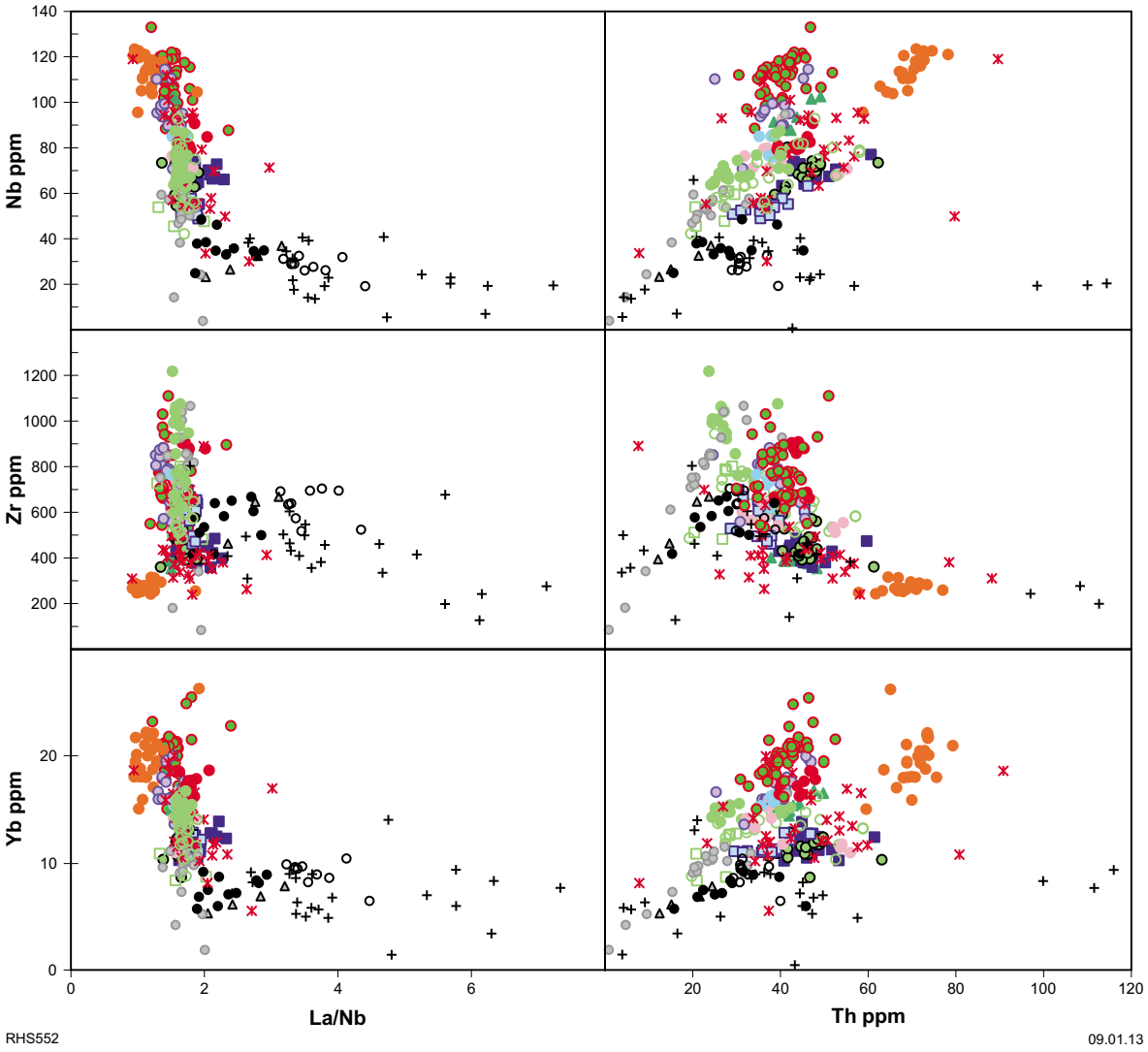

Figure 29. Compositional variation diagrams showing variations in Th content and La/Nb ratio versus selected trace elements for felsic rocks of the Warakurna Supersuite (symbols as in Fig. 16)

the mafic parental magma of the eastern magmas was more depleted in Nb, Ta, Zr, Hf, and HREE than the HF magmas.

The Alcurra Dolerite dykes are regionally extensive, whereas the eastern magmas are comagmatic with the massive (unlayered) G2 gabbros that intrude major shear zones throughout the region to the east of the Talbot Sub-basin. The G2 gabbros and intrusive examples of the eastern magmas (regional leucogranite dykes) are commonly extensively and intricately mingled. The least contaminated G2 gabbros have the highest MgO contents (up to 12.7 wt%) and Mg# (up to 73, typically >60) of all the older than 1000 Ma regional mafic magmas, but also have amongst the highest La/Nb ratios and lowest $\varepsilon_{Nd(t)}$ values. They show MORB-like depleted mantle HFSE patterns, but have Th and LREE enrichments reflecting small degrees of crustal contamination (Fig. 30). Invoking G2 gabbros, rather than Alcurra Dolerite, as the mafic parental magma component of the eastern magmas would explain the relative depletions of Nb, Ta, Zr, Hf, and HREE in the eastern magmas compared to HF magmas.

Hence, the HF magmas and the eastern magmas are likely derived from slightly different mantle source regions; the G2 source for the eastern magmas was more depleted and the G2 magmas also appear to represent higher degree partial melts than the Alcurra-type magmas. Nevertheless, the contrasting trends in terms of $\varepsilon_{Nd(t)}$ vs SiO_2 (or La/Nb) (Fig. 24), suggest that the proportion of crustal material incorporated in the eastern magmas increased as the magmas evolved, whereas the HF magmas (or most likely their Alcurra-type parental magmas) were contaminated early, and remained closed to further crustal addition.

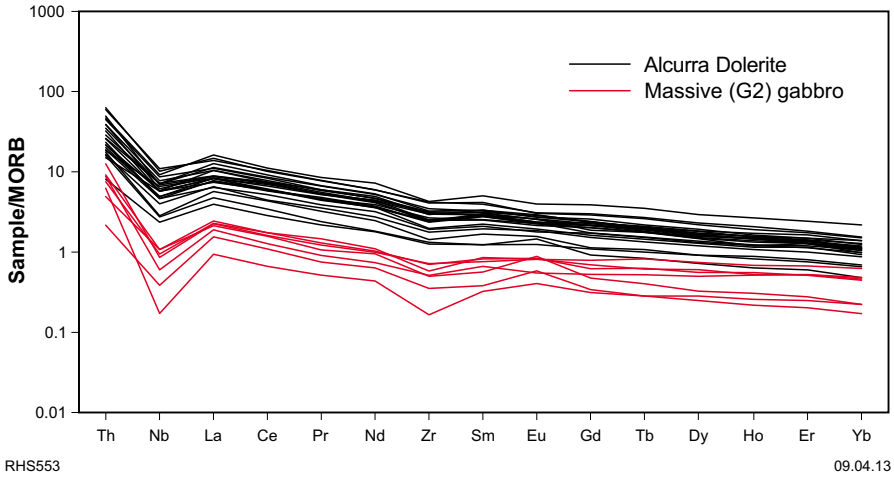

Figure 30. MORB-normalized incompatible trace element spider diagram comparing the Alcurra Dolerite with massive (G2) gabbro (normalizations are from Sun and McDonough, 1989)

Talbot Sub-basin

On nearly all compositional variation diagrams, the evolved dacitic compositional ranges of the HF magmas (~65–70% SiO_2) lie within the range for the less-evolved felsic rocks of the Talbot Sub-basin (Figs 18 and 19). This is consistent with the isotopic similarity among rhyolites of the Talbot Sub-basin, the HF magmas, and the closely associated range of Alcurra-type magmas. Magmas within the compositional range of basaltic andesite to andesite are not seen in the Talbot Sub-basin. This might reflect the rapid natural evolution of fractionating tholeiitic magmas (i.e. very small temperature drop across this silica range; e.g. Turner and Rushmer, 2009), although the more mafic to intermediate HF magmas are found in the Blackstone Sub-basin. For this reason we suggest that HF-type magmas fed the magma chambers of the Talbot Sub-basin volcanic system(s), but they ascended from lower crustal sources as dacites. This suggestion is also based on the lack of zircon age inheritance in the rhyolites. Notably, HF-type dacites represent about 80–85% crystallization of a primitive Alcurra-type magma. If HF-type magmas are parental to the main body of rhyolitic magmas of the Talbot Sub-basin, the further enrichments in Th, LREE, and Nb to produce the average compositions of the rhyolites of the sub-basin increases this figure to >90% crystallization.

Viewing all of the felsic volcanic rocks of the Talbot Sub-basin together allows a few generalizations to be made about magma compositional evolution. The most primitive felsic magmas of the Talbot Sub-basin were likely to have dacitic silica contents between those of the least silica-rich crystal-rich (~65 wt%) and crystal-poor rocks (~70 wt%). Those magmas, nevertheless, were highly evolved, Fe-rich, Mg-poor, and strongly enriched in incompatible trace elements (HFSE, REE, Th, and U). In the HF magmas, SiO_2 and Ba contents are positively correlated, indicating that the magmas did not crystallize K-feldspar, at least until SiO_2 concentrations exceeded 67 wt% (Fig. 19). The more primitive rocks of the Talbot Sub-basin overlap the trend for the HF magmas, suggesting that they also did not crystallize K-feldspar. This is consistent with petrographic observations. However, for the main Talbot Sub-basin population, Ba, Sr, and Eu concentrations, and Eu/Eu* ratios (Eu* = expected concentration of Eu obtained extrapolating between Sm and Gd on a normalized REE spider diagram; Eu/Eu* quantifies a 'Eu anomaly'), are negatively correlated with SiO_2 content, reflecting removal of feldspar (plagioclase and K-feldspar; Fig. 19). Unlike the HF magmas, the Talbot Sub-basin magmas all appear to have reached zircon saturation, and Zr and SiO_2 concentrations are negatively correlated. Zircon removal could explain why LREE have typically become enriched within most groups, but M–HREE either remain at constant concentrations or are depleted. However, zircon crystallization cannot explain why the M–HREE in the HF magmas change from incompatible to compatible behaviour at ~70 wt% SiO_2. This requires an alternative HREE-rich phase, possibly minerals of the chevkinite group.

Most of the stratigraphic units of the Talbot Sub-basin show very limited geochemical variation. The Mount Palgrave Group comprises a series of geographically or stratigraphically restricted units of individually distinctive but limited compositional range (Figs 18 and 19). The same appears to be true for the Hilda and Wururu Rhyolites. Thus, each stratigraphic group comprises one or more discrete and relatively geochemically homogeneous eruptive magma batches, each reflecting a slightly different set of compositions or processes. The only clear exceptions to this (other than the HF magmas) are the Kaarnka rhyolite (A) and rhyolite (B) units, which both show a more extended variation of silica content of ~10 wt%. This perhaps reflects the difference between

sampling a compositionally homogenous chamber in a single, rapid and chamber-emptying eruption, and more episodic sampling over a period that allowed magma compositions to evolve via processes such as fractional crystallization. Alternatively, the Kaarnka rhyolite (A) and rhyolite (B) units may have been erupted from compositionally zoned chambers.

Geochronological data presented earlier indicate that eruption of the individual stratigraphic groups within the Talbot Sub-basin was separated by periods greater than those of typical magmatic systems. Hence, there can be no direct genetic relationship between most of these groups in terms of a single liquid line of descent. This is also suggested by subparallel to parallel (stacked) trends formed by many of the felsic magmas on plots of SiO_2 vs REE and HFSE (e.g. Nb, Zr, Y; Fig. 19), which reflect slight variations in source compositions and/or the mineralogy of residual or fractionating assemblages. Possible exceptions to this are the subvolcanic Kaarnka and Pussy Cat porphyritic rhyolite intrusions, the Kaarnka quartz-rhyolite unit, most components of the Winburn granite, and likely a few high-silica samples of the Kaarnka rhyolite (B) unit. Together, these show a common narrow variation in ratios of the most incompatible trace elements (e.g. Th/Nb) that distinguish these rocks from all other magmas, except the Kathleen Ignimbrite (Fig. 22). These units are also geographically associated within, and to the southwest of, the Kaarnka caldera, and geochronological and stratigraphic relationships permit a common magmatic time frame corresponding to the deposition of the lower part of the Kaarnka Group. Furthermore, these rocks together form continuous geochemical trends similar to those of the compositionally extended Kaarnka rhyolite (A) and rhyolite (B) units, although at different trace element concentrations (e.g. Yb vs SiO_2; Fig. 19). The suggestion that the Kathleen Ignimbrite is also part of this association is strongly supported by field evidence that it is in contact with, and of similar age to, subvolcanic Pussy Cat porphyritic rhyolite intrusions. The Kathleen Ignimbrite forms an evolved extension to the compositional trends defined by the porphyritic magmas for most elements, with extreme enrichments in Th, Nb, HREE, Rb, and F. However, higher Th/La and Nb/La ratios distinguish the Kathleen Ignimbrite.

The Kathleen Ignimbrite has F concentrations (~5400 ppm) up to double those of any other magma group of the Talbot Sub-basin. In high-silica magmas like the Kathleen Ignimbrite, strong enrichments in F are thought to promote F-complexation with incompatible trace elements, and lead to marked changes in the mineral-melt partitioning behaviour of those elements (e.g. Irber, 1999). The results are evolved magmatic compositions with unusual REE-fractionation patterns (e.g. birdwing patterns) — the 'lanthanide tetrad effect' (e.g. Irber, 1999) — and marked deviation from chondritic ratios for elements with close ionic charge and radii (e.g. Y/Ho and Zr/Hf; Auwera et al., 2003). Normalized REE patterns for the Kathleen Ignimbrite (Fig. 20) do show a degree of concave–convex behaviour that could be ascribed to the tetrad effect, particularly for the third (Gd–Ho) and fourth (Er–Lu) tetrads, as defined by Masuda et al. (1987). In addition, Y/Ho and Zr/Hf ratios do show clear deviation from chondritic values (Fig. 31). These observations strongly suggest that trace element behaviour within the highly evolved Kathleen Ignimbrite was not controlled entirely by expected mineral-melt partitioning. Non-chondritic Y/Ho and Zr/Hf ratios, strong enrichments in HREE, and slight depletions in LREE (hence high Th/La and Nb/La ratios) are plausibly the result of high F contents in the melts. Thus, despite their high Th/La and Nb/La ratios, a direct genetic relationship between the Kathleen Ignimbrite and the subvolcanic Kaarnka and Pussy Cat porphyritic rhyolite intrusions and the Kaarnka quartz-rhyolite unit is very plausible.

As noted above, variations in Th/Nb ratio (and Th/M–HREE ratio) define two broad magma groups (Fig. 22): a high Th/Nb ratio (and high Th/M–HREE and Nb/Zr ratios) group incorporating the subvolcanic porphyritic rhyolite intrusions, the Kaarnka quartz-rhyolite unit and the Kathleen Ignimbrite; and a low Th/Nb ratio (and low Th/M–HREE and Nb/Zr ratios) group incorporating rocks of the Mount Palgrave and Cassidy Groups. This distinguishes the units of extreme regional continuity (Mount Palgrave and Cassidy Groups) from units within and associated with the Kaarnka caldera. Notably, the Kaarnka rhyolite (A) and rhyolite (B) units, although part of the Kaarnka Group, appear to fall within the latter regional (low Th/Nb ratio) group.

It is possible that the groups with high- and low-Th/Nb ratios reflect two broadly distinct parental compositions, perhaps ultimately related to compositional variations in the Alcurra-type mafic source. Alternatively (or additionally), these differences might reflect variations in physical conditions within subvolcanic chambers. For example, most analyses of the high-level Winburn granite clearly belong to the group represented by high Th/Nb ratios (Kaarnka caldera), so we can reasonably speculate that this caldera-forming association developed within a very shallow chamber. Estimates based on the zircon-saturation thermometer of Watson and Harrison

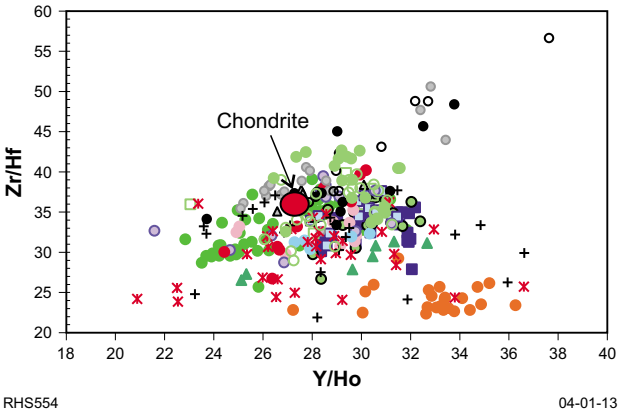

Figure 31. Compositional variation diagram showing variations of Y/Ho versus Zr/Hf ratios for felsic rocks of the Warakurna Supersuite (symbols as in Fig. 16). Chondritic values are from Sun and McDonough (1989).

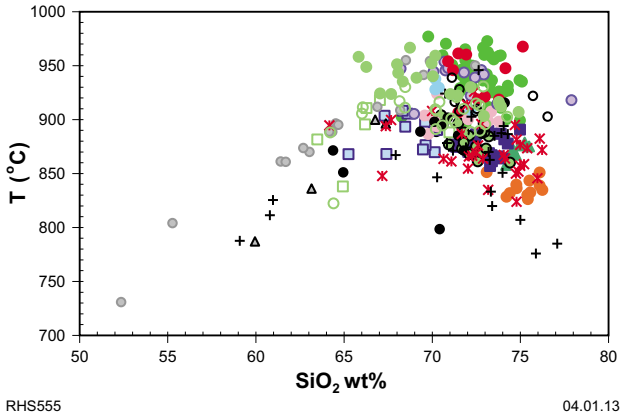

Figure 32. Magmatic temperature estimates for felsic rocks of the Warakurna Supersuite using the Zr-saturation thermometer of Watson and Harrison (1983) (symbols as in Fig. 16)

(1983) suggest that these magmas also underwent zircon-saturation at much lower temperatures (~900°C; Fig. 32), and at similar or lower silica concentrations, than magmas of the group with low Th/Nb ratios (~980°C), perhaps also indicative of a shallower magma chamber. Hence, it is possible that magmas of the group with high Th/Nb ratios were simply derived from a higher level, lower temperature part of a magmatic chamber system. In this case, high Th/M–HREE and Nb/Zr ratios might relate to earlier zircon saturation. However, higher Th/Nb ratios are more difficult to explain unless correspondingly lower chamber pressures promoted the development of more-volatile-rich magmas with higher fO_2 that crystallized earlier, and more abundant magnetite (the only petrographically observed phase with D_{Nb}>>1).

The alternative suggestion — that the groups with high- and low- Th/Nb ratios reflect two broadly distinct parental compositions — is perhaps supported by the geochronological data (stratigraphic levels L1–L12). Earlier, it was indicated that geochronological samples yielding the most unimodal age components (MWSD closest to 1) also yielded restricted mean ages in the 1081–1071 Ma age range. These samples are from stratigraphic levels L6–L8 and from the Winburn granite; that is, they represent the group with high Th/Nb ratios. This leads to the suggestion that most rocks at these stratigraphic levels were indeed erupted or remobilized from a compositionally distinctive chamber now exposed as the Winburn granite. Stratigraphic and geochronological relationships indicate that the main high Th/Nb ratio component of the Winburn granite was emplaced before eruption of stratigraphic level L2, but did not become a viable source for eruption or remobilization until after deposition of stratigraphic level L5.

Despite the small differences noted above, there does not appear to be any clear fundamental change in felsic magmatic composition within the Talbot Sub-basin with time. Thus, it is likely that the thermal structure of the crust, magma-forming processes, and Alcurra-type source compositions did not significantly change throughout the protracted (>30 m.y.) volcanic history of the sub-basin. On a more regional scale, it appears that earlier (>1070 Ma) felsic magmas of the Bentley Basin (and Bentley Supergroup) — the Smoke Hill Volcanics of the Blackstone Sub-basin and the rocks of the Finlayson Sub-basin — were derived from a more depleted mantle source and perhaps incorporated slightly greater amounts of crustal material (or were more susceptible to crustal contamination) than the younger preserved rhyolites of the Talbot Sub-basin. However, antecrysts older than 1070 Ma in rhyolites of the Talbot Sub-basin do not show any clear decrease in the proportion of non-radiogenic Nd (Fig. 33), indicating that non-radiogenic crustal material was never a significant component of the Talbot Sub-basin magmatic system.

Discussion — processes and physical conditions

Extent and volume of volcanic rocks

Field relationships and patterns of geochemical variation unambiguously indicate that the observed stratigraphic thickness of the volcanic succession within the Talbot Sub-basin does not involve structural thickening. The maximum combined thickness of volcanic rocks (~12.7 km) is clearly never realised in any single traverse, but the thickest continuous stratigraphic section still contains >8 km of volcanic rocks, of which 70% is rhyolite. Such a thickness is quite extraordinary. It greatly exceeds the typical preserved stratigraphic thickness of most silicic LIPs (e.g. Etendeka, Parana and the Okhotsk-Chukotka Volcanic Belt of northeastern Russia; Ewart et al., 2004; Peate et al., 1990; Tikhomirov et al., 2012) as well as the preserved felsic volcanic successions in volcanic centres and basins in plate-boundary settings and intracontinental rift basins like the Adama Basin, where a 4 km thickness of volcanic sequences represents about 25 m.y. of development of the Main Ethiopian rift (e.g. Wolfenden et al., 2004). Possible intracontinental exceptions include the Neogene volcanic accumulation in the Eastern Snake River Plain of North America, which based on geophysical evidence is speculated to be ~7 km thick (Cathey and Nash, 2004), and the Late Cretaceous Kap Washington Group in northern Greenland, which contains >5 km thickness of rhyolite-dominated rocks (Thorarinsson et al., 2012).

The extent of preserved outcrop of the Talbot Sub-basin is ~5200 km^2. Assuming an average thickness of volcanic rocks of ~6 km, the preserved combined outcrop of mafic and felsic magma then represents volumes of 9360 km^3 of mafic magma and 21 840 km^3 of felsic magma. This is a large enough volume of felsic magma to represent 48 super-volcano eruptions (each ≥450 km^3; e.g. Sparks et al., 2005). The geochemical and isotopic evidence presented here indicates that the rhyolite evolved through a process that involved >90% crystallization of Alcurra-

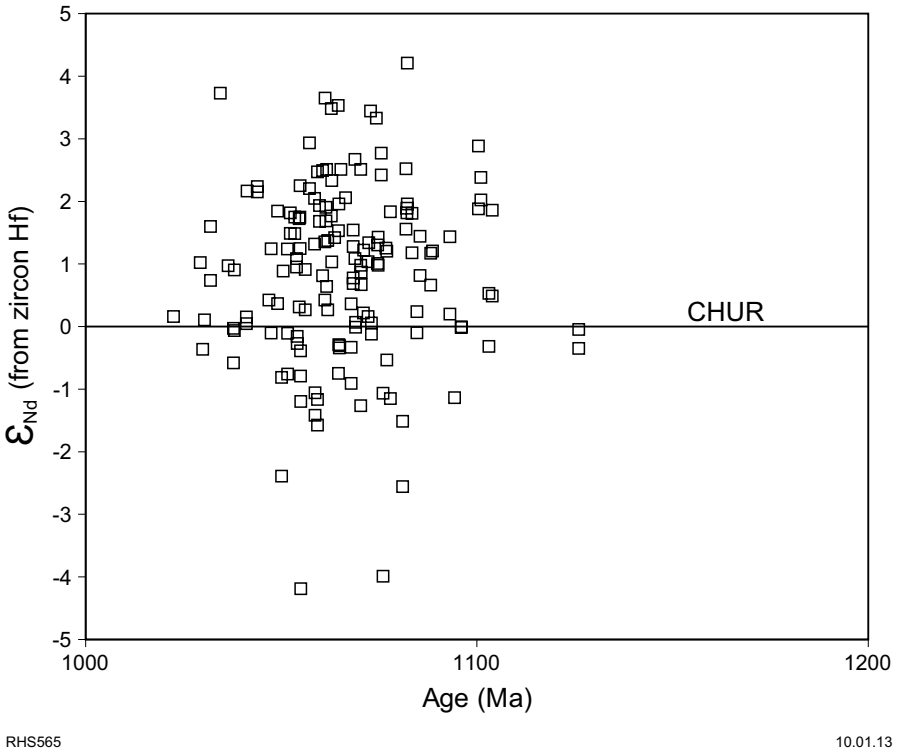

Figure 33. Nd-isotopic compositions of zircons from rocks of the Talbot Sub-basin calculated from Hf-isotopic data assuming a terrestrial array (e.g. Vervoort et al., 1999)

type mafic magmas. This means that the initial volume of mafic magma required to derive the preserved volume of felsic volcanic rock is approximately 218 400 km^3, with a total of 227 760 km^3 of mantle-derived magma required to produce the total preserved felsic and mafic volcanic pile. Notably, of the total required mantle-derived magma, <5% erupted as basalt.

It is likely that the Talbot Sub-basin originally extended beyond its currently preserved limits and, along with other sub-basins of the Bentley Basin, formed a thick volcanic succession covering a region of at least 50 000 km^2. Extending the above calculation over this interpreted original basin size requires an original mafic magma volume of approximately 2.19×10^6 km^3 extracted from the mantle during formation of the Bentley Basin. Isotopic evidence presented here indicates that a significant proportion of the felsic magmas to the east of the Talbot Sub-basin have incorporated crustal material. However, the relative proportion is exaggerated by the depleted nature of the mantle-derived (G2) parental component. In any case, the effect that this might have on the above calculation is probably more than compensated for because the calculation did not include the Mummawarrawarra Basalt, at the base of the Ngaanyatjarra Rift, which was originally thick enough to have at least locally formed the country rock to the layered Giles (G1) intrusions. Nor did the calculation include the huge volumes of unseen mafic magma likely required to trigger super-volcanic felsic eruptions (e.g. Leeman et al., 2008).

Both the Warakurna Supersuite and the Giles Event have previously been linked with a mafic LIP (the 1075–1070 Ma Warakurna LIP; e.g. Wingate et al., 2004; Fig. 1), and this includes one of the world's largest layered mafic intrusions — the layered Giles (G1) intrusion (Fig. 2). However, the Warakurna LIP is merely a spontaneous expression of a much larger and longer-lived system that included development of the Bentley Basin. The minimum estimated extrusive volume of felsic magma for the Talbot Sub-basin alone exceeds that of several recognized silicic LIPs (e.g. Altiplano-Puma in the central Andes, Taupo Volcanic Zone of New Zealand; Bryan et al., 2008), without including comagmatic rhyolites in the adjoining sub-basins.

Modern concepts of subvolcanic felsic magma chambers

Modern concepts of the dynamics of felsic magma chambers suggest that many large-volume, silicic volcanic rocks erupt from melt-rich lenses within the upper portions of large, vertically extended subvolcanic crystal mush chambers (e.g. Hildreth, 2004; Bachmann and Bergantz, 2008). These systems cool (or heat; e.g. Annen, 2009) to a rheological lock-up point where the proportion of crystals is too high (40–60% crystals; e.g. Marsh, 1981; Bachmann and Bergantz, 2008) for the system to convect, but it is still sufficiently permeable for interstitial melt to migrate.

Crystal–melt separation is most efficient within a narrow crystallinity window of ~50–70% crystals, and modelling shows that large crystal-poor cupolas or chambers can be generated over geologically reasonable time scales, even for highly viscose melts (Dufek and Bachmann, 2010). A mush chamber may hover at or near this near-solidus state for an indefinite period, with melt proportions varying down to effectively full crystallization, depending on the tectonomagmatic system's ability to maintain an appropriate thermal gradient. Perturbations in the local or regional thermal gradient locally or regionally vary the relative proportions of crystals and interstitial melt in these mush chambers. These freeze-and-thaw cycles may have many causes, including magmatic underplating, influx and mixing of new magma batches (recharge), or addition of volatile components (e.g. CO_2, F, H_2O) through processes such as gas sparging (Bachmann and Bergantz, 2006). During a thaw cycle, increased volumes of interstitial melt may migrate and pond, forming melt-rich portions of the chamber that can erupt to yield crystal-poor rhyolite. Rapid and substantial thaw cycles may lead to wholesale remobilization, stirring, and homogenization of the mush, and can cause catastrophic eruptions of regionally voluminous crystal-rich dacite that represent the largest volcanic eruptions known on Earth (e.g. Bachmann and Bergantz, 2008).

First-order compositional variations in volcanic rocks derived through such processes should be controlled primarily by the varying proportions of crystals and melt (i.e. the proportions of phenocrysts and vitric groundmass) and should be practically indistinguishable from the effects of fractional crystallization. In addition, processes of contamination and assimilation will be invisible as long as all components are cognate.

Mush chamber models have been applied mainly to calc-alkaline felsic volcanic rocks, typically in continental arc settings (i.e. the cold-wet-oxidized rhyolites of Christiansen and McCurry, 2008 and Bachmann and Bergantz, 2008). The relevance of such models to the hot-dry-reduced rhyolites found at intracontinental hotspots and rifts has been questioned (Christiansen and McCurry, 2008), particularly where geochemical modelling can also relate the rhyolites to comagmatic basaltic parental magmas through extreme fractional crystallization (e.g. Streck and Grunder, 2008). One of the main reasons for this is that, although intermediate rocks with compositions appropriate for the source mush reservoirs are frequently associated with cold-wet-oxidized rhyolites, they are rarely associated with hot-dry-reduced rhyolites. However, Bachmann and Bergantz (2008) suggested that this is an entirely predictable consequence of crystallizing hot-dry magmas that is essentially equivalent to the 'Daly Gap' (i.e. gap in silica content range) and is explicable within the crystal mush model. In the case of the Talbot Sub-basin, relatively crystal-rich and low-SiO_2 magmas, such as the Kaarnka rhyolite (A) and rhyolite (B) units, subvolcanic Kaarnka porphyritic rhyolite intrusions and crystal-rich ignimbrites, and several low-silica members of the Winburn granite, have compositions that would most closely approach those of source mush reservoirs.

One predictable consequence of repeated magma recharge, mixing, and freeze-and-thaw events is very complex mineral textures and compositional zonation patterns, like those seen in the rhyolites of the Talbot Sub-basin. These include strong dissolution embayments and multiple and discordant regrowth patterns in feldspars (Figs 5 and 15). For recent felsic volcanic rocks, U-series disequilibrium geochronological techniques are precise enough to distinguish the ages of individual zircon and plagioclase growth zones, and detailed geochronological studies using such dating techniques have provided several important conclusions (Reid et al., 1997; Simon et al, 2008; Schmitt et al., 2010; Storm et al., 2011, 2012; Eppich et al., 2012; Ruprecht and Cooper, 2012; Stelten and Cooper, 2012). These studies indicate that freeze-and-thaw cycles generally operate on time scales of tens to hundreds of thousands of years. More importantly, mineral growth may terminate up to 250 k.y. prior to eruption, requiring that the minerals reside in a chamber or mush zone over periods equivalent to several eruptive events. There also appears to be a decoupling between instantaneous eruption (or eruption trigger) events and the longer-term crystallization state of a crystal mush. However, although continuous zircon growth periods can span up to several tens of thousands of years (e.g. Storm et al., 2011), reflecting a particularly long-lived melt, the isothermal conditions required for this are usually not sustained over such periods, and certainly not over the period of rhyolitic volcanism inferred here for the Talbot Sub-basin. Periods of non-growth, or residence (particularly long-term), are more likely in a subsolidus state where crystals are shielded from melt. This supports the concept of a complex dynamic chamber in which local areas periodically switch between a subsolidus state and mush. Age and compositional fingerprinting of specific crystal components has shown that various parts of such a magma system may evolve separately and require an inhomogeneous thermal regime within the larger chamber system. This is typically attributed to local emplacement of mafic magmas into, or beneath, the chamber (e.g. Storm et al., 2011) and, in at least some cases, these mafic magmas provide a material contribution (i.e. mix) to the felsic magmatism (e.g. Czuppon et al., 2012). However, the age and compositional fingerprinting also indicate that partially molten reservoirs have communicated over distances of several kilometres to produce hybrid magmas (e.g. Schmitt et al., 2010).

Large-scale chamber systems, mush processes, and the subvolcanic Talbot Sub-basin

Even though direct cogenetic relationships (i.e. single magma batches) among most of the rhyolite units of the Talbot Sub-basin can be ruled out, the rhyolitic magmatism reflects a very long-lived magmatic system. The volumes of felsic magma produced and the degree of crystallization of Alcurra-type parental magmas that the rhyolitic compositions require (>90%) require that a substantial volume of mantle-derived magma was transferred into the crust, processed to produce felsic (dacitic?) melts, and likely transferred to higher crustal levels. Some of the erupted rhyolites are of super-volcano volume and each requires a correspondingly

large subvolcanic chamber. Integrating this over the total period of volcanism requires an extraordinarily large and long-lived subvolcanic chamber system (or systems). The dacitic magmas that likely fed the chamber system(s) were zircon-undersaturated, but clearly reached saturation within the chamber system(s). Thus, the total lack of inherited zircons within any of the rhyolite units suggests that the erupted units were all derived within a small number of closely related chamber systems (possibly a single system) lacking any effective access to basement or country rock. The vertical extent of the chamber system(s) can be loosely constrained. The maximum depth corresponds to the 4–6 kbar (14–21 km) constraint on the evolution of the Alcurra Dolerite. The minimum constraint is effectively within a few kilometres of the surface and is based on the geochemical evidence that the Winburn granite is part of the association of the subvolcanic porphyritic rhyolite intrusions, Kaarnka Group quartz-rhyolite, and Kathleen Ignimbrite, and intrudes into earlier Talbot Sub-basin volcanic products. The Kaarnka quartz-rhyolite component of this association locally also intrudes potential ring dykes related to the Kaarnka caldera cluster.

Several petrographic observations can be interpreted as supporting the suggestion that the Winburn granite was a subvolcanic mush chamber. The granite is dominated by porphyritic rocks with granophyric textures reflecting low-pressure disequilibrium processes (e.g. quenching). Several samples contain relatively few phenocrysts (melt-rich pockets?), comprising between 35 and 50% rounded and strongly embayed quartz, and subhedral complexly rimmed and commonly embayed feldspar, all separated by a distinctive granophyric groundmass (Fig. 5). Such textures reflect rapid solidification of a very melt-rich magma and are similar to the products of repeated magma recharge, mixing, and freeze-and-thaw events in a mush chamber.

Individual units (stratigraphic groups, formations, or units therein) of the Talbot Sub-basin are typically of very limited compositional range, likely reflecting the instantaneous emptying of compositionally homogeneous and mostly crystal-poor magma chambers. Rarer crystal-rich units (subvolcanic porphyritic rhyolite intrusions, Kaarnka quartz-rhyolite) show a wider range in composition controlled primarily by melt–feldspar separation. In these rocks, strongly embayed, disaggregated and multiply resorbed and regrown feldspar and quartz phenocrysts, similar to those of the Winburn granite, are abundant. These probably reflect significant cannibalization of older dormant or extinct parts of the chamber system(s) during renewed magmatism. However, a more compelling case for this can be made with the complex antecrystic zircon age components that are present in all of the rhyolites.

Cases where antecrysts dominate the zircon population are typically also the crystal-rich units (e.g. subvolcanic porphyritic rhyolite intrusions, Hilda rhyolite) and require that large volumes of near-solidified (or indeed solidified) material were largely to completely remobilized, possibly during several events. A good example of this is the subvolcanic Pussy Cat porphyritic rhyolite intrusion that was emplaced stratigraphically above the Kathleen Ignimbrite, but that has a mean SHRIMP zircon U–Pb age older than, and beyond error of, the mean age of units of the Eliza Formation. Some of these antecryst-dominated crystal-rich units are, perhaps, the equivalents of the 'Monotonous Intermediates' of Hildreth (1981) which, in modern cold-wet-oxidized rhyolite systems are believed to approximate the bulk composition of a source mush reservoir (e.g. Bachmann et al., 2002, 2005). The observation that the crystal-poor rhyolites (e.g. Eliza Formation, Thomas Rhyolite) tend to have fewer antecrysts suggests that these rocks originated from magmas freed of early-crystallized components.

Hence, despite the hot-dry-reduced nature of the Talbot Sub-basin rhyolites, this felsic magma system appears to share many characteristics which, in modern systems, can be explained in terms of long-lived subvolcanic mush chamber processes. However, periods of only 0.1 – 1.0 m.y. are typically suggested for the duration of modern long-lived mush chambers (e.g. Bachmann et al., 2002; Storm et al., 2011). Although it is clear that the Talbot Sub-basin rhyolites do not reflect a single event, gaps between individual events cannot be detected using U–Pb dating of zircon. Thus, magmatism likely represents a near-continuous series of similar, very large-volume to super-volcano eruptive events, over a period of >30 m.y. Although this is extraordinary in itself, what is most extraordinary about felsic magmatism within the Talbot Sub-basin is evidence for the repetitive recycling of cognate components throughout that entire period. This requires that the continuous series of magmatic events all used that same plumbing, or magmatic chamber system(s), and is consistent with the geographically stationary loci of volcanism and, in this regard, the Talbot Sub-basin volcanic system (or systems) is very unusual. How the heat required to produce and sustain magma chambers was continuously delivered to upper crustal regions over a time frame of >30 m.y. is discussed below. The lower crustal or mantle conditions and wider tectonic setting that permitted this are addressed later under the heading The Talbot Sub-basin and its relevance to the tectonic evolution of the Giles Event.

Thermal state and eruption triggers

Plutonic or batholithic masses typically accumulate over periods of several millions to a few tens of millions of years (e.g. de Saint Blanquat et al., 2011; Davis et al., 2012). As a result, individual pulses of magma are likely to be separated by sufficient time to cool before emplacement of the next pulse, so pluton-wide temperatures cannot increase to the level at which they can produce or sustain melt-rich mushes or magma chambers (e.g. Glazner et al., 2004; Annen, 2009). Large-volume eruptions like those that characterize the entire >30 m.y. history of Talbot Sub-basin volcanism require very large magma chambers. Annen (2009) modelled the thermal constraints on accumulation of large, eruptible silicic magma chambers during growth of an upper-crustal pluton via incremental addition of felsic sills, and found that these can only form during periods of magma fluxes > 10^{-2} to 10^{-1} km^3/yr.

Assuming the minimum 30 m.y. time frame, the flux of HF-type dacitic magmas into the proposed Talbot Sub-basin magma chamber system(s) was only 1×10^{-3} km^3/yr. To attain fluxes that approach the minimum required by Annen (2009), the actual cumulative period over which eruptible chambers were under construction and were sustained must have been less than about 6 m.y., or roughly 10% of the minimum depositional duration of the sub-basin. The application of Annen's models to the Talbot Sub-basin system, however, reflects a minimum cumulative period of chamber life because it does not take into account heat sources other than the effects of the addition of silicic sills. If additional significant heat sources were acting on or within the chamber system, it is likely that large chambers of eruptible material were larger, more frequently developed, and longer lived. Nevertheless, these calculation stress the above inference that volcanism was clearly not continuous throughout the evolution of the Talbot Sub-basin.

Thus, the evolution of the Talbot Sub-basin requires at least the punctuated maintenance of temperatures high enough to force regions of the chamber system(s) into a partially molten state over a period one to two orders of magnitude longer than that of typical magmatic systems. Given the hot-dry-reduced (Fe-rich tholeiitic) compositions of the volcanic rocks, the temperatures required to mobilize or rejuvenate mush chambers would have been high. This is also indicated by magmatic temperature estimates including values >900°C, using the Zr-saturation thermometer of Watson and Harrison (1983), which is likely appropriate given the geochemical trends for Zr and the observation that zircon crystallized throughout the volcanic history of the sub-basin.

Leeman et al. (2008) studied the thermal constraints on production of recent rhyolites in the Snake River Plain – Yellowstone area of North America. For some of these rhyolites, ^{18}O-depletion requires a source previously altered by meteoric water, and constrain melting depths to mid–upper crustal levels (<20 km); thermometry constrains melting temperatures to >900°C. Although compositionally similar to the Snake River Plain – Yellowstone rhyolites, our data clearly indicate that the rhyolites of the Talbot Sub-basin have a dominant mantle component, that they likely migrated as parental dacitic magmas from their source, and that they ponded at mid–upper crustal levels as part of a mush chamber. Nevertheless, the suggestion that the volcanism reflects periodic partial remobilization of this mush chamber still requires transient mid–upper crustal temperatures possibly >900°C, so the models of Leeman et al. (2008) are likely relevant. These models require that large volumes of mafic magma are emplaced into the crust, in the form of dykes, to raise ambient crustal temperatures to the required levels. In this regard, the model is similar to that of Annen (2009), but utilizes more-thermally favourable mafic dykes. To produce the modelled volume of the low-δ^{18}O rhyolites of the Snake River Plain – Yellowstone area at 900°C in the mid–upper crust, a cumulative intrusive thickness of 16 km of mafic magma is required, and heating requires a 4 m.y. period. If mafic magmatism ceases, temperatures rapidly decay below <900°C, depending on the actual depth of the system. Such time frames might be appropriate for typical volcanic cycles, but scaling the model to account for the >30 m.y. duration of Talbot Sub-basin volcanism requires unrealistic volumes of mafic intrusions that need to be accommodated within the crust, which must then undergo extreme extension. However, like the models of Annen (2009), these models assume a normal geothermal gradient prior to mafic intrusion.

The 1220–1150 Ma Musgrave Orogeny, which preceded the Giles Event, was an extraordinary event characterized by virtually continuous UHT metamorphism, with a geothermal gradient up to 40°C km^{-1}, as a result of effectively complete removal of the lithospheric mantle (Smithies et al., 2010, 2011). The crustal thickness at the end of this event was possibly <35 km (Smithies et al., 2011). Although this crust comprised anhydrous and extremely refractory material, our geochronological data indicate virtually continuous zircon-producing events spanning the period between the end of the Musgrave Orogeny and the beginning of the Giles Event, and Smithies et al. (2010, 2011) have suggested that the two tectonothermal events might be viewed as a continuum. Even if a 'normal' crust–mantle structure was re-established immediately after the Musgrave Orogeny, the slow rates of thermal diffusion mean that mid–upper crustal temperatures would have remained high throughout the Giles Event, simply as a result of the Musgrave Orogeny. Currie and Hyndman (2006), for example, showed that following UHT conditions at the base of the crust in some hot backarcs, conductive cooling took about 75 m.y. to reduce the excess crustal heat flow by ~50%.

In addition to this residual (Musgravian) conductive heat, the early stages of the Giles Event involved an enormous transfer of mantle-derived mafic magma to upper crustal levels, as required by the models of Leeman et al. (2008). Emplacement of the regional-scale layered Giles (G1) intrusion, in particular, as well as the locally voluminous massive (G2) gabbros, occurred within the period during which the Talbot Sub-basin developed, and the ~10-km-thick Jameson intrusion arm of the Giles (G1) intrusion is locally in contact with the Winburn granite. Hence, it is plausible that the ambient mid–upper crustal temperature was maintained at an unusually high level throughout the Giles Event. This would significantly reduce the amount of additional heat (e.g. by basalt intrusion) required to from or sustain an eruptible felsic magma chamber (e.g. Rowe et al., 2007; Annen, 2009).

It is also clear from the stratigraphy of the Talbot Sub-basin that voluminous mafic magma, compositionally distinct from the G1 and G2 magmas, was transported through the crust throughout the entire volcanic history of the sub-basin. Synvolcanic mafic dykes locally account for up to 25% (by volume) of the Winburn granite and of the stratigraphically lowest preserved rhyolites; extrapolating similar proportions to depth also provides an enormous source of heat. Bachmann and Bergantz (2006) and Huber et al. (2011) suggested that single, large mafic intrusions or underplates lack the capacity

to distribute sufficient heat over a sufficiently large area to produce significant amounts of crustal melt. However, swarms of closely spaced mafic intrusion, like those observed within the Winburn granite, would be much more efficient, particularly if the rate of intrusion was high (e.g. Annen, 2009). Each of the compositionally unique felsic stratigraphic formations of the Talbot Sub-basin either includes, or is separated by, a significant thickness of mafic lava, and each of the eight separate mafic units also has a unique composition. This strongly supports the suggestion that mafic magmatism is indeed one of the main triggers of felsic magmatism in the Talbot Sub-basin.

Hildreth and Wilson (2007) discussed additional processes that might trigger escape of interstitial melt from a permeable silicic mush. According to these authors, as a mush becomes increasingly crystal rich and rigid, interstitial melt becomes increasingly volatile rich, less viscous, and more prone to escape under the effects of gravity (particularly in thick mush chambers), shearing flow, gas-driven filter pressing, or external deformation. All of these processes are potentially relevant in the eruption of magmas of the Talbot Sub-basin. The effects of high F concentrations on reducing melt viscosities are well documented (e.g. Dingwell et al., 1985) and, in addition to the high (>900ºC) melt temperatures, would have been particularly relevant to the magmas of the Talbot Sub-basin. Aitken et al. (2012) also pointed out that active normal faults facilitated accommodation of large upper-crustal magma chambers in the Musgrave Province throughout the Giles Event. Movements on these faults are clearly potential eruption triggers.

Size of the Talbot Sub-basin magma chamber system(s)

Taking into account that high ambient mid–upper crustal temperatures might have been maintained throughout the Giles Event, the eight (at least) episodic mafic magmatic events that further elevated crustal temperatures and potentially triggered remelting or rejuvenation of potential chamber material still must have had an enormous cumulative intrusive thickness that requires accommodation. This is particularly the case because there is no geochemical evidence that mafic magmas physically mixed with the felsic reservoirs. Such large volumes of dense material should also leave indelible evidence of its existence.

Much of the presently preserved Talbot Sub-basin, in particular the eastern portion, is bounded by two northeast-trending faults, the easternmost of which is geophysically imaged as a crustal-scale fault (e.g. Aitken et al., 2012; Fig. 34). These two faults also bound an 81 × 71 km (~5800 km^2) region shown by gravity data to be underlain by unusually dense crust. One plausible model is that this dense crust reflects the accumulation of the mafic intrusions required to thermally remobilize the felsic mush chamber. This region also corresponds to the highest crustal level preserved in the western Musgrave region; the bounding faults typically juxtapose this region against crust of higher metamorphic grade. It is possible that large volumes of mafic magma were accommodated in these regions by vertical movement within this crustal block. According to Cruden and

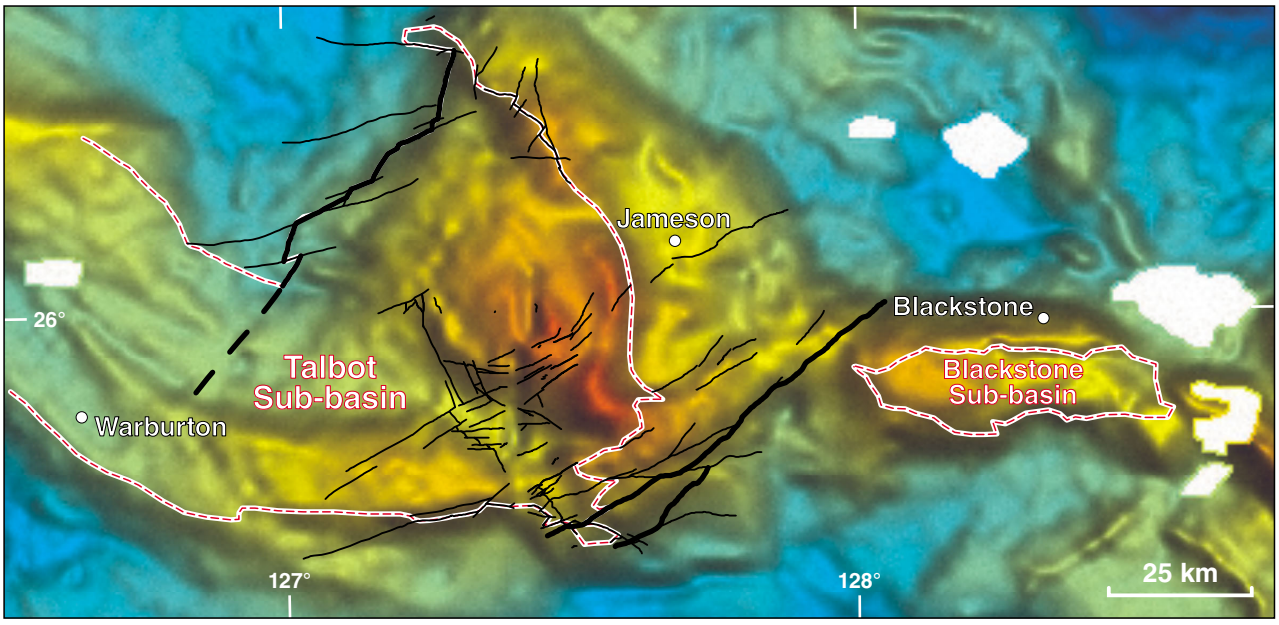

RHS570 09.01.13

Figure 34. Gravity image of the west Musgrave Province showing outlines of the Talbot and Blackstone Sub-basins and faults (major faults, thick black lines; minor faults, thin black lines) partially defining the extent of dense crust (orange and yellow) beneath the eastern Talbot Sub-basin

McCaffrey (2001), large volumes of magma can be accommodated in the upper levels of a chamber system by floor depression along brittle faults, and compensated for by ductile flow at deeper chamber levels. Similarly, Aitken et al. (2012) suggested that the large layered G1 Giles intrusions were accommodated in the crust by simultaneous vertical movement along bounding faults in a manner akin to growth faults in depositional basins. Hence, the faulted boundaries of this block are akin to the margins of a regional-scale caldera-like structure, and this region encloses the Kaarnka caldera cluster. It is possible that this region effectively outlines the combined horizontal extent of the Talbot Sub-basin subvolcanic chamber system(s). Because the maximum vertical extent of this system is ~21 km (see Large scale chamber systems, mush processes, and the subvolcanic Talbot Sub-basin), this (combined) chamber system could have had a volume of up to 121 800 km^3. The lack of any zircon inheritance within the Talbot Sub-basin rhyolites suggests the developing upper-crustal magma system had no effective contact with country-rock or basement components. Although the HF-type dacite might have been zircon-undersaturated, zircon was clearly an abundant accessory within the magmatic chamber system(s), so any country-rock zircons should have survived in the evolved rhyolite chambers. One explanation for the lack of inherited zircon is that country-rock or basement components were a volumetrically negligible part of the chamber system(s), which thus consisted almost entirely of parental HF-type dacite, mush chambers of varying crystal–melt proportions, eruptible rhyolite chambers, and mafic magma sills and chambers. Interestingly, the volumes of dacitic HF-type magmas required to form the Talbot Sub-basin rhyolites (roughly double the volume of rhyolite) would have allowed for the combined volume of this chamber system to include up to 60% mafic magma, consistent with the observed large gravity anomaly (Fig. 34) and with the huge volumes of mafic magma that Leeman et al. (2008) suggested were needed to produce the rhyolites like those of the Snake River Plain – Yellowstone region.

Magmatic evolution of the Talbot Sub-basin

In this section, we summarize the distinctive features of the Talbot Sub-basin volcanic system, as detailed above, and integrate them with other known and speculated aspects of the geology and geological evolution of the region. We then present a chronology of events and processes that controlled the geological evolution of this region from the end of the Musgrave Orogeny to the cessation of volcanic activity in the Talbot Sub-basin at c. 1030 Ma.

By the end of the Musgrave Orogeny, at around 1150–1120 Ma, the Musgrave Province had undergone 80–100 m.y. of UHT metamorphism, in either an intracontinental or distal backarc environment (e.g. Smithies et al., 2010, 2011). The crust was ~35 km thick and the lithospheric mantle had been removed, juxtaposing lower crust and asthenosphere. The lower crust was a largely homogenized anhydrous and refractory mixture of juvenile mafic material and Proterozoic intermediate basement. The period between the end of UHT conditions in the mid-crust and the beginning of the Giles Event was sufficiently short that regional geothermal gradients would still have been greatly elevated throughout the Giles Event, even without additional heat input.

Emplacement of the regional layered Giles (G1) intrusions (1078–1075 Ma) provided an enormous additional thermal input into the mid–upper crust. Massive (unlayered) gabbro (G2) (1078–1074 Ma) intruded immediately after the G1 intrusions and provided a further large input of heat. G2 gabbro was clearly emplaced along major, active crustal-scale structures or magmatic shear zones. Comagmatic and cogenetic felsic magmatism was also concentrated along these structures and ranged in scale from pluton-sized bodies (e.g. Tollu Pluton) to extensively and intricately mingled granite and G2 gabbro intrusions. The regional leucogranite dyke suite was part of this magmatism and the Smoke Hill Volcanics (Blackstone Sub-basin) were its volcanic expression. This group of felsic magmas was different from those of the Talbot Sub-basin in that the primary G2-like mantle component was derived from a source more depleted than the source for the Alcurra Dolerite, and also included larger amounts of lower-crustal melt. Compared with the Alcurra Dolerites, the depleted compositions, combined with typically higher MgO contents (and Mg#) suggest that the primary G2 magmas were significantly higher temperature melts, which may explain the higher proportion of crustal contamination. The observed mingling relationships were upper-crustal features involving cogenetic (cognate) components. They resulted from contemporaneous feeding of both unfractionated G2 gabbro (from deep crustal chambers) and fractionated and variably contaminated felsic magmas (from upper crustal chambers) into the same active shear zones.

Based on the range of ages of antecrysts, at least limited felsic volcanism in the Talbot Sub-basin commenced at the same time, or before, emplacement of the layered Giles (G1) and massive gabbro (G2) intrusions and could have immediately followed deposition of the Kunmarnara Group. Felsic volcanism in the Finlayson Sub-basin was also early — possibly part of the Kunmarnara Group itself — whereas the Tollu Group in the Blackstone Sub-basin was deposited at c. 1075–1071 Ma after uplift and partial erosion of the layered Giles (G1) intrusion.

This means that the Alcurra-type magmas that were ultimately parental to the rhyolites of the Talbot Sub-basin started to under- and intra-plate the crust below that region of the Talbot Sub-basin at the same time that emplacement of G2-type magmas was elsewhere leading to the evolution of the eastern magmas. Hence, the mantle beneath the region was compositionally heterogeneous at this stage. The geographical range of Alcurra- and G2-type magmatism overlapped throughout much of the west Musgrave Province. However, evidence of G2-type magmas is not found in the Talbot Sub-basin, the western most occurrence being at Nebo-Babel (Godel et al., 2011), marginal to the sub-basin, within the Barrow Range – Cavenagh Corridor (Fig. 2). It is possible that large

volumes of Alcurra-type magmas beneath the Talbot Sub-basin simply masked any input from the source of the G2-type magma within that area. Even in the area to the east of the Talbot Sub-basin, Alcurra-type magmatism outlived G2-type magmatism, as observed in the Blackstone Sub-basin, where dacite of the Hogarth Formation overlies the eastern magmas of the Smoke Hill Volcanics.

Extensive under- and intra-plating of Alcurra-type magmas beneath the Talbot Sub-basin (in particular) led to a lower-crustal hot zone, a thermally mature mush zone where earlier mafic sheets partially re-melted and newly intruded sheets incompletely crystallized (e.g. Annen et al., 2006; Solano et al., 2012). Pre-existing basement was only a very minor component within this zone. Prior basement melting during the Musgrave Orogeny had already produced anhydrous, ferroan Pitjantjatjara Supersuite granites enriched in incompatible trace elements. Hence, the remaining basement was anhydrous and refractory. Any further melting would have yielded highly evolved and highly enriched low-volume melts. Even very minor (<4%) incorporation of this material into the juvenile melts would have led to the observed enrichments of Th, LREE, and HFSE within the Alcurra Dolerite.

Hybrid combinations of partial melts of the earlier mafic sheets, residual melts from incompletely crystallized mafic magmas, and primitive mafic magmas themselves, formed and migrated to mid–upper crustal levels. Here, they contributed to the evolving Talbot Sub-basin magma chamber system(s). The hybrid melts reached dacitic silica contents and represented an average evolved liquid to residual solid ratio of ~1:5.

The Talbot Sub-basin magma chamber system(s) developed during the >30 m.y. magmatic history of the sub-basin into a fault-bounded volume of 5800 km^2 areal extent and up to 21 km deep. It was effectively devoid of zircon-bearing country rock or basement components. The dacitic magmas ascending from the lower-crustal mafic mush hot zone contributed to approximately 40% of the volume of the system(s) over time. The other 60% was mafic material (Alcurra-type magmas), representing the chambers that both fed the basaltic stratigraphy of the Talbot Sub-basin and provided one of the significant primary eruption triggers for felsic volcanism. The large lateral extent of the combined chamber system is preserved as a positive gravity anomaly (Fig. 34) that reflects a high proportion of residual mafic material. The huge magmatic inputs were accommodated by downward moment along bounding and internal normal faults, which were active at all mid–upper crustal levels. At the subvolcanic to surface level, the Kaarnka caldera cluster developed.

The parental dacitic component of the chamber system(s) formed an interconnected series of chambers. The physical and compositional nature of these chambers depended on where they sat with respect to new inputs of mafic magma, and changed as the chamber system(s) evolved. Thus, these bodies included relatively cool and fully crystallized (subsolidus and fertile) dacite, distal to new mafic intrusions; fully crystallized and variably residual (depleted) plagioclase-rich bodies representing crystal accumulations after partial to full extraction of rhyolitic melts; variable combinations of crystals and interstitial melt (mush chambers), in proximity to newly accumulated mafic bodies; and crystal-poor rhyolite chambers representing potentially eruptible pockets of migrated melt.

The distinctive basalt–rhyolite cyclicity of the Talbot Sub-basin clearly implicates mafic magmatism as the main mechanism for periodically producing or rejuvenating mush chambers, and this was probably greatly facilitated by the long-lived regionally high geothermal gradient. The extreme efficiency of rhyolite–crystal separation and the magma fluxes required to promote melt chambers capable of super-volcano eruptions may have been additionally facilitated by seismic activity along faults within and bounding the combined chamber system and through the filter-pressing process that resulted from this activity. Melt–crystal separation was probably also strongly enhanced because of the high magmatic temperatures and F-rich compositions of the Talbot Sub-basin rhyolites.

Most of the individual stratigraphic units of the Talbot Sub-basin show very limited geochemical variation; they comprise one or more discrete and geochemically homogeneous magma batches, each reflecting a unique set of compositions or processes that was the outcome of a single, rapid chamber-emptying eruption. However, the Kaarnka rhyolite (A) and rhyolite (B) units show more extended ranges of silica content, perhaps reflecting either more episodic eruption over a period that allowed magma compositions to evolve via processes such as fractional crystallization, or eruption from a compositionally zoned chamber.

Although the areal extent (5800 km^2) and volume (121 800 km^3) of the combined chamber system was very large, the actual volume of primary Alcurra-type magma required to produce the preserved erupted and subvolcanic components of the Talbot Sub-basin was ~227 760 km^3. These estimates might suggest that only a portion of the true size of the combined Talbot Sub-basin magma chamber system is still geophysically detectable, or that magma chamber systems other than the Talbot Sub-basin system directly contributed to volcanism within the Talbot Sub-basin. However, a distinction needs to be made between the chamber system and the source region that feeds that system. For example, geophysical modelling of the High Lava Plains – Snake River Plains region of North America suggests there has been significant lateral migration there of magma in the lower crust and uppermost mantle into the lower crustal plumbing systems of recent voluminous volcanism (Eagar et al., 2011; Kelbert et al., 2012). Recent seismic reflection data (Neumann, 2013) show that the Moho beneath the Talbot Sub-basin and the area immediately to the north (Mitika Zone) is unusually deep, at approximately 60 km. No strong seismic reflectors are observed within the deep crust, and its seismic properties are consistent with a mafic underplate. Although a significant amount of the crustal thickening might be attributed to the younger (c. 570 Ma) Petermann Orogeny, it is equally possible that a large component of it also reflects a mafic underplate that developed as part of the magmatic evolution of the Ngaanyatjarra Rift (e.g. Aitken et al., 2012), and included regional reservoirs that fed the Talbot Sub-basin magma chamber system(s).

The Talbot Sub-basin and its relevance to the tectonic evolution of the Giles Event

Limited regional exposure and preservation limits the accuracy of magma volume calculations presented earlier, but those for felsic magma volumes in Talbot Sub-basin are probably reasonably robust minimum values. Even if our estimates of magmatic volume and magmatic-duration were overestimated by a factor of two, this volcanism still clearly records one of the world's longest-lived and most voluminous known felsic volcanic systems. An outstanding feature of this 'felsic' system is that it is fundamentally mafic, and mantle derived, and more so than most comparable super-sized intracontinental volcanic systems, such as the Snake River Plain – Yellowstone system. Its products represent one of the world's largest contributions of juvenile felsic material to the continental crust outside a subduction environment. Its evolution is clearly a reflection of fundamentally significant processes that go beyond the crustal scale and must have had a major bearing on the tectonic evolution of the region. In the section below, we discuss the possible tectonic setting of the Talbot Sub-basin, Ngaanyatjarra Rift, and the Giles Event.

The Warakurna Supersuite and the Giles Event have already been linked with a mafic LIP — the Warakurna LIP (Wingate et al., 2004). Previous models for the Warakurna Supersuite and the Giles Event invoked the arrival of a single mantle plume, probably beneath the Musgrave Province (Wingate et al., 2004; Morris and Pirajno, 2005; Godel et al., 2011). The basis for this interpretation included the short (about 5 m.y.) duration of LIP-scale magmatism, the vast regional span of dolerite intrusions, and the known (e.g. the layered Giles G1 intrusion) and inferred massive volume of mafic magmas involved. However, as discussed earlier, the Warakurna LIP is really a relatively early and spontaneous expression of a much larger and longer-lived system. That larger system — the Giles Event and the Ngaanyatjarra Rift (Evins et al., 2010) — includes the Bentley Basin, with a magmatic life known to span at least 50 m.y. (1090–1040 Ma; Edgoose et al., 2004; Appendix), including more than 30 m.y. of felsic volcanism within the Talbot Sub-basin alone, and possibly considerably longer (maximum potential duration determined here is between 1116 ± 28 Ma and 1110 ± 20 Ma). Within that larger basin, the minimum estimated extrusive volume of felsic magma for the Talbot Sub-basin alone exceeds that of several known silicic LIPs (e.g. Altiplano-Puma in the central Andes, Taupo Volcanic Zone of New Zealand; Bryan et al., 2008).

Mafic dykes with clear OIB-type compositions (Fig. 35) cross-cut c. 1068 Ma gabbros at Nebo-Babel, immediately east of the Talbot Sub-basin. Godel et al. (2011) viewed these as clear evidence for the Warakurna plume. They also suggested that the Alcurra-type magmas required a garnet-residual source and, thus, magma upwelling from a deep (>80 km) asthenospheric region.

Calculated at c. 1070 Ma, the Nd-isotopic composition of most of the OIB samples is considerably more radiogenic than depleted mantle sources (Fig. 36). The minimum age of the OIB dykes is actually unconstrained and it is only with assumed initial ages of <730 Ma that all of the samples have sensible isotopic compositions similar to, or less radiogenic than, depleted mantle (Fig. 36). This is also the age of minor dolerite dykes that intrude the Musgrave Province, and of the Mudtank carbonatite (Black and Gulson, 1978) in the southern Northern Territory. The OIB dykes may reflect a mantle plume, but they have no relevance to the Warakurna Supersuite, the Ngaanyatjarra Rift, or the Giles Event. Similarly, the inference that the Alcurra-type magmas are high-pressure melts is based on their high La/Yb ratios. As shown earlier, these features are better explained by crustal contamination, and there is no reason to infer a deep asthenospheric source.

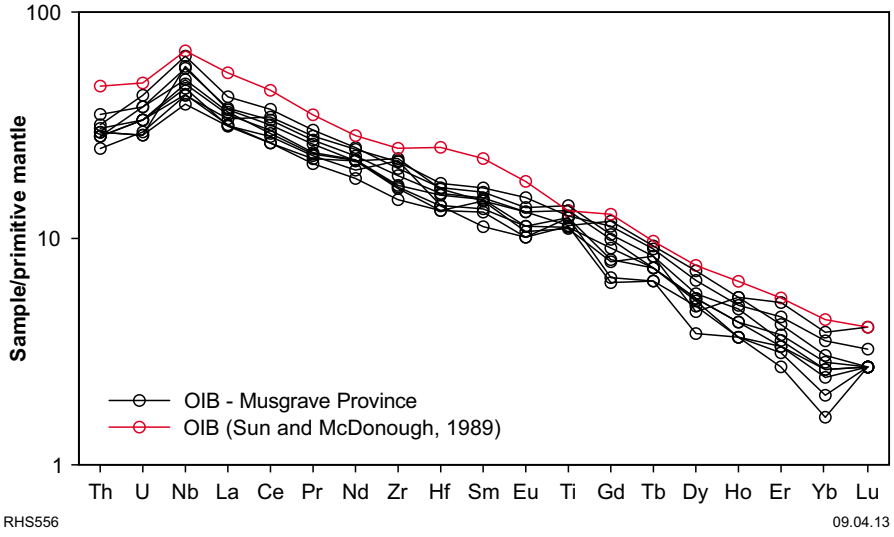

Figure 35. Primitive mantle-normalized incompatible trace element spider diagrams for late OIB dykes of the Musgrave Province (normalizations are from Sun and McDonough, 1989)

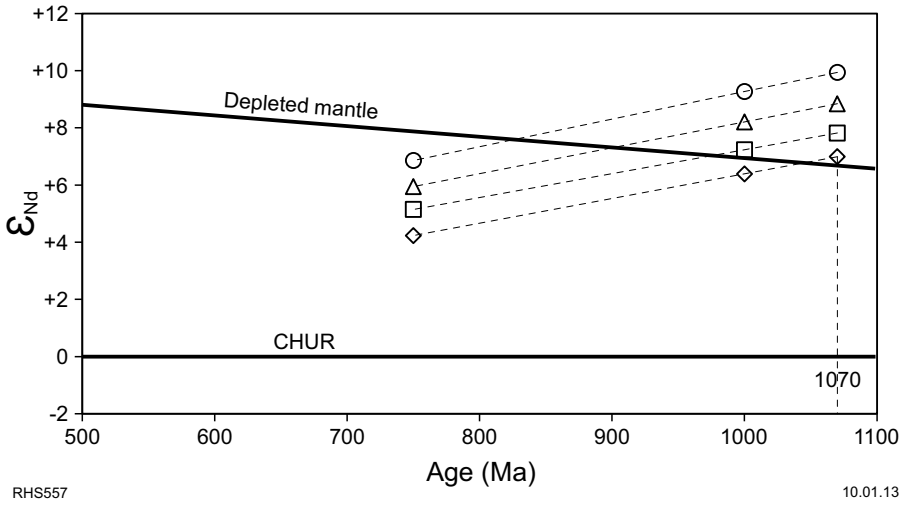

Figure 36. Nd-isotopic evolution diagram for four samples of late OIB dykes of the Musgrave Province. Data from Godel et al. (2011) and GSWA WACHEM database <geochem.dmp.wa.gov.au/geochem/>.

Evins et al. (2010) suggested that the magmatic history of the Ngaanyatjarra Rift was too long and complex to be the result of a simple, single mantle plume. Although the overall setting is likely one of (far field) intracontinental transtension, the structural history involves several phases of transpression, including a period of localized basin inversion, which Evins et al. (2010) tentatively related to a far-field effect of the collision of India with the West Australian Craton, about 1000 km to the west during the c. 1080 Ma Pinjarra Orogeny (Wilde, 1999; Fitzsimons, 2003). According to Evins et al. (2010) the magmatic and structural history of the Ngaanyatjarra Rift is more akin to a long-lived failed intracontinental rift.

The geological evolution of the Ngaanyatjarra Rift shows many close similarities with that of the Mezoproterozoic Midcontinental Rift in North America (Evins et al., 2010; Aitken et al., 2012). The Midcontinental Rift system has traditionally been regarded as a result of a large asthenospheric plume (e.g. Nicholson and Shirey, 1990; Hanson et al., 2004). Hanson et al. (2004) have temporally and spatially correlated the rift and the Umkondo LIP in southern Africa, to outline a superplume centred between the two provinces. Extensive and voluminous mafic to felsic magmatism in the Midcontinental Rift system is represented by the Keweenawan Supergroup, mainly between c. 1108 and 1094 Ma (e.g. Vervoort and Green, 1997), with a period of waning volcanism continuing until c. 1086 Ma (Hanson et al., 2004). However, Heaman et al. (2007) showed that that mafic magmatism there actually extended for at least 60 m.y. Because drift rates suggest that North America probably moved more than 2000 km over this period, Hollings et al. (2012) proposed that this magmatism cannot reflect a single stationary mantle plume, but may better fit a cluster of plumes. At face value, the alternative view would be that this magmatism simply does not reflect a plume at all. In the case of the Ngaanyatjarra Rift and the Giles Event, the evolution of the Talbot Sub-basin favours that alternative.

Perhaps the closest analogy to the Talbot Sub-basin volcanic system(s) in terms of magma range, composition, volume, and volcanic style is the Miocene Snake River Plain – Yellowstone system (e.g. Bonnichsen et al., 2008; Branney et al., 2008; Christiansen and McCurry, 2008; McCurry et al., 2008). This system has been active for approximately 16 m.y. (Bonnichsen et al., 2008), but over that period there has been a systematic, age-progressive northeastward shift in the focus of volcanism, defined by a ~700 km chain of caldera structures, the active Yellowstone caldera being the youngest and easternmost. This province is widely regarded as a classic example of a plume-generated continental hotspot track formed as North America migrated over the stationary Yellowstone plume at ~2 cm/yr (e.g. Bindeman et al., 2007; Shervais and Hanan, 2008; Pierce and Morgan, 2009; Coble and Mahood, 2012). Although the plume interpretation has been challenged (e.g. Faccenna et al., 2010; James et al., 2011; Fouch, 2012), the main contentious issues appear to be the depth from which asthenospheric upwelling occurs and the role of an actively subducting slab in locating upwelling zones. The concept of a laterally stationary mantle upwelling zone and a migrating plate appears to be widely accepted.

In the Talbot Sub-basin, Yellowstone-style, high-temperature, super-volcano class eruptions occurred over a minimum period of about 30 m.y., at least double the duration of the Miocene Snake River Plain – Yellowstone system. Not only is the Talbot Sub-basin system bimodal throughout its entire history, but the felsic component is effectively of direct mantle origin; together, the amount of felsic and mafic magmatism represents an extraordinarily large magma input. The most remarkable feature of the

Talbot Sub-basin system is that this all occurred at the one locality. There is no evidence of a regional age-progressive trend in magmatism; using a conservative rate of plate motion of ~2 cm/year, it can be estimated that the sub-basin region would have migrated >600 km away from any initially stationary asthenospheric heat source. A plume cluster does not offer a satisfactory solution because it would require that plate migration fortuitously located the Bentley Basin alone over each new plume within that cluster. The more likely conclusion is that the reasons for, or controls on, magmatism in the Talbot Sub-basin are specifically attached to the lithosphere rather than to the underlying asthenosphere. The paradox, then, is how such enormous volumes of magma were produced over such a long period from a mantle source that was apparently tied to the lithospheric plate.

Recent volcanism within the Jemez Mountains volcanic field, part of the Rio Grande Rift system in New Mexico, presents a similar problem. There, voluminous intracratonic bimodal volcanism has been localized within a small (~4900 km^2) area for approximately the last 20 m.y. (Wolff et al., 2005; Rowe et al., 2007). Within this restricted area, the longevity of volcanism indicates that the controls on the location of magmatism reside within the lithosphere, and the lithospheric mantle is thought to be the magma source (Wolff et al., 2005). Periods of maximum volcanic activity coincide with periods of extension related to the evolution of the Rio Grande Rift (Rowe et al., 2007), and the underlying cause of magmatism is thought to be the effect this lithospheric extension has on underlying fertile mantle (Wolff et al., 2005).

During the Musgrave Orogeny, the Musgrave Province was in a relatively unusual tectonic situation; there was a thin hot piece of Proterozoic crust locked into the middle of a rigid architecture comprising three older, thick and refractory cratonic masses (Smithies et al., 2010, 2011; Fig. 37). Following lithospheric removal at the beginning of the Musgrave Orogeny, this natural asthenospheric upwelling zone may have prevented or retarded re-establishment of a normal crustal geothermal gradient and the development of new, thick lithospheric mantle, perhaps because it was positioned where the effects of any far-field stresses would have been readily amplified. The prevailing tectonic regime throughout the Musgrave Orogeny was likely one of continuously failed rifting — transtension with periods of transpression.

Whether or not the Musgrave Orogeny and the Giles Event can be viewed as a continuum is difficult to assess, although there is no evidence that the prevailing tectonic regimes fundamentally differed (e.g. Evins et al., 2010; Smithies et al., 2011). Evidence for UHT conditions does not extend beyond c. 1120 Ma (Smithies et al., 2010, 2011). However, the geochronological record shows virtually continuous zircon-forming events between c. 1120 and 1090 Ma. Even if the decline of lower- to mid-crustal temperatures below UHT conditions at c. 1120 Ma indicates that the thermal driver of the Musgrave Orogeny had waned, rates of thermal diffusion are such that the geothermal gradient at the beginning of, and throughout, the Giles Event would have been significantly higher than normal (e.g. Currie and Hyndman, 2006), simply as a result of the Musgrave Orogeny itself. In addition, because

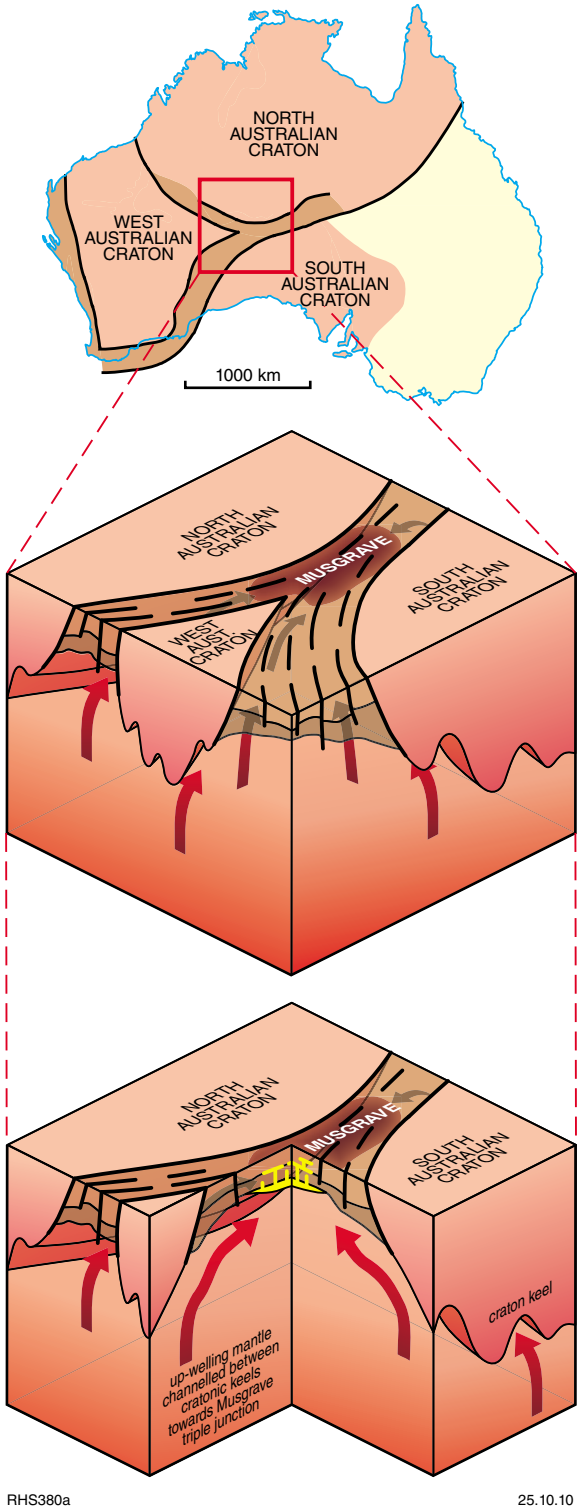

Figure 37. Block diagrams showing the influence of crustal blocks on the tectonothermal evolution of the Musgrave Province during the Musgrave Orogeny

the west Musgrave Province remained a focus of mantle-derived magmatism during the Giles Event, it seems equally reasonable to suggest that this might relate in some way to the crust–mantle architecture established during the Musgrave Orogeny. In this sense, although the magmatic products of the Warakurna LIP extend well beyond the Musgrave Province, it is very likely that the Giles Event and Ngaanyatjarra Rift would have been fundamentally different if not for the precursor Musgrave Orogeny.

According to Aitken et al. (2012), the Ngaanyatjarra Rift is very different to most modern rifts in that overall extension was very limited and was actually a response to magmatism-induced crustal thickening and the gravitational collapse of the crustal column. Evins et al. (2010) and Aitken et al. (2012) identified several stages of deformation accompanying rift development after the emplacement of the G1 Giles intrusions, including significant localized shortening. Throughout the history of the rift, overall crustal extension was probably less than 20 km, but magmatic additions saw net crustal thickening of the order of 15 km. Such systems of magmatism-dominated rifting might have dominated in the Precambrian, reflecting weaker strain localization due to decreased lithospheric rigidity under warmer Proterozoic conditions (Aitken et al., 2012).

The western part of the Talbot Sub-basin, including the Kaarnka caldera cluster, lies at the junction of three crustal-scale structures, each with histories that pre-date the Giles Event (e.g. Smithies et al., 2010, 2011; Aitken et al., 2012). These include the northeast-trending Cavenagh Fault, the northwest-trending Mann and Hinckley faults and the north-trending Lasseter-Mundrabilla shear zone. Given the elevated geothermal gradients, thinner crust, and unique lower-crustal architecture of the region, the volcanic evolution of the Ngaanyatjarra Rift and the Talbot Sub-basin may be linked to episodic tectonic adjustments along these crustal scale structures, perhaps as a far-field effect of the c. 1080 Ma Pinjarra Orogeny (e.g. Wilde, 1999; Fitzsimons, 2003), as suggested by Evins et al. (2010).

Thus, within the context of a Proterozoic regime that promoted magmatism-driven rifting (e.g. Aitken et al., 2012), the west Musgrave Province was unusual in that it reflected an intracontinental region of long-term high heat-flow as a result of a crustal architecture established during amalgamation of Proterozoic Australia. The pre – Giles Event crustal architecture possibly continued to actively channel upwelling mantle-derived heat and magma throughout the Giles Event. However, residual heat from earlier UHT conditions alone was possibly enough to ensure the magmatic evolution of the Ngaanyatjarra Rift as a thermally weakened region that responded to the far-field effects of tectonic processes operating along the margins of the combined craton, possibly including the c. 1080 Ma collision of India with the West Australian Craton. These far-field stresses may have been transferred through, and acted on, one or more of several large crustal-scale structures, resulting in progressive but episodic accumulation of a lower crustal mafic under- and inter-plate.

The evolution of the Talbot Sub-basin, and of the Bentley Basin and Ngaanyatjarra Rift in general, represents one of the world's largest intracontinental additions of juvenile felsic crust, through possibly the longest-lived sequence of super-volcanic eruptions. Lithospheric structure and thermal history are the controls on that evolution, and there is no apparent role for deep-seated mantle upwelling, or a mantle plume.

References

Aitken, ARA, Smithies, RH, Dentith, MC, Joly, A, Evans, S and Howard, HM 2012, Magmatism-dominated intracontinental rifting in the Mesoproterozoic: The Ngaanyatjarra Rift, central Australia: Gondwana Research, doi.org/10.1016/j.gr.2012.10.003.

Anderson, JL 1983, Proterozoic anorogenic granite plutonism of North America: Geological Society of America, Memoir 161, p. 133–154.

Annen, C 2009, From plutons to magma chambers: Thermal constraints on the accumulation of eruptible silicic magma in the upper crust: Earth and Planetary Science Letters, v. 284, p. 409–416.

Annen, C, Blundy, JD and Sparks, RSJ 2006, The genesis of intermediate and silicic magmas in deep crustal hot zones: Journal of Petrology, v. 47, p. 505–539.

Auwera, JV, Bogaerts, M, Liégeois, J-P, Demaiffe, D, Wilmart, E, Bolle, O and Duchesne, JC 2003, Derivation of the 1.0–0.9 Ga ferro-potassic A-type granitoids of southern Norway by extreme differentiation from basic magmas: Precambrian Research, v. 124, p. 107–148.

Bachmann, O and Bergantz, GW 2006, Gas percolation in upper-crustal silicic crystal mushes as a mechanism for upward heat advection and rejuvenation of near-solidus magma bodies: Journal of Volcanology and Geothermal research, v. 149, p. 85–102.

Bachmann, O and Bergantz, GW 2008, Rhyolites and their source mushes across tectonic settings: Journal of Petrology, v. 49, p. 2277–2285.

Bachman, O, Dungan, MA and Bussy, F 2005, Insights into shallow magmatic processes in large silicic magma bodies: the trace element record in the Fish Canyon magma body, Colorado: Contributions to Mineralogy and Petrology, v. 149, p. 338–349.

Bachman, O, Dungan, MA and Lipman, PW 2002, The Fish Canyon Magma Body, San Juan Volcanic Field, Colorado: Rejuvenation and eruption of an upper-crustal batholith: Journal of Petrology, v. 43, p. 1469–1503.

Betts, PG and Giles, D 2006, The 1800-1100 Ma tectonic evolution of Australia: Precambrian Research, v. 144(1–2), p. 92–125.

Bindeman, IN, Watts, KE, Schmitt, AK, Morgan, LA and Shanks, PWC 2007, Voluminous low $\delta^{18}O$ magmas in the late Miocene Heise volcanic field, Idaho: Implications for the fate of Yellowstone hotspot calderas: Geology, v. 35, p. 1019–1022.

Black, LP, Gulson, BL 1978, The age of the Mud Tank carbonatite, Strangways Range, Northern Territory: BMR Journal of Australian Geology and Geophysics, v. 3, p. 227–232.

Bodorkos, S and Wingate, MTD 2008, 174594: metamorphosed leucogabbro, Mirturtu Camp; Geochronology Record 716: Geological Survey of Western Australia, 4p.

Bodorkos, S, Wingate, MTD and Kirkland, CL 2008a, 174538: metamonzogranite, Mount Daisy Bates; Geochronology Record 712: Geological Survey of Western Australia, 4p.

Bodorkos, S, Wingate, MTD and Kirkland, CL 2008b, 174558: metamorphosed quartz diorite, Mount Fanny; Geochronology Record 713: Geological Survey of Western Australia, 4p.

Bodorkos, S, Wingate, MTD and Kirkland, CL 2008c, 174736: granofelsic metasyenogranite, Mount Fanny; Geochronology Record 717: Geological Survey of Western Australia, 4p.

Bodorkos, S, Wingate, MTD and Kirkland, CL 2008d, 174737: foliated metamonzogranite, Mount Fanny; Geochronology Record 718: Geological Survey of Western Australia, 5p.

Bodorkos, S, Wingate, MTD and Kirkland, CL 2008e, 174747: metagabbro, Mount Fanny; Geochronology Record 719: Geological Survey of Western Australia, 4p.

Bonnichsen, B, Leeman, WP, Honjo, N, McIntosh, WC and Godchaux, MM 2008, Miocene silicic volcanism in southwestern Idaho: geochronology, geochemistry, and evolution of the central Snake River Plain: Bulletin of Volcanology, v. 70, p. 315–342.

Boudreau, AE 1999, PELE-a version of the MELTS software program for the PC platform: Computers and Geosciences, v. 25, p. 201–203.

Branney, MJ, Bonnichsen, B, Andrews, GDM, Ellis, B, Barry, TL and McCurry, M 2008, 'Snake River (SR)-type' volcanism at the Yellowstone hotspot track: distinctive products from unusual, high-temperature silicic super-eruptions: Bulletin of Volcanology, v. 70, p. 293–314.

Bryan, SE and Ernst, RE 2008, Revised definition of large igneous provinces (LIPs): Earth Science Reviews, v. 86, p. 175–202.

Bryan, SE, Ewart, A, Stephens, CJ, Parianos, J and Downes, PJ 2000, The Whitsunday Volcanic Province, central Queensland, Australia: Lithological and stratigraphic investigations of a silicic-dominated large igneous province: Journal of Volcanology and Geothermal Research, v. 99, p. 55–78.

Bryan, SE, Ferrari, L, Reiners, PW, Allen, CM, Petrone, CM, Ramos-Rosique, A and Campbell, IH 2008, New insights into crustal contributions to large-volume rhyolite generation in the mid-Tertiary Sierra Madre Occidental Province, Mexico, revealed by U–Pb geochronology: Journal of Petrology, v. 49, p. 47–77.

Cathey, HE and Nash, BP 2004, The Cougar Point Tuff: Implications for thermochemical zonation and longevity of high-temperature, large-volume silicic magmas of the Miocene Yellowstone hotspot: Journal of Petrology, v. 45, p. 27–58.

Cawood, PA and Korsch, RJ 2008, Assembling Australia: Proterozoic building of a continent: Precambrian Research, v. 166, p. 1–38.

Chakhmouradian, AR, Cooper, MA, Medici, L, Hawthorne, FC and Adar, R 2008, Fluorine-rich hibschite from silicocarbonatite, Afrikanda Complex, Russia: crystal chemistry and conditions of crystallization: The Canadian Mineralogist, v. 46, p. 1033–1042.

Christiansen, EH and McCurry, M 2008, Contrasting origins of Cenozoic silicic volcanic rocks from the western Cordillera of the United States: Bulletin of Volcanology, v. 70, p. 251–267.

Coble, AC and Mahood, GA 2012, Initial impingement of the Yellowstone plume located by widespread silicic volcanism contemporaneous with Columbia River flood basalts: Geology, v. 40, p. 655–658.

Coleman, P 2009, Intracontinental orogenesis in the heart of Australia: structure, provenance and tectonic significance of the Bentley Supergroup, western Musgrave Block, Western Australia: Geological Survey of Western Australia, Record 2009/23, 50p.

Cruden, AR and McCaffrey, KJW 2001, Growth of plutons by floor subsidence: implications for rates of emplacement, intrusion spacing and melt-extraction mechanisms: Physics and Chemistry of the Earth, Part A, Solid Earth and Geodesy, v. 26, p. 303–315.

Currie, CA and Hyndman, RD 2006, The thermal structure of subduction zone back arcs: Journal of Geophysical Research, v. 111, B08404, doi:10.1029/2005JB004024.

Czuppon, G, Lukács, R, Harangi, S, Mason, PRD and Ntaflos, T 2012, Mixing of crystal mushes and melts in the genesis of the Bogács Ignimbrite suite, northern Hungary: An integrated geochemical investigation of mineral phases and glasses: Lithos, v. 148, p. 71–85.

Daniels, JL 1974, The geology of the Blackstone region, Western Australia: Geological Survey of Western Australia, Bulletin 123, 257p.

Davis, JW, Coleman, DS, Gracely, JT, Gaschnig, R and Stearns, M 2012, Magma accumulation rates and thermal histories of plutons of the Sierra Nevada batholith, CA: Contributions to Mineralogy and Petrology, v. 163, p. 449–465.

de Saint Blanquat, M, Horsman, E, Habert, G, Morgan, S, Vanderhaeghe, O, Law, R and Tikoff, B 2011, Multiscale magmatic cyclicity, duration of pluton construction, and the paradoxical relationship between tectonism and plutonism in continental arcs: Tectonophysics, v. 500, p. 20–33.

Dingwell, DB, Scarfe, CM and Cronin, DJ 1985, The effect of fluorine on viscosities in the system Na_2O-Al_2O_3-SiO_2: implications for phonolites, trachytes and rhyolites: American Mineralogist, v. 70, p. 80–87.

Dufek, J and Bachmann, O 2010, Quantum magmatism: Magmatic compositional gaps generated by melt-crystal dynamics: Geology, 38, p. 687–690.

Eagar, KC, Fouch, MJ, James, DE and Carlson, RW 2011, Crustal structure beneath the High Lava Plains of eastern Oregon and surrounding regions from receiver function analysis: Journal of Geophysical Research, v. 116, BO2313, doi:10.1029/2010JB007795, 2011.

Eaton, P 2010, Final report for funding agreement, Royalties for Region Co-Funded Government-Industry Drilling Program 2010, No. DA2009/048: Geological Survey of Western Australia, Statutory mineral exploration report A87820, 24 p. (unpublished).

Edgoose, CJ, Scrimgeour, IR and Close, DF 2004, Geology of the Musgrave Block, Northern Territory: Northern Territory Geological Survey, Report 15, 48p.

Eppich, GR, Cooper, KM, Kent, AJR and Koleszar, A 2012, Constraints on crystal storage timescales in mixed magmas: Uranium-series disequilibria in plagioclase from Holocene magmas at Mount Hood, Oregon: Earth and Planetary Science Letters, v. 317–318, p. 319–330.

Evins, PM, Smithies, RH, Howard, HM, Kirkland, CL, Wingate, MTD, Bodorkos, S 2010, Devil in the detail; the 1150–1000 Ma magmatic and structural evolution of the Ngaanyatjarra Rift, west Musgrave Province, Central Australia: Precambrian Research, v. 183(3), p. 572–588.

Evins, PM, Smithies, RH, Howard, HM and Maier, WD 2009, Holt. WA Sheet 4546: Western Australia Geological Survey, 1:100 000 Geological Series.

Ewart, A, Marsh, JS, Milner, SC, Duncan, AR, Kamber, BS and Armstrong, RA 2004, Petrology and geochemistry of Early Cretaceous bimodal continental flood volcanism of the NW Etendeka, Namibia, Part 2: Characteristics and petrogenesis of the high-Ti latite and high-Ti and low-Ti voluminous quartz latite eruptives: Journal of Petrology, v. 45, p. 107–138.

Faccenna, C, Becker, TW, Lallemand, S, Lagabrielle, Y, Funiciello, F and Piromallo, C 2010, Subduction-triggered magmatic pulses: A new class of plumes?: Earth and Planetary Science Letters, v. 299, p. 54–68.

Fitzsimons, ICW 2003, Proterozoic basement provinces of southern and southwestern Australia and their correlation with Antarctica: Geological Society, London, Special Publication 206, p. 93–130.

Fouch, MJ 2012, The Yellowstone hotspot: Plume or not?: Geology, v. 40, p. 479–480.

Frost, B and Frost, C 1997, Reduced rapakivi-type granites: the tholeiite connection: Geology, v. 25, p. 647–650.

Frost, BR, Barnes, CG, Collins, WJ, Arculus, RJ, Ellis, DJ and Frost, CD 2001, A geochemical classification for granite rocks: Journal of Petrology, v. 42, p. 2033–2048.

Gibson, GM and Ireland, TR 1996. Extension of Delamerian (Ross) orogen into western New Zealand: evidence from zircon ages and implications for crustal growth along the Pacific margin of Gondwana: Geology, v. 24, p. 1087–1090.

Giles, D, Betts, PG and Lister, GS 2004, 1.8–1.5-Ga links between the North and South Australian Cratons and the Early–Middle Proterozoic configuration of Australia: Tectonophysics, v. 380, p. 27–41.

Glazner, AF, Bartley, JM, Coleman, DS, Gray, W and Taylor, RZ 2004, Are plutons assembled over millions of years by amalgamation from small magma chambers?: Geological Society of America, Today, v. 14, p. 4–11.

Glikson, AY, Stewart, AT, Ballhaus, GL, Clarke, GL, Feeken, EHT, Level, JH, Sheraton, JW and Sun, S-S 1996, Geology of the western Musgrave Block, central Australia, with reference to the mafic–ultramafic Giles Complex: Australian Geological Survey Organisation, Bulletin 239, 206p.

Godel, B, Seat, Z, Maier, WD and Barnes, S-J 2011, The Nebo-Babel Ni-Cu-PGE sulfide deposit (West Musgrave Block, Australia): Part 2 – Constraints on parental magma and processes, with implications for mineral exploration: Economic Geology, v. 106, p. 557–584.

Gray, CM 1971, Strontium isotope studies on granulites: Australian National University, Canberra, PhD thesis (unpublished), 242p.

Grove, TL and Donnelly-Nolan, JM 1986, The evolution of young silicic lavas at Medicine Lake Volcano, California – implications for the origin of compositional gaps in calc-alkaline series lavas: Contributions to Mineralogy and Petrology, v. 92, p. 281–302.

Haapala, I and Rämö, OT 1990, Petrogenesis of the Proterozoic rapakivi granites of Finland: Geological Society of America, Special Papers, v. 246, p. 275–286.

Hanson, RE, Crowley, JL, Bowring, SA, Ramezani, J, Gose, WA, Dalziel, IWD, Pancake, JA, Seidel, EK, Blenkinsop, TG and Mukwakwami, J 2004, Coeval large-scale magmatism in the Kalahari and Laurentian cratons during Rodinia assembly: Science, v. 304, p. 1126–1129.

Heaman, LM, Easton, M, Hart, TR, Holling, P, MacDonald, CA and Smyk, M 2007, Further refinement of the timing of Mesoproterozoic magmatism, Lake Nipigon region, Ontario: Canadian Journal of Earth Sciences, v. 44, p. 1055–1086.

Hildreth, W 1981, Gradients in silicic magma chambers: implications for lithospheric magmatism: Journal of Geophysical Research, v. 86, p. 10153–10192.

Hildreth, W 2004, Volcanological perspectives on Long Valley, Mammoth Mountains, and Mono Craters: several contiguous but discrete systems. Journal of Volcanology and Geothermal Research, v. 136, p. 169–198.

Hildreth, W and Wilson, CJN 2007, Compositional zoning of the Bishop Tuff: Journal of Petrology, v. 48, p. 951–999.

Hollings, P, Smyk, M and Cousens, B 2012, The radiogenic isotope characteristics of dikes and sills associated with the Mesoproterozoic Midcontinent Rift near Thunder Bay, Ontario, Canada: Precambrian Research, v. 214–215, p. 269–279.

Howard, HM, Smithies, RH, Kirkland, CL, Evins, PM and Wingate, MTD 2009, Age and geochemistry of the Alcurra Suite in the west Musgrave Province and implications for orthomagmatic Ni–Cu–PGE mineralization during the Giles Event: Geological Survey of Western Australia, Record 2009/16, 16p.

Howard, HM, Smithies, RH and Pirajno, F 2007, Geochemical and Nd isotopic signatures of mafic dykes in the western Musgrave Complex, *in* Geological Survey of Western Australia Annual Review 2005–06: Geological Survey of Western Australia, Perth, p. 64–71.

Howard, HM, Smithies, RH, Pirajno, F and Skwarnecki, MS 2006, Bates, WA Sheet 4646: Geological Survey of Western Australia, 1:100 000 Geological Series.

Howard, HM, Smithies, RH, Werner, M, Kirkland, CL and Wingate, MTD 2011a, Geochemical characteristics of the Alcurra Dolerite (Giles Event) and its extrusive equivalents in the Bentley Supergroup, *in* GSWA 2011 Extended Abstracts: promoting the prospectivity of Western Australia: Geological Survey of Western Australia, Record 2011/2, p. 27–30.

Howard, HM, Werner, M, Smithies, RH, Kirkland, CL, Kelsey, DL, Hand, M, Collins, A, Pirajno, F, Wingate, MTD, Maier, WD and Raimondo, T 2011b, The geology of the west Musgrave Province and the Bentley Supergroup – a field guide: Geological Survey of Western Australia Record 2011/4, 119p.

Huber, C, Bachmann, O and Dufek, J 2011, Thermo-mechanical reactivation of locked crystal mushes: Melting-induced internal fracturing and assimilation processes in magmas: Earth and Planetary Science Letters, v. 304, p. 443–454.

Irber, W 1999, The lanthanide tetrad effect and its correlation with K/Rb, Eu/Eu*, Sr/Eu, Y/Ho and Zr/Hf of evolving peraluminous granite suites: Geochimica et Cosmochimica Acta, v. 63, p. 489–508.

James, DE, Fouch, MJ, Carlson, RW and Roth, JB 2011, Slab fragmentation, edge flow and the origin of the Yellowstone hotspot track: Earth and Planetary Science Letters, v. 311, p. 124–135.

Kelbert, A, Egbert, GD and deGroot-Hedlin, C 2012, Crust and upper mantle electrical conductivity beneath the Yellowstone Hotspot Track: Geology, v. 40, p. 447–450.

Kelsey, DE, Hand, M, Smithies, H, Evins, P, Clark, C and Kirkland, CL 2009, High-temperature, high-geothermal gradient metamorphism in the Musgrave Province, central Australia; potential constraints on tectonic setting, *in* Biennial Conference of Specialist Group for Geochemistry, Mineralogy and Petrology, Kangaroo Island, South Australia, 2009 *edited by* NE Timms, J Foden, KE Evans, and C Clark: Geological Society of Australia, Abstracts 96, 28.

King, RJ 2008, Using calculated pseudosections in the system NCKFMASHTO and SHRIMP II U–Pb zircon dating to constrain the metamorphic evolution of paragneisses in the Latitude Hills, West Musgrave Province, Western Australia: Geological Survey of Western Australia, Record 2009/15.

Kirkland, CL, Smithies, RH, Woodhouse, AJ, Howard, HM, Wingate, MTD, Belousova, EA, Cliff, JB, Murphy, RC and Spaggiari, CV 2013a, Constraints and deception in the isotopic record; the crustal evolution of the west Musgrave Province, central Australia: Gondwana Research, v. 23, p. 759–781.

Kirkland, CL, Wingate, MTD, Howard, HM and Smithies, RH, M 2013a, 185518: rhyolite, Barnard Rocks; Geochronology Record 1128: Geological Survey of Western Australia, (in press).

Kirkland, CL, Wingate, MTD and Smithies, RH 2013b, 187054: quartz diorite, Meewajarra Soak; Geochronology Record 1129: Geological Survey of Western Australia, (in press).

Kirkland, CL, Wingate, MTD and Bodorkos, S 2008a, 183496: orthogneiss, Mount West; Geochronology Record 747: Geological Survey of Western Australia, 5p.

Kirkland, CL, Wingate, MTD and Bodorkos, S, 2008b, 183459: charnockite, Latitude Hill, Geochronology Record 722: Geological Survey of Western Australia, 5p.

Kirkland, CL, Wingate, MTD and Bodorkos, S, 2008c, 183509: leucogranite dyke, Mount West; Geochronology Record 724: Geological Survey of Western Australia, 4p.

Kirkland, CL, Wingate, MTD and Bodorkos, S, 2008d, 193850: leucogranite dyke, Mount Fanny; Geochronology Record 748: Geological Survey of Western Australia, 4p.

Kirkland, CL, Wingate, MTD and Bodorkos, S, 2008e, 174761: porphyritic granite dyke, Bell Rock; Geochronology Record 721: Geological Survey of Western Australia, 4p.

Kirkland, CL, Wingate, MTD and Bodorkos, S, 2008f, 185509: leucogranite, Mount Aloysius; Geochronology Record 725: Geological Survey of Western Australia, 4p.

Kirkland, CL, Wingate, MTD, Evins, PM, Howard, HM and Smithies, RH 2009, 194354: Gabbro, north of Jameson Range; Geochronology Record 799: Geological Survey of Western Australia, 4p.

Leeman, WP, Annen, C and Dufek, J 2008, Snake River Plain – Yellowstone silicic volcanism: implications for magma genesis and magma fluxes, *in* Dynamics of crustal magma transfer, storage and differentiation *edited by* C Annen, and GF Zellmer: Geological Society, London, Special Publication 304, p. 235–259.

Li, Z-X 2000, Palaeomagnetic evidence for unification of the North and West Australian Cratons by ca. 1.7 Ga: new results from the Kimberley Basin of northwestern Australia: Geophysical Journal International, v. 142, p. 173–180.

Manning, CE and Bird, DY 1990, Fluorian garnets from the host rocks of the Skaergaard intrusion: Implications for metamorphic fluid composition: American Mineralogist, v. 75, p. 859–873.

Marsh, BD 1981, On the crystallinity, probability of occurrence, and rheology of lava and magma: Contributions to Mineralogy and Petrology, v. 78, p. 85–98.

Masuda, A, Kawakami, O, Dohmoto, Y and Takenaka, T 1987, Lanthanide tetrad effects in nature: Two mutually opposite types W and M. Geochemical Journal, v. 21, p. 119–124.

McCurry, M, Hayden, KP, Morse, LH and Mertzman, S 2008, Genesis of post-hotspot, A-type rhyolite of the Eastern Snake River Plain volcanic field by extreme fractional crystallization of olivine tholeiite: Bulletin of Volcanology, v. 70, p. 361–383.

Medlin CC in prep., The volcanology, geochemistry, and evolution of a shallow marine intra-caldera, rheomorphic ignimbrite succession: The Mesoproterozoic Kathleen Formation, west Musgrave Province, central Australia: Monash University, Clayton, Victoria, PhD thesis (unpublished).

Morris, PA and Pirajno, F 2005, Geology, geochemistry, and mineralization potential of Mesoproterozoic sill complexes of the Bangemall Supergroup, Western Australia: Geological Survey of Western Australia, Report 99, 75p.

Murakami T, Chakoumakos BC, Ewing RC, Lumpkin GR and Weber WJ 1991, Alpha-decay event damage in zircon: American Mineralogist, v. 76, p. 1510–1532.

Myers, JS, Shaw, RD and Tyler, IM 1996, Tectonic evolution of Proterozoic Australia: Tectonics, v. 16, p. 1431–1446.

Nekvasil, H, Dondolini, A, Horn, J, Filiberto, J, Long, H and Lindsley, DH 2004, The origin and evolution of silica-saturated alkalic suites: an experimental study: Journal of Petrology, v. 45, p. 693–721.

Neumann, NL (editor) 2013, Yilgarn – Officer Basin – Musgrave Province seismic and MT workshop notes: Geoscience Australia, 189p.

Nicholson, SW and Shirey, SB 1990, Midcontinental Rift volcanism in the Lake Superior region: Sr, Nd and Pb isotopic evidence for a mantle plume origin: Journal of Geophysical Research, v. 95, p. 10851–10868.

Pankhurst, RJ, Riley, TR, Fanning, CM and Kelley, SP 2000, Episodic silicic volcanism in Patagonia and the Antarctic Peninsula: chronology of magmatism associated with the break-up of Gondwana: Journal of Petrology, v. 41, p. 605–625.

Pearce, JA, Harris, NBW and Tindle, AG 1984, Trace element discrimination diagrams for the tectonic interpretation of granitic rocks: Journal of Petrology, v. 25, p. 956–983.

Peate, DW, Hawkesworth, CJ, Mantovani, MSM and Shukowsky, W 1990, Mantle plumes and flood basalt stratigraphy in the Paraná, South America: Geology, v. 18, p. 1223–1226.

Pierce, KL and Morgan, LA 2009, Is the track of the Yellowstone hotspot driven by a deep mantle plume? Review of volcanism, faulting, and uplift in light of new data: Journal of Volcanology and Geothermal Research, v. 188, p. 1–25.

Reid, MR, Coath, CD, Harrison, TM and McKeegan, KD 1997, Prolonged residence times for the youngest rhyolites associated with Long Valley Caldera: ^{230}Th-^{238}U ion microprobe dating of young zircons. Earth and Planetary Science Letters, v. 150, p. 27–39.

Rowe, MC, Wolff, JA, Gardner, JN, Ramos, FC, Teasdale, R and Heikoop, CE 2007, Development of a continental volcanic field: petrogenesis of pre-caldera intermediate and silicic rocks and origin of the Bandelier magmas, Jemez Mountains (New Mexico, U.S.A): Journal of Petrology, v. 48, p. 2063–2091.

Ruprecht, P and Cooper, KM 2012, Integrating the uranium-series and elemental diffusion geochronometers in mixed magmas from Volcán Quizapu, Central Chile: Journal of Petrology, v. 53, p. 841–871.

Schmitt, AK, Stockli, DF, Lindsay, JM, Robertson, R, Lovera, OM and Kislitsyn, R 2010, Episodic growth and homogenization of plutonic roots in arc volcanoes from combined U-Th and (U-Th)/He zircon dating: Earth and Planetary Science Letters, v. 295, p. 91–103.

Seat, Z 2008, Geology, petrology, mineral and whole-rock chemistry, stable and radiogenic isotope systematics and Ni–Cu–PGE mineralisation of the Nebo–Babel intrusion, west Musgrave, Western Australia: University of Western Australia, Perth, PhD thesis (unpublished).

Sheraton, JW and Sun, S-S 1995, Geochemistry and origin of felsic igneous rocks of the western Musgrave Block: AGSO Journal of Australian Geology and Geophysics, v. 16, p. 107–125.

Shervais, JW and Hanan, BB 2008, Lithospheric topography, tilted plumes, and the track of the Snake River-Yellowstone hot spot: Tectonics, v. 27, TC5004, doi:10.1029/2007TC002181.

Shirey, S, Klewin, K, Berg, J and Carlson, R 1994, Temporal changes in the sources of flood basalts: isotopic and trace element evidence from the 1100 Ma old Keweenawan Mamainse Point Formation, Ontario, Canada: Geochimica et Cosmochimica Acta, v. 58, p. 4475–4490.

Simon, JI, Renne, PR and Mundil, R 2008, Implications of pre-eruptive magmatic histories of zircons for U–Pb geochronology of silicic extrusions: Earth and Planetary Science Letters, v. 266, p. 182–194.

Smithies, RH, Howard, HM, Evins, PM, Kirkland, CL, Kelsey, DE, Hand, M, Wingate, MTD, Collins, AS and Belousova, E 2011, High-temperature granite magmatism, crust-mantle interaction and the Mesoproterozoic intracontinental evolution of the Musgrave Province, Central Australia: Journal of Petrology, v. 52(5), p. 931–958.

Smithies, RH, Howard, HM, Evins, PM, Kirkland, CL, Kelsey, DE, Hand, M, Wingate, MTD, Collins, AS, Belousova, E and Allchurch, S 2010, Geochemistry, geochronology and petrogenesis of Mesoproterozoic felsic rocks in the western Musgrave Province of central Australia and implication for the Mesoproterozoic tectonic evolution of the region: Geological Survey of Western Australia, Report 106, 73p.

Smithies, RH, Howard, HM, Evins, PM and Maier, WD 2009, Blackstone, WA Sheet 4545: Western Australia Geological Survey, 1:100 000 Geological Series.

Solano, JMS, Jackson, MD, Sparks, RSJ, Blundy, JD and Annen, C 2012, Melt segregation in deep crustal hot zones: a mechanism for chemical differentiation, crustal assimilation and the formation of evolved magmas: Journal of Petrology, v. 53, p. 1999–2026.

Sparks, RSF, Self, S and Working Group 2005, Super-eruptions: global effects and future threats (2nd edition): Geological Society of London Working Group Report, Geological Society, London, 24p.

Stacey, JS, and Kramers, JD, 1975, Approximation of terrestrial lead isotope evolution by a two-stage model: Earth and Planetary Science Letters, v. 26, p. 207–221.

Stelten, ME and Cooper, KM 2012, Constraints on the nature of the subvolcanic reservoir at South Sister volcano, Oregon from U-series dating combined with sub-crystal trace-element analysis of plagioclase and zircon: Earth and Planetary Science Letters, v. 313–314, p. 1–11.

Storm, S, Shane, P, Schmitt, AK and Lindsay, JM 2011, Contrasting punctuated zircon growth in two syn-erupted rhyolite magmas from Tarawera volcano: Insights to crystal diversity in magmatic systems: Earth and Planetary Science Letters, v. 301, p. 511–520.

Storm, S, Shane, P, Schmitt, AK and Lindsay, JM 2012, Decoupled crystallization and eruption histories of the rhyolite magmatic system at Tarawera volcano revealed by zircon ages and growth rates: Contributions to Mineralogy and Petrology, doi:10.1007/s00410-011-0682-8.

Streck, MJ and Grunder, AL 2008, Phenocryst-poor rhyolites of bimodal, tholeiitic provinces: the Rattlesnake Tuff and implications for mush extraction models: Bulletin of Volcanology, v. 70, p. 385–401.

Sun, S-S and McDonough, WF 1989, Chemical and isotopic systematics of oceanic basalts; implications for mantle composition and processes, *in* Magmatism in the ocean basins *edited by* AD Saunders and MJ Norry: Geological Society of London, Special Publication 42, p. 313–345.

Sun, S-S, Sheraton, JW, Glikson, AY and Stewart, AJ 1996, A major magmatic event during 1050–1080 Ma in central Australia, and an emplacement age for the Giles Complex: AGSO Journal of Australian Geology and Geophysics, v. 24, p. 13–15.

Thorarinsson, SB, Holm, PM, Duprat, HI and Tegner, C 2012, Petrology and Sr-Nd-Pb isotope geochemistry of Late Cretaceous continental rift ignimbrites, Kap Washington peninsula, North Greenland: Journal of Volcanology and Geothermal Research, v. 219–220, p. 63–86.

Tikhomirov, PL, Kalinina, EA, Moriguti, T, Makishima, A, Kobayashi, K, Cherepanova, I Yu and Nakamura, E 2012, The Cretaceous Okhotsk-Chukotka Volcanic Belt (NE Russia): Geology, geochemistry, magma output rates, and implications on the genesis of silicic LIPs: Journal of Volcanology and Geothermal Research, v. 221–222, p. 14–32.

Turner, S and Rushmer, T 2009, Similarities between mantle-derived A-type granites and voluminous rhyolites in continental flood basalt provinces: Earth and Environmental Science Transactions of the Royal Society of Edinburgh, v. 100, p. 51–60.

Vervoort, JD and Green, JC 1997, Origin of evolved magmas in the Midcontinent rift system, northeast Minnesota: Nd-isotopic evidence for melting of Archean crust: Canadian Journal of Earth Sciences, v. 34, p. 521–535.

Vervoort, JD, Patchett, PJ, Blichert-Toft, J and Albarède, F 1999, Relationships between Lu–Hf and Sm–Nd isotopic systems in the global sedimentary system: Earth and Planetary Science Letters, v. 168 (1–2), p. 79–99.

Wade, BP, Barovich, K, Hand, M, Scrimgeour, IR and Close, DF 2006, Evidence for early Mesoproterozoic arc magmatism in the Musgrave Block, central Australia: implications for Proterozoic crustal growth and tectonic reconstructions of Australia: Journal of Geology, v. 114, p. 43–63.

Wade, BP, Kelsey, DE, Hand, M and Barovich, KM 2008, The Musgrave Province: stitching north, west and south Australia: Precambrian Research, v. 166, p. 370–386.

Watson, EB and Harrison, MT 1983, Zircon saturation revisited: temperature and composition effects in a variety of crustal magma types: Earth and Planetary Science Letters, v. 64, p. 295–304.

Wendt, I and Carl, C 1991, The statistical distribution of the Mean Squared Weighted Deviation: Chemical Geology, v. 86(4), p. 275–285.

Werner, M, Howard, HM and Smithies, RH 2012, Mount Eveline, WA Sheet 4345: Geological Survey of Western Australia, 1:100 000 Geological Series.

Whitaker, ML, Nekvasil, H, Lindsley, DH and Difrancesco, NJ 2007, The role of pressure in producing compositional diversity in intraplate basaltic magmas: Journal of Petrology, v. 48, p. 365–393.

Whitaker, ML, Nekvasil, H, Lindsley, DH and McCurry, M 2008, Can crystallization of olivine tholeiite give rise to potassic rhyolites? – an experimental investigation: Bulletin of Volcanology, v. 70, p. 417–434.

White, RW, Clarke, GL and Nelson, DR 1999, SHRIMP U–Pb zircon dating of Grenville-age events in the western part of the Musgrave Block, central Australia: Journal of Metamorphic Geology, v. 17, p. 465–481.

Wilde, SA 1999, Evolution of the western margin of Australia during the Rodinian and Gondwanan supercontinent cycles: Gondwana Research, v. 2, p. 481–499.

Winchester, JA and Floyd, PA 1977, Geochemical discrimination of different magma series and their differentiation products using immobile elements: Chemical Geology, v. 20, p. 325–343.

Wingate, MTD, Pirajno, F and Morris, PA 2004, Warakurna large igneous province: a new Mesoproterozoic large igneous province in west-central Australia: Geology, v. 32, p. 105–108.

Wolfenden, E, Edinger, C, Yirgu, G, Deino, A and Ayalew, D 2004, Evolution of the northern Main Ethiopian rift: birth of a triple junction: Earth and Planetary Science Letters, v. 224, p. 213–228.

Wolff, JA, Rowe, MC, Teasdale, R, Gardner, JN, Ramos, FC and Heikoop, CE 2005, Petrogenesis of pre-caldera mafic lavas, Jemez Mountains Volcanic Field (New Mexico, USA): Journal of Petrology, v. 46, p. 407–439.

York, D 1966, Least-squares fitting of a straight line: Canadian Journal of Physics, v. 44, p. 1079–1086.

Appendix

GSWA geochronological data for the Warakurna Supersuite in the west Musgrave Province

GSWA Sample No.	Published age (Ma)[a]	Rock type	Report status (2012)	Geochronology Record No.
187177	1026 ± 25	Rhyolite/dacite	Published	847
185415	1052 ± 5	Rhyolite/dacite	Preliminary	
187054	1055 ± 10	Gabbro	Preliminary	
174691	1057 ± 6	Rhyolite/dacite	Published	1048
195673	1059 ± 6	Rhyolite/dacite	Preliminary	
194454	1062 ± 6	Gabbro	Published	962
189580	1063 ± 8	Rhyolite/dacite	Published	961
194637	1064 ± 7	Granite	Published	963
195678	1064 ± 5	Rhyolite/dacite	Preliminary	
174690	1065 ± 5	Rhyolite/dacite	Published	995
189563	1065 ± 9	Granite	Preliminary	
195230	1065 ± 9	Rhyolite/dacite	Preliminary	
187256	1066 ± 9	Granite	Published	913
191716	1067 ± 9	Granite	Published	916
194354	1067 ± 8	Gabbro	Published	799
195116	1067 ± 6	Rhyolite/dacite	Preliminary	
185518	1068 ± 7	Rhyolite/dacite	Preliminary	
195114	1068 ± 5	Rhyolite/dacite	Preliminary	
194763	1070 ± 7	Gabbro	Published	964
194800	1070 ± 6	Rhyolite/dacite	Preliminary	
195115	1070 ± 10	Rhyolite/dacite	Preliminary	
191728	1071 ± 8	Rhyolite/dacite	Published	917
195723	1071 ± 5	Rhyolite/dacite	Published	939
183474	1072 ± 8	Granite	Published	723
185583	1073 ± 6	Granite	Published	765
191706	1073 ± 7	Rhyolite/dacite	Published	915
189561	1073 ± 8	Rhyolite/dacite	Preliminary	
205119	1073 ± 23	Granite	Preliminary	
174589	1074 ± 3	Granite	Published	715
185407	1074 ± 6	Rhyolite/dacite	Preliminary	
190256	1074 ± 4	Rhyolite/dacite	Preliminary	
174761	1075 ± 7	Granite	Published	721
185509	1075 ± 3	Granite	Published	725
194762	1076 ± 7	Granite	Published	966
174662	1077 ± 6	Granite	Published	909
183847	1078 ± 4	Granite	Published	1059
195231	1079 ± 8	Granite	Preliminary	

NOTE: (a) Results cited in the text are derived from 207-correction of U–Pb data in the GSWA Geochronology Record series available at <www.dmp.wa.gov.au/geochron/> and thus may differ slightly from results cited in this table (see Geochronology section in main text for details).

This report presents new geological, geochemical, isotopic, and geochronological data from the felsic volcanic sequences of the Bentley Supergroup in the Mesoproterozoic Ngaanyatjarra Rift – the main crustal expression of the Mesoproterozoic Giles Event. In one region of the rift – the Talbot Sub-basin – at least 20 separate felsic volcanic units can be recognized, forming layers of very high-temperature (some >900˚C) rhyolitic and rheomorphic ignimbrites and rhyolitic flows, some of super-volcano size (i.e. >450 km^3 of material erupted). These accumulated over a period of >30 m.y. and likely contributed to a silicic large igneous province. The rhyolites are interleaved with regional tholeiitic basalt flows compositionally equivalent to the Alcurra Dolerites that formed the Warakurna Large Igneous Province, also during the Giles Event. Both the dolerite and the rhyolites are genetically related to the same parental mantle-derived magma. The minimum volume of juvenile parental magma required to form the volcanic units of the Talbot Sub-basin was 227 000 km^3. The volume of juvenile parental magma required to form all units intruded, extruded or erupted during the > 50 m.y. duration of the Giles Event was possibly more than 2.19 × 10^6 km^3. Crustal structure and thermal history were the primary controls on magmatic and tectonic evolution, rather than deep-seated mantle upwelling or mantle plume activity.

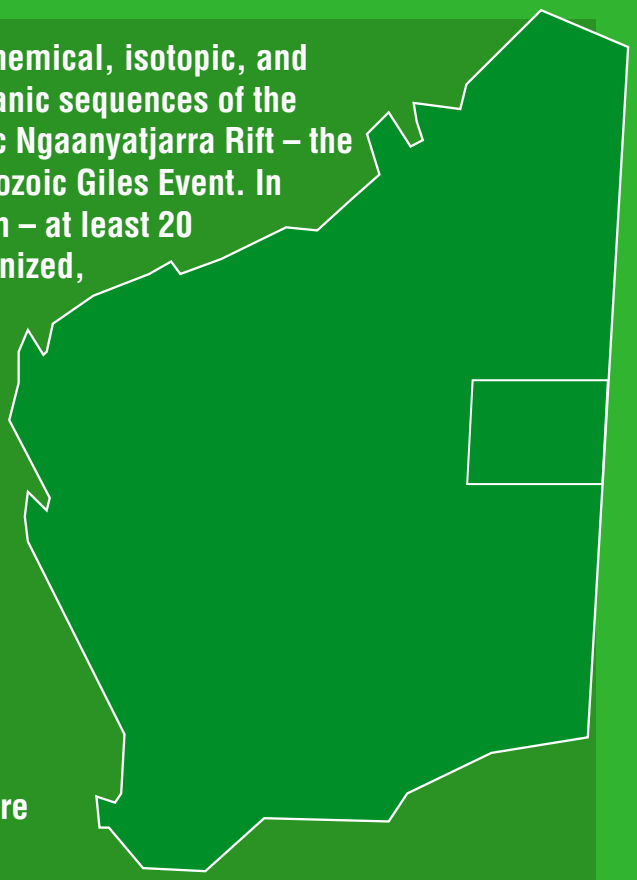

Further details of geological products and maps produced by the Geological Survey of Western Australia are available from:

Information Centre
Department of Mines and Petroleum
100 Plain Street
EAST PERTH WA 6004
Phone: (08) 9222 3459 Fax: (08) 9222 3444

www.dmp.wa.gov.au/GSWApublications

Smithies et al.

GEOCHEMICAL EVOLUTION OF RHYOLITES OF THE TALBOT SUB-BASIN AND ASSOCIATED FELSIC UNITS OF THE WARAKURNA SUPERSUITE

REPORT 118